

**MODELING, DESIGN, FABRICATION AND  
CHARACTERIZATION OF MINIATURIZED PASSIVES AND  
INTEGRATED EM SHIELDS IN 3D RF PACKAGES**

A Dissertation

Presented to

The Academic Faculty

by

Srikrishna Sitaraman

In Partial Fulfillment  
of the Requirements for the Degree  
Doctor of Philosophy in the  
School of Electrical and Computer Engineering

Georgia Institute of Technology  
DECEMBER 2015

Copyright© 2015 by SRIKRISHNA SITARAMAN

**MODELING, DESIGN, FABRICATION AND  
CHARACTERIZATION OF MINIATURIZED PASSIVES AND  
INTEGRATED EM SHIELDS IN 3D RF PACKAGES**

Approved by:

Dr. Rao R. Tummala, Advisor  
School of Electrical and Computer  
Engineering  
*Georgia Institute of Technology*

Dr. Peter J. Hesketh  
School of Mechanical  
Engineering  
*Georgia Institute of Technology*

Dr. John Papapolymerou  
School of Electrical and Computer  
Engineering  
*Georgia Institute of Technology*

Dr. Markondeya Raj Pulugurtha  
School of Electrical and Computer  
Engineering  
*Georgia Institute of Technology*

Dr. Andrew F Peterson  
School of Electrical and Computer  
Engineering  
*Georgia Institute of Technology*

Date Approved: August 18, 2015

*Dedicated to my parents, sister, and fiancée.*

## ACKNOWLEDGEMENTS

I would like to thank and express my sincere gratitude to my advisor Prof. Rao Tummala for giving me the opportunity to work on a leading edge project at the Georgia Tech 3D systems packaging research center. He has been a constant source of inspiration. His vision and advice has greatly helped in shaping my thesis. I am extremely grateful for having been mentored and advised by Prof. Tummala.

I would also like to thank my mentor Dr. Raj for his invaluable support and mentorship over the years. His technical depth has helped guide me every step of the way. I have learnt much more than I could have ever hoped for. Next, I would like to thank my committee members: Prof. Andrew Peterson, Prof. John Papapolymerou, Prof. Peter Hesketh, and Dr. Venky Sundaram for being part of my PhD committee and for all the valuable suggestions and feedback. I would like to extend special thanks to Dr. Venky Sundaram, Dr. Junki Min, Dr. Fuhun Liu, and Dr. Vanessa Smet for their timely guidance through the years.

I have had the privilege to work with a very knowledgeable and enthusiastic team at the Georgia Tech PRC and I would like to thank Dr. Himani Sharma, Prof. Klaus Jergen Wolter, Dr. Melinda Varga, Mr. Sung Jin Kim, and Mr. Nitesh Kumbhat for all of their invaluable support over the course of my stay at Georgia Tech. Next I would like to thank the PRC staff: Karen May, Patricia Allen, Brian McGalde, Tracy Monroe, Chris White, and Jason Bishop for their patient support over my stay at the GT PRC. I would also like to extend a special thanks to all the visiting engineers: Yoichiro Sato (AGC), Tomonori Ogawa (AGC), Yuya Suzuki (Zeon Chemicals), Toshitake Seki (NGK-NTK), Makoto Kobayashi (Namics Corporation), Satomi Kawamoto (Namics Corporation), Yutaka Takagi (NGK-NTK), Charlie Russel (AVX), and Ryuta Furuya (Ushio).

My stay in Atlanta would not have been as good but for the support of my friends: Vijay Narayanan, Prasaanth Muralidharan, Mithun Udayakumar, Gopi Sundaresan, Gokul Kumar, Vijay Sukumaran, Koushik Ramachandran, Saumya Gandhi, Dibyajat Mishra, Kaushiik Bhaskaran, Sudarsanan Krishnan, Vignesh Somasundaram, Uppili Raghunathan, Swarrnna Karthik Parthasarathy, Srikanth Dwarakanath, Shreyas Srinivas, Karthik Raghavan, Chandrashekar Nair, Bhupender Singh Chauhan, Ninad Sahane, Xian Qin, Sadia Khan, Vivek Sridharan, Nithya Sankaran, Bruce Chou, Brett Sawyer, Timothy Huang, Kaya Demir, Zihan Wu, Chinmay Honrao, William Vis, Tapobrata, Qiao Chen, Hao Lu, Gary Menezes, Yushu Wang, Jialing Tong, Min Suk Kim, Teng Sun, Parthasarathy Chakraborty, Florian Nebe, and Tailong Shi. Lastly I would like to thank my parents who have made me what I am today. I am extremely grateful for the love and support of my family.

# TABLE OF CONTENTS

	Page
ACKNOWLEDGEMENTS .....	iv
LIST OF TABLES .....	viii
LIST OF FIGURES .....	ix
SUMMARY .....	xiii
CHAPTER 1: INTRODUCTION .....	1
Strategic Need .....	1
Objectives of this Research .....	9
Research Challenges.....	10
Approach to RF Module Integration with Thin Passives and EMI Shields .....	12
Research Tasks .....	15
CHAPTER 2: LITERATURE SURVEY.....	17
Passive Miniaturization .....	17
EMI Shielding .....	23
RF Module Integration .....	34
Summary and Thesis R&D Focus .....	39
CHAPTER 3: MINIATURIZATION OF WLAN DIPLEXER.....	42
Objectives .....	42
Approach .....	43
Modeling and Design of Novel Filters .....	44
Fabrication and Characterization of Filters .....	56
Design and Demonstration of 3D IPD Diplexer.....	59
Summary.....	67

CHAPTER 4: MINIATURIZED COMPONENT-LEVEL EMI SHIELDING.....	69
Objectives .....	69
Approach .....	70
Modeling EM Radiation in RF Modules .....	71
Analytical Material Modeling - Material and Multi-layer Stack-up Design .....	74
Modeling and Design of Component-level EMI Shields .....	85
Fabrication and Characterization of EMI Shields .....	90
Summary.....	93
CHAPTER 5: DESIGN AND DEMONSTRATION OF MINIATURIZED RF MODULES .....	95
Objectives .....	95
Module Description .....	96
Design and Simulation of WLAN RF Module on Organic Substrate .....	98
Fabrication, Assembly, and Characterization of RF Module on organic substrates .....	107
Design and Simulation of RF Module on Glass Substrate .....	113
Fabrication and Characterization of RF Modules on Glass Substrates .....	119
Summary.....	122
CHAPTER 6: SUMMARY AND FUTURE WORK .....	124
Key Contributions .....	127
Future Research Directions .....	127
List of Publications.....	129
REFERENCES .....	131

## LIST OF TABLES

	Page
Table 1 Parameters and Targets of the Proposed Research .....	9
Table 2 Parameters and Targets for WLAN Diplexers.....	15
Table 3 Parameters and Targets for EMI Shielding.....	15
Table 4 Parameters and Targets for RF Modules .....	16
Table 5 Parameters and Targets for EMI shielding .....	42
Table 6 Inductor and Capacitor Values .....	47
Table 7 Performance Specifications of the WLAN Diplexer .....	59
Table 8 Targets for EMI Shielding .....	69
Table 9 List of Material Properties .....	79
Table 10 Design Rules for the Shield Structure.....	85
Table 11 Targets for Module Design.....	96

## LIST OF FIGURES

	Page
Figure 1: Estimated number of devices with wireless connectivity. ....	1
Figure 2: Evolution of RF modules: a) Traditional RF modules, b) Future ultra-miniaturized RF modules. ....	2
Figure 3: Trends in passive and active integration. ....	3
Figure 4: Miniaturized multi-layer WLAN diplexer by TDK. ....	5
Figure 5: Module with embedded discrete SMT components [7]. ....	6
Figure 6: RF Module with embedded thin-film passives [8]. ....	6
Figure 7: Metallic cans employed in EMI shielding [15]. ....	8
Figure 8: Conformally coated metallic shield for over-mold packages [17]. ....	8
Figure 9: Compartment-based over-mold shielding [18]. ....	8
Figure 10: Via-array based shield structures. ....	9
Figure 11: Challenges with RF module miniaturization: a) Trade-off between performance, loss and size; b) EM interference vs. proximity. ....	11
Figure 12: RF front-end module integration trend (Source: Arjun Ravindran, TDK-EPCOS). ....	12
Figure 13: 3D IPAC approach for miniaturization, performance and cost. ....	13
Figure 14: Band-pass filters designs using transmission line elements; a) schematic, b) resonator configuration, c) fabricated substrate top view [9]. ....	18
Figure 15: Band-pass filters using broad-side coupled striplines on LTCC substrates; a) Layout of filter, b) 3-D view of substrate with ground planes [25]. ....	19
Figure 16: Compact band-pass filter: a) component design, and b) substrate stack-up [27]. ....	20
Figure 17: (a) Equivalent circuit, and (b) frequency response, of a LTCC-based filter [27]. ....	20
Figure 18: (a) WLAN band-pass filters using lumped elements, (b) on organic substrates. [11]. ....	21
Figure 19: Modified low-order filter with transmission zeros, on organic substrate: (a) schematic, (b) response. [11]. ....	21
Figure 20: WLAN band-pass filters on glass wafers using single-side processing: (a) schematic, (b) response. [28]. ....	22
Figure 21: Band-pass filters on thin glass with TPVs: (a) Layout view, (b) cross-section of fabricated sample [12]. ....	22
Figure 22: EM interference between various components in a SOP substrate. ....	24
Figure 23: (a) 3D model of on-chip inductor, and (b) current density on the surface for various shields at 20MHz. ....	24
Figure 24: Coupling between a component and a transmission line. ....	25
Figure 25: Coupling between PA and LNA dies: a) system-level schematic, (b) component-level schematic. ....	25
Figure 26: Coupling between two RF dies: (a) Dicing to eliminate substrate coupling, (b) measured isolation. ....	26
Figure 27: (a) 3-D model to study EMI coupling into trace on a board, (b) PA response for different noise coupling. ....	26

Figure 28: (a) Coupling between digital and RF signals in mixed-signal systems, (b) grounded via wall as a shield. ....	27
Figure 29: (a) Digital-RF Coupling and, (b) RF sensitivity improved through shield design techniques. ....	27
Figure 30: Magnetic field shielding by providing a low-reluctance path. ....	28
Figure 31: (a) Schematic of multiple layers, (b) equations for H-field shield effectiveness. ....	28
Figure 32: Multiple layers of magnetic and non-magnetic layers as EMI shield. ....	29
Figure 33: Thin multi-layer stack with high shielding effectiveness at frequencies close to the FMR (ferromagnetic resonance) frequency. ....	30
Figure 34: (a) 3-D EM and experimental set-up to measure shield effectiveness, (b) measured shielding effectiveness. ....	30
Figure 35: Multiple layers of NiFe and insulator used for shielding at high frequencies. ....	31
Figure 36: Single-component package with EM shield to suppress external interference. ....	31
Figure 37: Metallic cans employed in EMI shielding [15]. ....	32
Figure 38: Conformally coated metallic shield for over-mold packages [17]. ....	32
Figure 39: Compartment-based over-mold shielding [18]. ....	32
Figure 40: (a) RF SiP design, and (b) shielding structure. ....	33
Figure 41: Via-array based shield structures. ....	33
Figure 42: Single-chip WLAN 802.11b/g Front End Module [2]. ....	34
Figure 43: RF module with embedded planar diplexers on LTCC substrate: (a) Layout, (b) fabricated sample [46]. ....	35
Figure 44: 3-D view of a LTCC front end module. ....	35
Figure 45: WLAN module on LCP substrate with embedded passives and surface mounted actives. ....	36
Figure 46: Embedded actives substrate for high-density integration. ....	36
Figure 47: Schematic of chip-last embedded actives substrate. ....	37
Figure 48: WLAN RF receiver module schematic cross-section. ....	37
Figure 49: Glass provides the best combination of advantages from ceramic, organic and silicon. ....	38
Figure 50: RF IPD on glass wafers - single-side processing; a) cross-section stack-up, b) assembled IPD component. ....	39
Figure 51: Stack-up cross-section of a 3D glass substrate. ....	39
Figure 52: Stack-up of the glass substrate. ....	44
Figure 53: Perspective view of the innovative filter structure layout. ....	45
Figure 54: Simulated filter responses for two polymer thicknesses. ....	46
Figure 55: Equivalent circuit model of the proposed filter. ....	47
Figure 56: Correlating the EM and circuit simulation of the filter. ....	47
Figure 57: Magnitude and phase of insertion loss. ....	48
Figure 58: Group-delay through the filter. ....	48
Figure 59: Simulated filter pass-band insertion loss for different line widths. ....	50
Figure 60: Simulated filter transmission zero for different line widths. ....	50
Figure 61: Variation in pass-band center frequency for different (a) polymer thicknesses, (b) spiral lengths. ....	51
Figure 62: Simulated filter responses for X-Y misalignment between the metal layers. .	52

Figure 63: Top-view of the filter layout with secondary spiral and capacitor plate.....	53
Figure 64: Simulated filter responses of the filter with and without secondary spirals....	53
Figure 65: Top-view of the filter layout with grounded spirals.....	54
Figure 66: Simulated filter responses with and without ground spirals.....	54
Figure 67: Top-view of the filter layout with grounded capacitor.....	55
Figure 68: Simulated filter responses with and without ground capacitors.....	55
Figure 69: Process flow for fabrication of the ultra-thin glass substrate with TPVs.....	56
Figure 70: Measurement and top view optical image of fabricated BPF structure on 30 $\mu$ m thin glass.....	57
Figure 71: Simulation-measurement performance correlation of the filter.....	58
Figure 72: Substrate stack-up and design rules for 4ML diplexer fabrication.....	60
Figure 73: 3D view of the initial diplexer design.....	61
Figure 74: Simulated response of (a) low-band filter, (b) high-band filter.....	61
Figure 75: (a) Fabricated diplexer substrate, (b) RF Probing of diplexer.....	62
Figure 76: Diplexer measurement results: (a) Low-Band (b) High-band.....	62
Figure 77: Modified substrate stack-up and design rules for 4ML diplexer fabrication..	63
Figure 78: 3D view of the initial diplexer design.....	64
Figure 79: Simulated response of (a) low-band filter, (b) high-band filter.....	64
Figure 80: Conceptual 3D view of a 3DIPD WLAN diplexer component.....	65
Figure 81: 3D view of the revised low-band filter design.....	66
Figure 82: Simulated response of the revised low-band filter.....	66
Figure 83: Top-view of the fabricated revised low-band design.....	67
Figure 84: Measured performance of the revised low-band design.....	67
Figure 85: Top view of the typical simulation setup.....	72
Figure 86: EM coupling between package elements.....	73
Figure 87: Wave impedance with varying distance from an EM source radiating at 5GHz.....	75
Figure 88: The various mechanisms associated with EM shielding.....	76
Figure 89: Comparison of shielding effectiveness of different materials.....	80
Figure 90: Shield effectiveness with varying thickness of the shield metal.....	81
Figure 91: Proposed unit stack-up.....	82
Figure 92: Mechanism of EM shielding in the proposed multi-layer stack.....	83
Figure 93: Comparison of simulated shield effectiveness of the proposed multi-layer stack and single-layer copper.....	84
Figure 94: Simulation set-up showing transmission lines separated by a trench-based shield.....	86
Figure 95: Comparison of TL-TL coupling in presence of via-arrays and trenches.....	86
Figure 96: Simulation setup of the via-array shields, (a) with continuous via pad, and (b) discrete via pads.....	87
Figure 97: Comparison of TL-TL coupling in presence of trenches and different via-arrays configurations.....	87
Figure 98: Lateral view of via-array shields to compare the aperture for different scenarios.....	88
Figure 99: 3D view of the trench-based shield extending above the plane of the signal lines.....	89
Figure 100: Comparison of TL-TL coupling for different trench configurations.....	89

Figure 101. Top-view of the substrate with the laser-ablated trench and blind-vias.....	90
Figure 102. Fabrication process of multi-layer glass substrates.....	91
Figure 103. Transmission lines with via-array and trench shields, fabricated on ultra-thin glass substrates.....	92
Figure 104. Comparison of measured TL-TL coupling in the presence of via-arrays and trenches. ....	92
Figure 105: Components of a WLAN sub-system.....	97
Figure 106: LNA Module schematic, as seen on TriQuint's datasheet.....	98
Figure 107: Stack up structure of the 3 metal-layer module.....	99
Figure 108. Top view of M2 layer in the LNA module design. ....	100
Figure 109: Layout of the WLAN band-pass filter.....	100
Figure 110: Simulated performance of the ban-pass filter.....	101
Figure 111: WLAN receiver module (a) schematic cross section and 3D view, and (b) top view. ....	102
Figure 112. Simulation flow used for analyzing the receiver module layout. ....	102
Figure 113: Top view of the WLAN receiver 3D model.....	103
Figure 114: Characteristics of output RF signal path. ....	104
Figure 115: Coupling from DC pad to RF signal path.....	104
Figure 116. Agilent ADS set-up to extract LNA die S-parameters. ....	105
Figure 117. Complete package model created in Agilent ADS, indicating signal flow. ....	105
Figure 118. Complete receiver model simulated using HFSS and Agilent ADS. ....	106
Figure 119: Image of the test vehicle mask layout. ....	107
Figure 120: Fabrication process steps.....	108
Figure 121: Images of, a) substrate prior to assembly, and b) top view of die cavity. ...	108
Figure 122: RF receiver module after assembly (left: top view, right: X-ray image). ...	109
Figure 123: Cross section of RF receiver module. ....	109
Figure 124. Measured response of LNA modules. ....	110
Figure 125: Measured response of RF receiver module. ....	111
Figure 126: Comparison of the simulated and the measured responses of the filter. ....	112
Figure 127: Comparison of the simulated and the measured responses of the receiver. ....	112
Figure 128: Stack-up cross-section of the multilayer glass substrate. ....	114
Figure 129: Top-view of the diplexer layout. ....	115
Figure 130: Simulated response of the diplexer. ....	115
Figure 131: (a) Schematic cross-section, and (b) top-view, of the WLAN RF receiver module.....	116
Figure 132: Top-view of the output section of the WLAN RF receiver module.....	117
Figure 133: Simulated response of the output section of the WLAN RF receiver module.....	118
Figure 134: Simulated coupling of the output section of the WLAN RF receiver module.....	118
Figure 135: Measured response of the low-band BPF of the diplexer. ....	120
Figure 136: ADS schematic to estimate the low-band response of RF module on glass.....	120
Figure 137: Estimated low-band response of WLAN RF module on glass substrate. ...	121

## SUMMARY

Smart systems require both high-performance and miniaturized functional components, and their integration into ultra-miniaturized modules and systems. To achieve these objectives, this thesis focuses on two key passive-component building block technologies: diplexers and EMI shields, for higher performance and miniaturization, and their integration with actives using an innovative 3D Integrated Passive and Active Components (3D IPAC) concept.

An innovative structure for thin-film band-pass filters is proposed and analyzed. This structure is employed in the design, fabrication, and development of 3D IPD diplexers on glass substrates with double-side metallization electrically connected by through-vias. Through modeling, design, fabrication and characterization of the WLAN 3D IPD glass diplexers, the proposed filter structure is shown to enable miniaturized and high-performance RF passives.

Component-level shield structures are developed to provide electromagnetic interference isolation between thin-film passives that are placed less than 100  $\mu\text{m}$  apart. Four-metal-layered glass substrates were designed, fabricated and characterized to demonstrate the shield effectiveness of metallized trench and via-array-based shields. The integration of such shields in miniaturized WLAN RF modules enables up to 60dB EM isolation in the frequency range of 1- 20GHz.

Advanced RF module technologies based on 3D IPAC concept were designed and demonstrated with ultra-thin low-loss organic and glass substrates, integrating WLAN actives with miniaturized diplexer and EM shields. Double-side integration of such

high-performance components on ultra-thin glass substrates enables up to 8x volume miniaturization including 2.5x reduction in area.

Thus, the advanced components demonstrated in this research, vis-a-vis miniaturized diplexers and component-level EMI shields; integrated with actives in ultra-thin glass substrates using the 3D IPAC concept, can enable highly-miniaturized smart systems with multiband wireless communication capabilities.

# CHAPTER 1

## INTRODUCTION

### Strategic Need

The growing need to access information and media content, along with security, healthcare and many others, is leading to the proliferation of smart systems such as smartphones, tablets, wireless health and environmental sensors, and appliances. As illustrated in Figure 1, tens of billions of such systems are estimated to be connected wirelessly with one other in the next decade through multiple Radio Frequency (RF) communication standards such as GPS, WLAN, GSM and Bluetooth. Integrating multiple wireless standards in phones, watches and other wearable electronic systems requires ultra-miniaturized and high-performance, multi-functional RF modules.

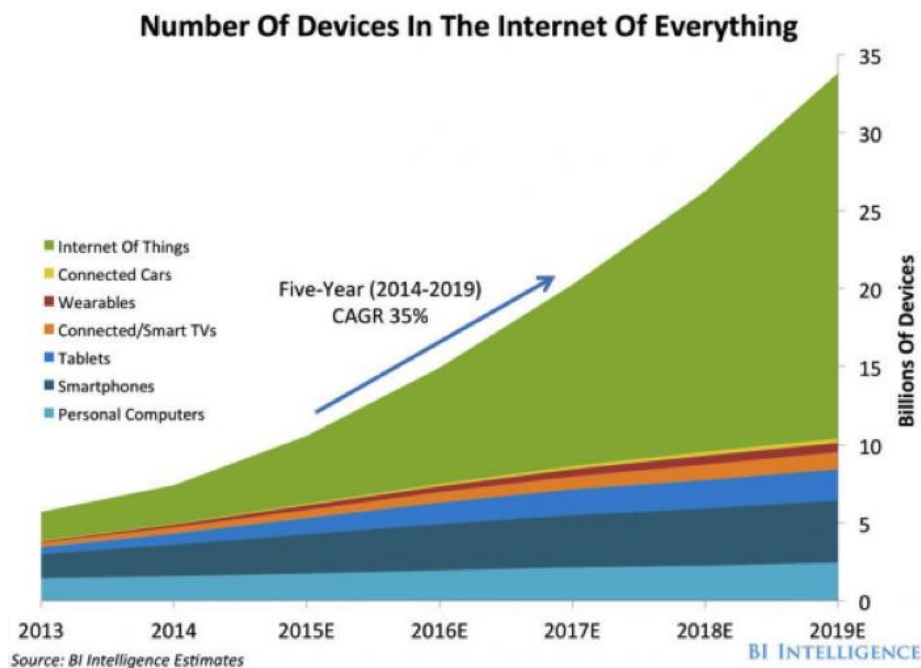


**Figure 1:** Estimated number of devices with wireless connectivity.

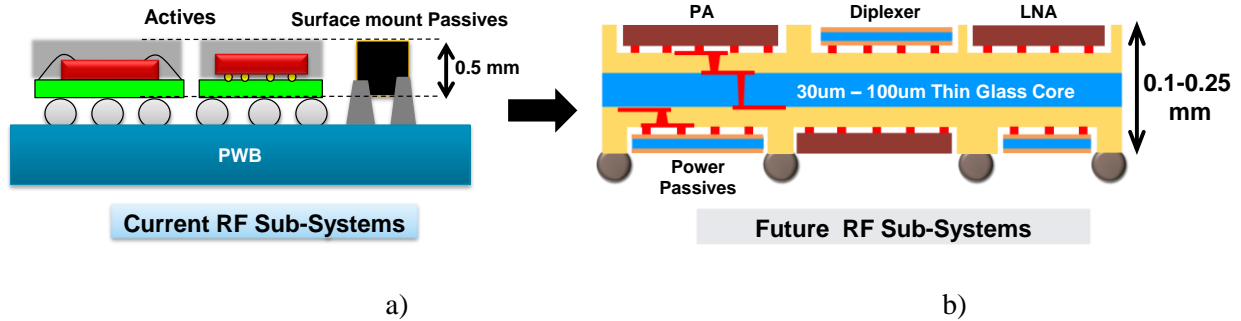


**Figure 2:** Evolution of RF modules: a) Traditional RF modules, b) Future ultra-miniaturized RF modules.

Traditional RF modules [1] feature actives and passives in individual thick packages, assembled on printed wiring boards, as shown in Figure 2a, resulting in low-performance and high cost; compared with a glass-based systems realized using 3D double-side component integration, envisioned in Figure 2b. To miniaturize and improve the performance of such RF modules, several advances in RF actives have been reported [2] over the past three decades. In spite of these, only incremental improvements in performance and miniaturization have been possible at the module- and system-level. This is because the overall size is dominated by other components such as passives, EMI shields, thermal structures and interconnections. Thus, performance enhancement, while miniaturizing RF modules, can be realized through five key building blocks: a) ultra-thin low-noise high-gain actives, b) thin-film low-loss RF and power passives, c) high-density active and passive component integration with minimal electromagnetic interference, d) miniaturized and efficient thermal dissipation, and e) interconnections with least signal and power losses.

Continuous advances in on-chip design, as mentioned earlier, have enabled miniaturization and integration of actives [2]. These include RF actives with very low noise and high gain, through optimal design of GaN or CMOS SOI dies, in less than 100 microns thickness. Discrete passive components with low-temperature co-fired ceramics (LTCC) have provided the best RF performance. However, these components are typically 0.3-0.9 mm thick, resulting in module thicknesses of above 1mm. To facilitate passive component miniaturization,

a number of low-loss thick-film and thin-film dielectrics are being developed for RF and power applications [3, 4]. In addition to such dielectric materials, miniaturization trend among passives include array of discretes, and integrated passive devices (IPDs) using silicon and glass substrates [5], as depicted in Figure 3.

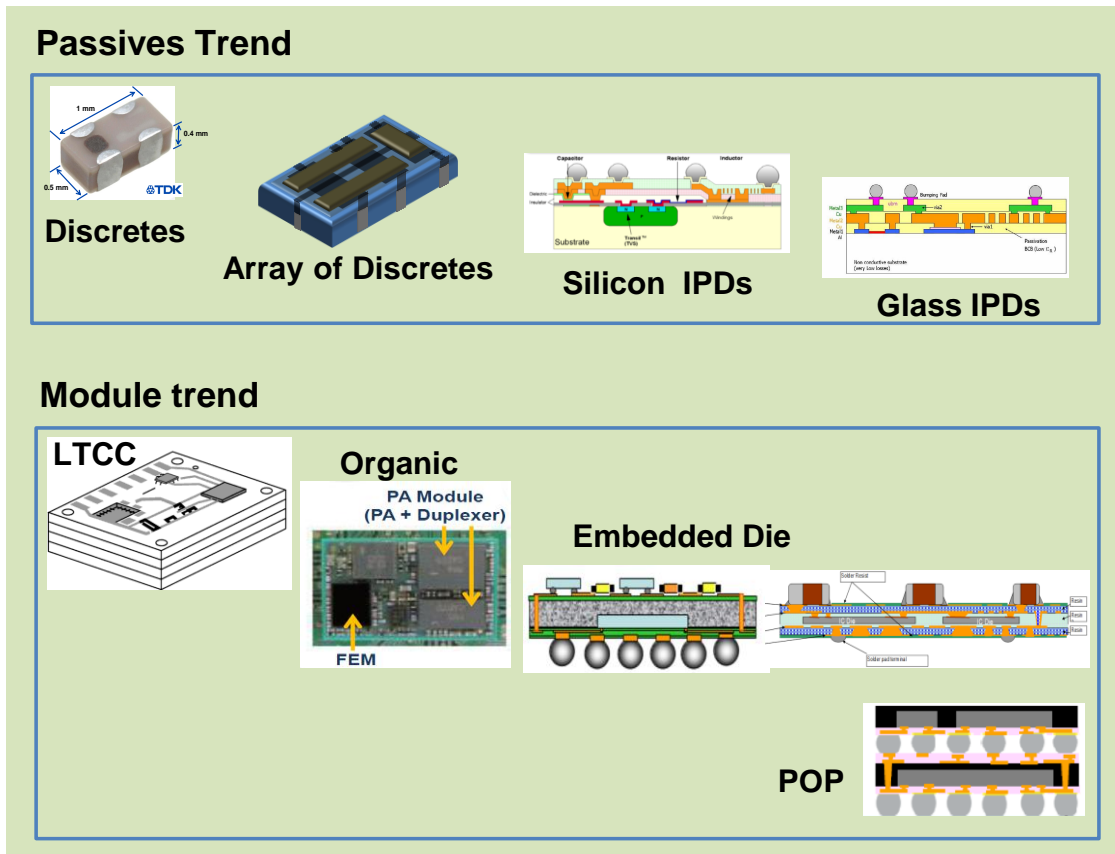


**Figure 3:** Trends in passive and active integration.

Further, to support the functionality and miniaturization requirements of consumer products such as smartphones, the system components that are typically mounted on the PWB board, are gradually migrating into the package substrates, increasing the package size, cost and complexity. Integration of actives and passives is being achieved through a number of embedded and non-embedded approaches, as shown in Figure 3. Passive and active integration in RF modules traditionally evolved with low-temperature co-fired ceramic substrates. The primary

reason is the superior properties of LTCC such as low dielectric loss, low moisture absorption, high reliability based on hermetic nature of ceramics, high temperature-stability and ability to form complex 3D multi-layered circuits. The technology eventually migrated to organic laminate packaging because of cost and higher component density from fine-line and multi-layered wiring. The process in embedding technologies such as wafer level fan-out [6], begins with embedding the actives, followed by surface-mounting or embedding the discrete passives. Such an embedding structure reduces the total thickness. The drive for form-factor reduction in radio sub-systems in both z and x-y direction has led to the evolution of embedded die-package architectures with dies facing up or down. This also reduces insertion loss by minimizing package parasitics. Embedded wafer-level ball grid array (eWLB) approaches based on fan out wafer-level package (FO-WLP) have achieved improved miniaturization and performance.

Both LTCC and organic laminate substrates co-exist in today's smartphones. Organic substrates that are ~0.3-0.5 mm thick form the preferred platform for today's modules, with up to two-metal layers on each side of the core. The lines and spaces are approaching 15-20  $\mu\text{m}$  with vias of 100  $\mu\text{m}$  in leading-edge RF substrates. Thin-film embedded passives such as RF inductors are seen in organic laminates for certain applications where tolerance is not critical. High-performance passives are also made from SAW (surface acoustic wave), BAW (bulk acoustic wave) devices that are packaged separately and assembled on the package or board. Shielding structures are provided for each packaged device to create isolation between individual packages. However, passive component miniaturization with performance enhancement has remained as a fundamental challenge. Further, to address the increasing EM interference between components in highly integrated modules, there is a need to develop effective package-integrated EMI shields. These two aspects are described in the next two sections.

## Passive Component Miniaturization and integration

Today's passive components are predominantly based on LTCC substrates. These are thick (>350 microns) and are manufactured and assembled as individual devices or packages as shown in Figure 4.

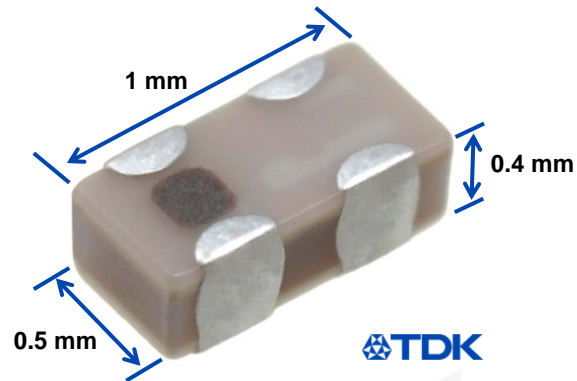


**Figure 4:** Miniaturized Multi-layer WLAN diplexer by TDK.

This approach is eventually expected to limit the miniaturization and performance at the functional-module level, and subsequently the entire system. The major concerns with such discrete RF passives are: 1) they contribute an additional 150-450 microns to the thickness of the package, 2) the number of passives is much higher than the number of actives which increases the size of today's 2D modules, and 3) the interconnection parasitics increase the loss and deteriorate the module performance.

To address these limitations with discrete passives, there is an increasing trend to embed the passives [7] in the substrate to reduce the distances from actives to less than 200 $\mu$ m while improving performance and conserving space, as shown in Figure 5.

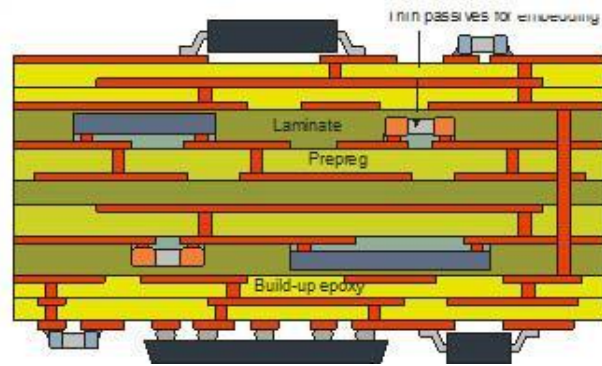


**Figure 5:** Module with embedded discrete SMT components [7].

However, this approach is limited by the component thickness (require  $<0.15$  mm). On the other hand, embedded thin-film passives, as shown in Figure 6, address the limitations of discrete passives and have been actively pursued for miniaturizing RF modules for more than two decades [8] [9-12] but still suffer from large thicknesses, tolerance, yield, testability and overall manufacturability.

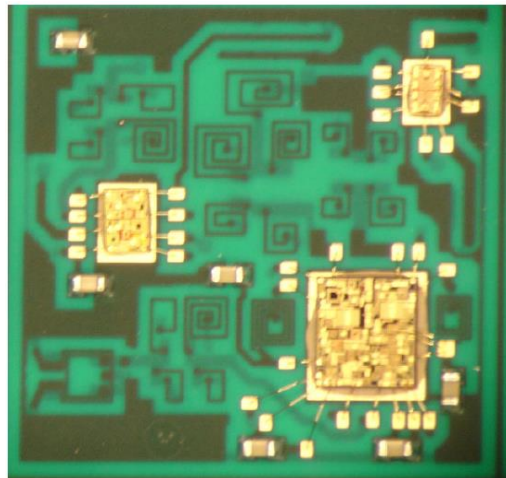


**Figure 6:** RF Module with embedded thin-film passives [8].

To develop ultra-miniaturized and high-performance embedded passives that match the size and performance of current LTCC passive components, new design approaches are required

for thin-film passives; to effectively utilize ultra-thin and dimensionally-stable substrate materials with high dielectric constant and low loss.

### Integrated EMI shielding

In traditional modules with individually- packaged components, the component density is limited by the component sizes and tolerance of the pick-and-place assembly processes. Hence the electromagnetic interference (EMI) between components could be mitigated by spatial separation between the components. However, in miniaturized modules with high-density of component integration of ultra-thin actives and passives, it is essential to address the electromagnetic interference (EMI) issues between components within the package that are spaced with distances of 50-200 microns from each other. Additionally, unlike traditional modules where each package component featured an EMI shield [13], miniaturized multicomponent packages demand integrated shielding approaches to achieve sufficient signal isolation within a package. To meet the requirements for highly-integrated and miniaturized RF modules, conceptually illustrated in Figure 1b, new strategies are required to miniaturize the passive components as thin-films, integrate them into ultra-high densities with least interconnection parasitics, while also mitigating the EMI issues.

A number of methods are being employed to address the electromagnetic interference between components at different levels of a system hierarchy. Traditional EM shields were developed to comply with FCC regulations on radio frequency interference – to protect electrical systems from external EM interference and to prevent outward radiation. In traditional modules, the components were packaged individually and assembled on a printed circuit board [14]. In such cases, EM isolation between components was predominantly achieved through spatial isolation, and metallic cans were employed to shield one sub-module from another [15], as depicted in Figure 7.

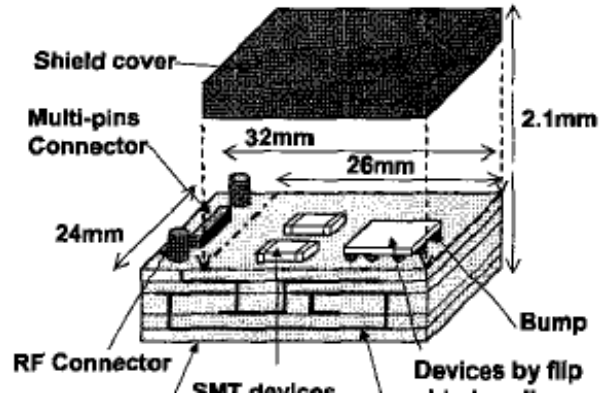


Figure 7: Metallic cans employed in EMI shielding [15].

Since metallic cans were thick and could also detune [16] the devices enclosed, conformal coating approaches were adopted [17] as shown in Figure 8. Alternatively, metallic shielding inside the over-mold have also been developed [18], as depicted in Figure 9.

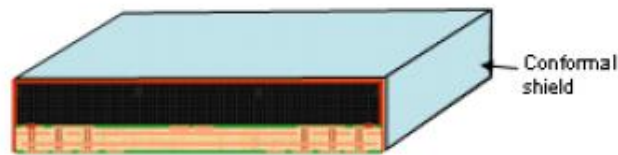


Figure 8: Conformally coated metallic shield for over-mold packages [17].

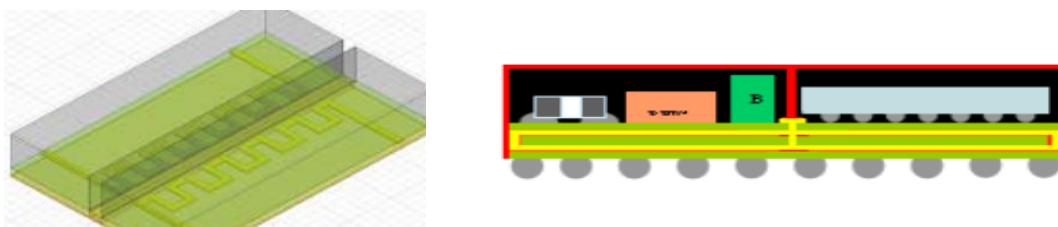


Figure 9: Compartment-based over-mold shielding [18].

In addition, via-based shield approaches have been explored [19-22] to isolate components in a package or board. An example of via-array based shielding is shown in Figure 10.

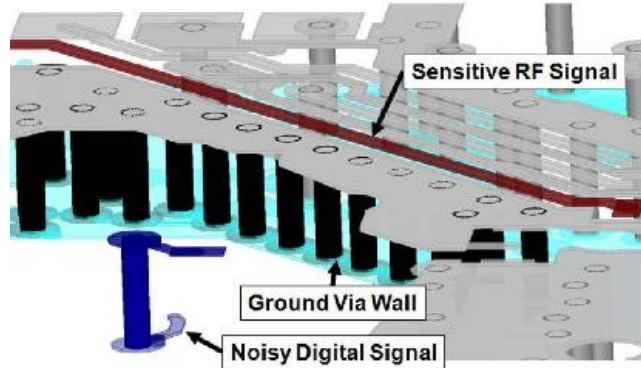


Figure 10: Via-array based shield structures.

However, the higher component-density, enabled by the increasing miniaturization of components, necessitates the development of miniaturized and highly effective shielding techniques to address the increased EM interference between components in a single package.

### Objectives of this Research

The objectives of this research are to model, design, fabricate, and characterize ultra-miniaturized RF components and wireless local area network (WLAN) modules with integrated diplexer and component-level EMI shields with potential lower cost than other approaches

Table 1

Parameters and Targets of the proposed research

#	Parameter	Prior Work	Proposed	Challenges
1	Diplexer size	1 mm x 0.5 mm x 0.5mm	1mm x 0.5 mm x 0.15 mm <b>&gt;3x volume reduction</b>	Selectivity better with more LC, but increases size and loss.
2	EMI isolation	>30 dB at >3mm separation (package level)	>30 dB at <1mm separation (component level ) <b>&gt;2x volume reduction and better performance</b>	Isolation is more effective with thicker shields which are far from interference source.
3	Module size	3.5mm x 3mm x 0.85 mm	2.5 mm x 2 mm x 0.3 mm <b>&gt;5x Miniaturization</b>	2D integration. → Large Area. Large component thicknesses EM interference with proximity.

As shown in the first row of Table I, the goals for passive miniaturization are to achieve the performance specifications of commercial ceramic chip-type RF passives in highly miniaturized form-factors. As described in the second row of Table I, the goal of EMI shielding is to integrate component-level electromagnetic (EM) isolation with the same performance as a package-level shielding. The target for RF module miniaturization is to achieve more than 3x volume miniaturization, as presented in the third row of Table I.

## **Research Challenges**

### Diplexer Miniaturization

The challenge in the design and fabrication of passives is to achieve miniaturization with simultaneous performance-enhancement. The key performance metrics are pass-band insertion loss, Q-factor, and out-of-band rejection. Electrical design of passives is driven by trade-offs between size, performance and cost. Passive designs based on lumped elements (individual inductors and capacitors) with high filter order (more than 2) are predominantly favored for passives in LTE and WLAN modules. Such passives have good selectivity but occupy more volume (area and thickness) because of the large number of inductors and capacitors required. Further, the size of each inductor and capacitor is limited by the inductance and capacitance densities supported by the substrate technology. Increasing the number of components to improve the component density also increases the insertion loss as illustrated in Fig. 2a. Moreover, thin-film embedded components face limitations such as achieving good tolerance, testability, reworkability and defect-driven yield losses.

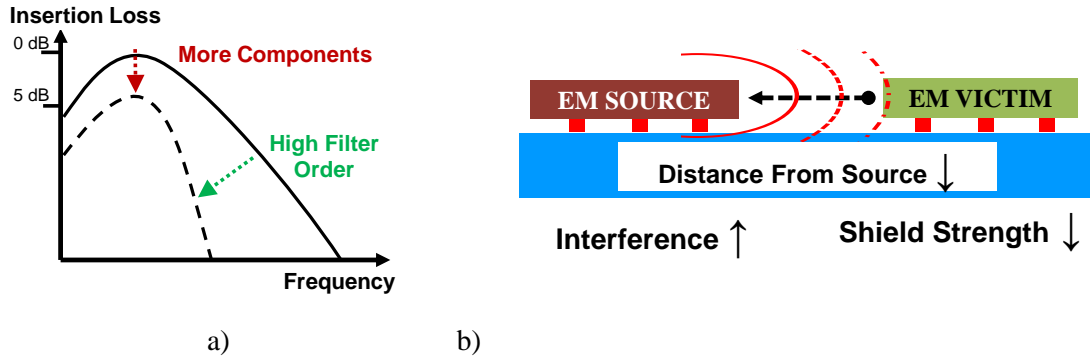


**Figure 11:** Challenges with RF module miniaturization: a) Trade-off between performance, loss and size; b) EM interference vs. proximity.

### Integrated EMI shielding

Any miniaturized RF module requires several active and passive components placed in close proximity to one another. All of them radiate electromagnetic fields of different strengths and frequencies. The region around an EM source is divided into near-field (distance  $< \lambda/2\pi$ ) and far-field (distance  $> \lambda/2\pi$ ). The typical distance of separation between components in RF modules is around 2-6 mm. This indicates that the components lie in the near-field region of each other for frequencies less than 8 GHz. Therefore, all components require electromagnetic interference (EMI) shields to suppress any radiation arising from components, and also to prevent external interference from entering into the components. Moreover, in the near field region, the electric and magnetic fields are decoupled and the magnetic fields have lower wave impedance and hence are very difficult to be shielded. State-of-the art EMI shields provide sufficient isolation between packages on a board. However, when integrating multiple components in a single package, there is a need to isolate components from one another within the package, and the thickness of the shield becomes a limiting factor in the miniaturization. The effectiveness of EMI shields reduces with decreasing shield thickness. Further, as indicated in Figure 2b, with increasing proximity between components, the EM interference increases and the shielding effectiveness decreases. Hence careful shield design and material selection is required for such component-level EMI shielding.

## Module miniaturization

High-performance and cost-effective module integration for RF sub-systems require fully-integrated front-end components for each frequency band including multimode PA, duplexers, RF switches and matching networks. This is indicated in Figure 12 based on the trend from discrete front-end modules to integration for each band.

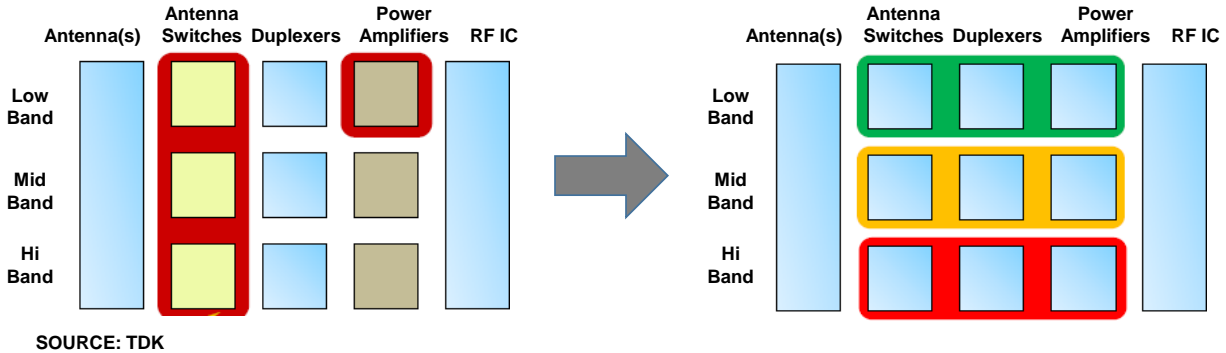


**Figure 12:** RF Front-end module integration trend (Source: Arjun Ravindran, TDK-EPCOS).

Such an integration requires miniaturized passives such as diplexers and filters, integrated with high-power components such as power amplifiers (PA), which are a critical source of EM radiation. Hence, the key challenges in RF module development include design of miniaturized passives integrated with component-level EM shielding.

### **Approach to RF module integration with thin passives and EMI Shields**

#### 3D IPAC RF module Concept

To integrate multiple heterogeneous components, an innovative 3D IPAC (Integrated Passives with Active Components) strategy is being pioneered by GT-PRC to achieve unparalleled miniaturization and performance enhancement [3]. The 3D IPAC concept, illustrated in Figure 3, consists a) of an ultrathin substrate ~ 30-100 microns in thickness, b) made of glass with ultra-low electrical loss, c) with ultra-short interconnection length between actives and passives enabled by through-package-vias (TPVs) for double-sided assembly of

active and passive components separated by only about 50-100 microns of interconnect length, d) embedded and surface-assembled ultra-thin actives and passives, e) using ultra-short and low-temperature Cu-Cu interconnections, f) integrated thermal and EMI shielding structures.

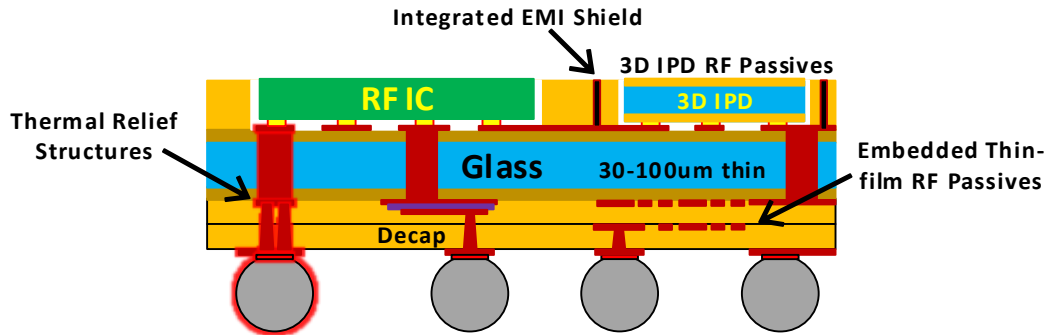


**Figure 13:** 3D IPAC approach for miniaturization, performance and cost.

### Diplexer miniaturization

The volume miniaturization of passives is achieved by developing in-substrate embedded passives or through separate, testable and yieldable ultra-thin glass substrates with through-vias and double-side thin-film passive components, referred to as 3D IPDs, as shown in Figure 13. Glass being a dimensionally stable material with excellent surface finish, just like silicon, enables fabrication of passives with fine features with good accuracy. Further, employing ultra-thin build-up polymers with low loss and high permittivity facilitates miniaturization of passives without compromising on performance. In this research, a unique filter layout is developed that best utilizes the benefits of such substrate materials. A semi-lumped passive structure combining individual inductors and capacitors is proposed and developed. Such a structure increases the volume utilization by eliminating the need for spatial isolation between inductors and capacitors as in a traditional lumped element design.

### Integrated EMI shielding

The high-density integration of components enabled by the 3D IPAC concept requires integrated electromagnetic shielding between the components. To achieve component-level EMI

shielding, metallized trenches are fabricated around the required components through- precisely- formed and metallized cavities in the build-up layers. Such EMI shield trenches offer good lateral isolation between different radiating elements as they have no discontinuity in the lateral direction. Since the metal thickness in these trenches is limited to a few microns, careful analysis is required for selecting the shield materials and to determine the shield effectiveness of these trenches.

#### Module miniaturization:

The 3D IPAC concept can be perceived as the next step in module evolution from ceramic to organic to silicon substrates, towards improved performance, miniaturization and cost. The TPVs enable double-side integration of components, thus reducing the X-Y footprint of the modules at least by half. Further, the ability to embed or integrate the active and passive devices with high precision reduces the interconnect length between actives and passives. Glass is as an ideal material for passive realization [5] because it combines the benefits of ceramics for ultra-low loss, and organic packages for large-area and low-cost processing, and silicon for high-density and lithographic precision. Polymer build-up dielectrics with low loss (loss tangent  $< 0.005$ ) and high dielectric constant onto these thin glass substrates enable high capacitance and inductance densities with high Q-factor. Fine-pitch through-via formation using low-cost substrate processing tools and processes such as laser vias and double-side wet metallization techniques will be utilized for interconnecting the components on both sides [23].

## Research Tasks

Three group of research tasks are proposed, to address the challenges, and to accomplish the objectives specified using Table , Table , and Table I. The tasks along with their subtasks are detailed below.

### Miniaturization of WLAN Diplexer

Table 2

Parameters and Targets for WLAN Diplexers

Parameter	Goal
Size	1mm x 0.5mm x 0.15 mm
Frequency	2-5GHz (WLAN)
Insertion Loss of filter	0.5 -1 dB
Out-of-band Rejection	>15dB

- a. **Modeling and design of novel filters:** Propose a novel filter layout structure, extract its equivalent circuit using full-wave EM simulation and tune the structure to achieve the target filter characteristics.
- b. **Fabrication and characterization of the filters:** Fabricate and characterize the designed filters, and correlate the measured performance with simulations.
- c. **Design and demonstration of WLAN 3D IPD diplexer:** Model and design a WLAN diplexer based on the novel filter concept to match the performance of commercial components. The 3D IPDs are then fabricated and characterized to compare their performance against that of commercial components.

### Model, design and fabricate component-level EMI shielding

Table 3

Parameters and Targets for EMI shielding

Parameter	Goal
EMI Shielding	30 – 60 dB
Frequency	1-20 GHz

<b>Distance</b>	<b>&lt; 100 <math>\mu\text{m}</math></b>
<b>Integrated Shield thickness</b>	<b>&lt; 100 <math>\mu\text{m}</math></b>

- d. Modeling of EM radiation in RF modules:** Model the electromagnetic propagation and interference between different passive elements in a typical RF module using electromagnetic simulations. From these simulations, develop guidelines for the placement and orientation of these elements in miniaturized RF modules.
- e. Analytical modeling – Material and multi-layer stack-up design:** Study the shield effectiveness of different materials and stack-ups using analytical modeling.
- f. Modeling and design of component-level EMI shields:** Propose component-level shield structure and study its shield effectiveness through 3D EM simulations.
- g. Fabrication and characterization of EMI shields:** Demonstrate the effectiveness of the proposed shield structure through fabrication and characterization.

Design and Demonstration of ultra-miniaturized 3D RF modules

**Table I**  
**Parameters and Targets for RF Modules**

<b>Parameter</b>	<b>Goal</b>
<b>Number of Dies</b>	<b>2-3</b>
<b>Frequency</b>	<b>2-5GHz (WLAN)</b>
<b>Passives</b>	<b>Diplexer Power Caps (SMT)</b>

The final task is to model, design and demonstrate a 3D IPAC RF module containing WLAN actives, miniaturized embedded passives and integrated component-level EMI shielding. This is proposed to be carried out in (a) organic substrates with traditional passives, but without EMI shielding, followed by (b) glass substrate with miniaturized passives and integrated EM shielding.

## **CHAPTER 2**

### **LITERATURE SURVEY**

Advances in RF module technologies are primarily enabled by innovations in high-performance actives and passives, and integrating these with least electromagnetic interference (EMI). This chapter reviews three categories of these innovations that are relevant to the proposed research: a) miniaturization of passives using filters and diplexers as examples, b) EMI shielding, and c) passive and active integration into modules. The first part of this chapter describes the evolution of WLAN RF filters and diplexers. The second part of the chapter presents the recent progress in the study of electromagnetic coupling between components, and the development of shielding materials and structures. The last part describes the trends in high-density integration of active and passive components in miniaturized RF modules, and the advantages of glass as a substrate material and 3D IPAC as module integration.

#### **Passive Miniaturization**

A typical WLAN RF module comprises several passives such as matching networks, filters, diplexers, baluns, transmission lines and antennas. This section reviews miniaturization of passives using filters and diplexers as examples. A filter is a device that is used to selectively pass or stop electrical signals of a specific band of frequencies. Depending on the band of frequencies they pass, they are classified as low-pass filters, high-pass filters or band-pass filters. A diplexer is a combination of two filters such that an incoming signal is directed to one of the two output ports depending on its frequency. Since filters are the basis for developing diplexers, studying various filter technologies sufficiently encompasses the trend of diplexers.

Filters operating in the frequencies of 1GHz -10GHz are predominantly either electroacoustic type or planar-type. Electroacoustic filters such as surface-acoustic wave (SAW) and bulk acoustic wave (BAW) filters use a piezo material and are available as surface-mounted

components. Planar filters can be implemented either as embedded metal patterns in a multi-layered module substrate, or as separately-manufactured surface-mounted components. They are of two types: 1) Distributed element filters, implemented using transmission lines, and 2) Lumped element filters, realized as individual inductor and capacitors.

### Filters with Distributed-elements (Transmission Lines)

Traditionally, in-substrate filters and resonators were realized using transmission line elements that utilized edge-coupling and end-coupling [9, 24]. As illustrated in Figure 14, second-order WLAN filters with more than 30dB out-of-band rejection have been developed, with dimensions 2.6mm x 2.6mm x 0.5mm on a LTCC (low temperature co-fired ceramic) substrate [9]. However, since such coupling is relatively small, broadside-coupled striplines, such as the one shown Figure 15 were also employed [9] [25].

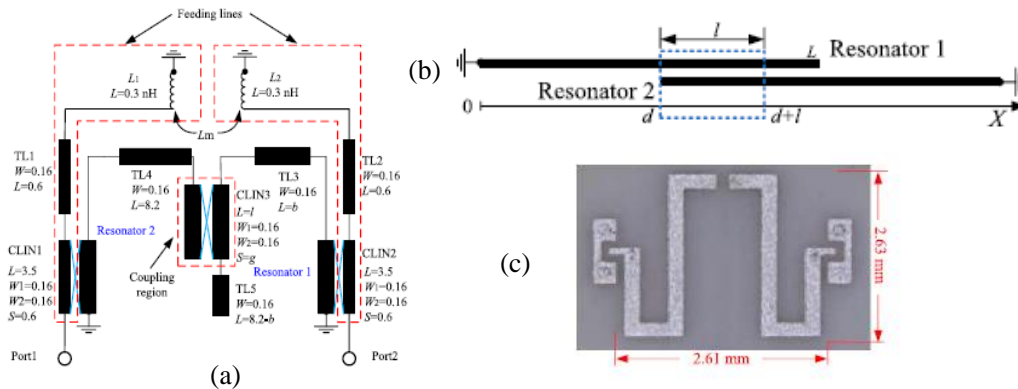


**Figure 14:** Band-pass filters designs using transmission line elements; a) schematic, b) resonator configuration, c) fabricated substrate top view [9].

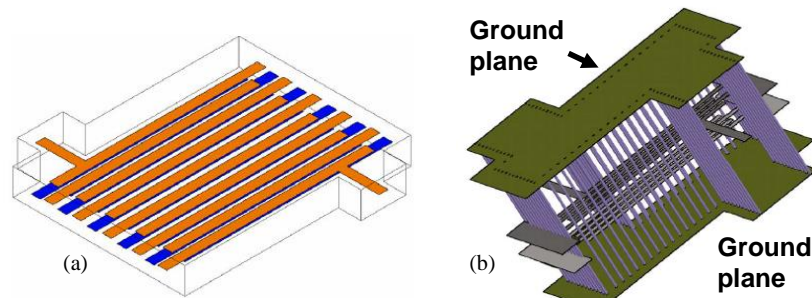


**Figure 15:** Band-pass filters using broad-side coupled striplines on LTCC substrates; a) Layout of filter, b) 3-D view of substrate with ground planes [25].

### Lumped element filters

Although transmission line-based filters exhibit sharp cutoff response, one major drawback is that their size is larger because the dimensions of the elements have to be comparable to the electromagnetic wavelength at the frequency of operation. To reduce the size of such components, filters were developed based on lumped-element passives. These lumped elements were realized as thin-films on multi-layer LTCC and organic substrates [11, 26, 27]. Such structures have been developed and optimized to achieve low-loss filter performance, with smaller volume occupancy compared to transmission-line based filters [27].

### *Filters on LTCC substrates*

Low-temperature co-fired ceramic (LTCC) technology was pioneered by Prof. Rao Tummala and his team at IBM starting in 1975. LTCC technology uses glass-ceramic or ‘glass + ceramic’ substrates to fabricate complex multi-layered 3D circuits, and are still widely employed for high-Q RF passives because glass-ceramics exhibit low signal losses, mechanical and electrical properties that are stable despite changes in frequency, temperature and humidity; good hermeticity, low CTE and high reliability, and easy processability with copper wiring. Filter designs on LTCC substrates occupy a large number of layers, sometime up to 15, with glass-ceramic substrates of permittivity ranging from 5-50 (Figure 16). Typical second-order

filter designs utilize two resonators connected using impedance inverters to each other and to the input and output [27], as illustrated in Figure 17.

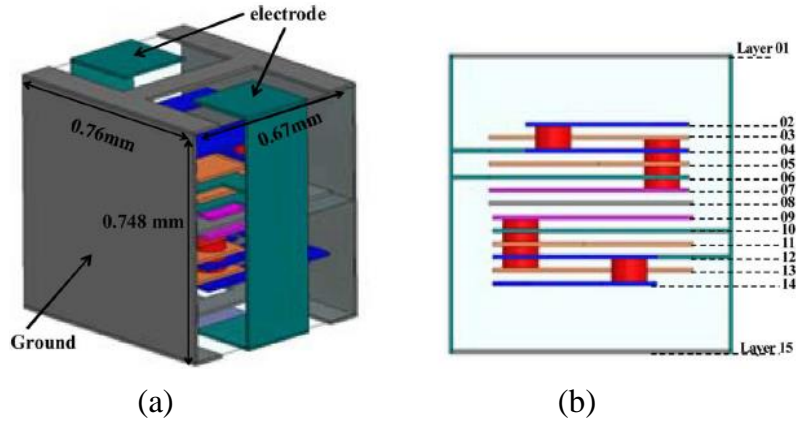


**Figure 16:** Compact band-pass filter: a) component design, and b) substrate stack-up [27].

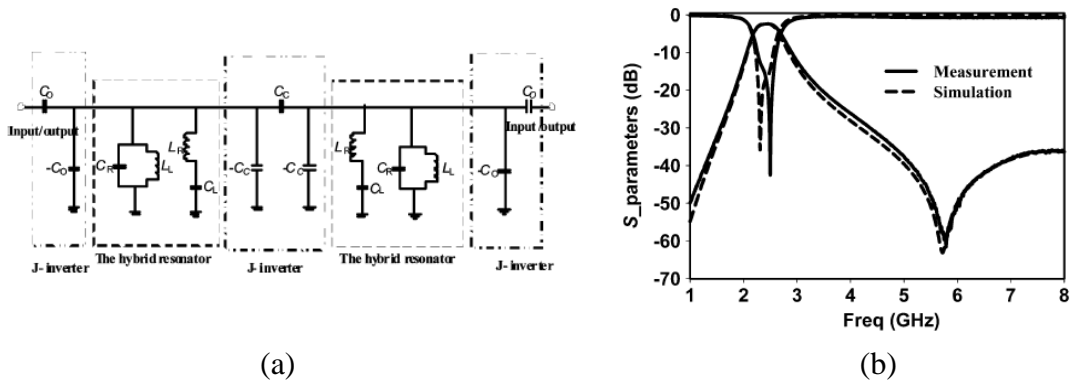


**Figure 17:** (a) Equivalent circuit, and (b) frequency response, of a LTCC-based filter [27].

### *Filters on organic substrates*

The need to reduce the thickness, cost, and number of layers for passive components, propelled the development of band-pass filters using lumped elements on multi-layer organic substrates [11]. The layout and cross-section of such a filter is shown in Figure 18. Filters on organic substrates typically occupy less than 8 metal layers. To reduce the size of filters without

compromising on the performance, lower-order filters can be designed with specific transmission zeros to improve the stop-band rejection, as illustrated in Figure 19.

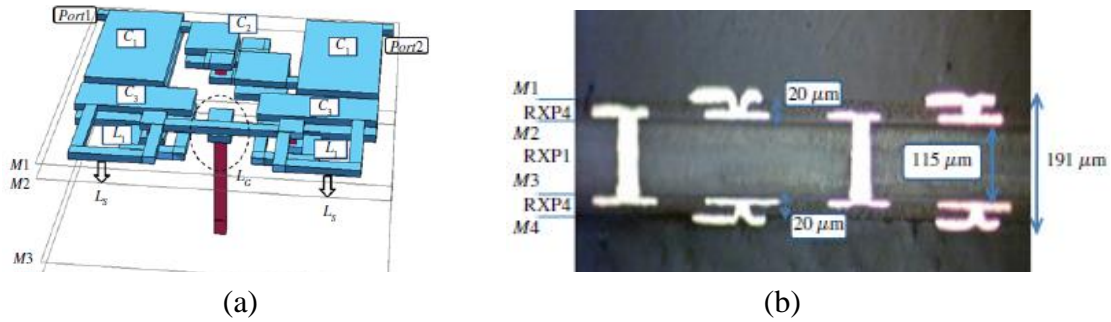


**Figure 18:** (a) WLAN band-pass filters using lumped elements, (b) on organic substrates. [11].

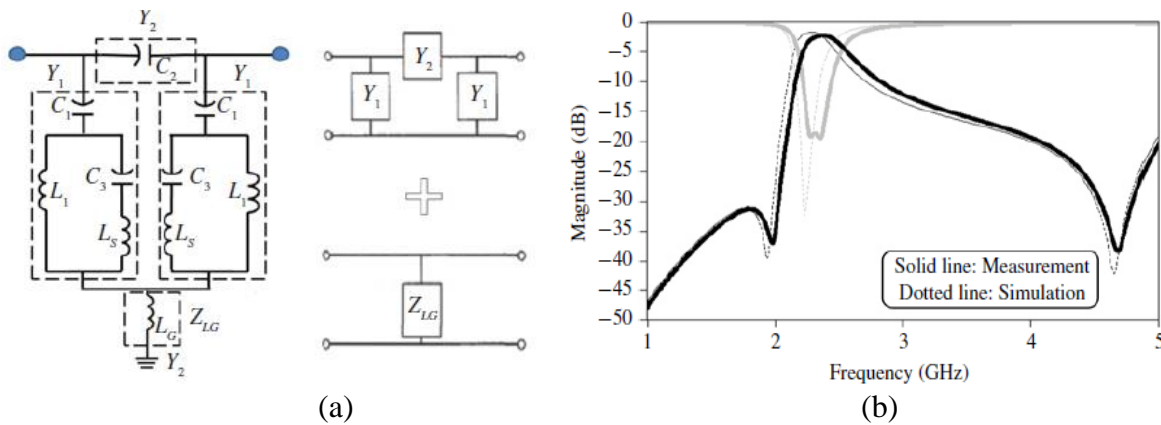


**Figure 19:** Modified low-order filter with transmission zeros, on organic substrate: (a) schematic, (b) response. [11].

### Filters on glass substrates

One major limitation in implementing RF passives on multi-layer organic substrates lies in achieving good alignment between patterns on multiple layers. This limitation arises due to the dimensional instability of organic materials. Driven by the need for stable, smaller, thinner, high-performance and low-cost components, there has been an evolution in passive component technology from LTCC and organics, eventually to glass substrates. Initially, compact lumped-

element-based band-pass filters were developed with single-side processed glass wafer-based IPD technology [28] using novel transformer-based coupled resonator designs as shown in Figure 20.

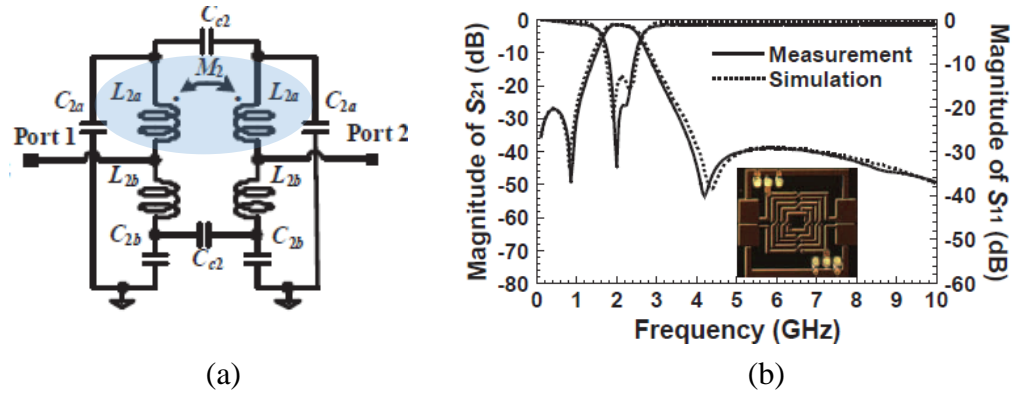


**Figure 20:** WLAN Band-pass filters on glass wafers using single-side processing: (a) schematic, (b) response. [28].

Since the size of wafers limits the device cost and throughput, ultra-thin panel-based glass substrates with through-vias is being pioneered by GT-PRC [12]. The presence of through package vias (TPVs) helps in miniaturization by enabling double-side integration of planar passives and surface-mount components on glass substrates. The TPVs have also been used as inductance elements to further miniaturize the filters.

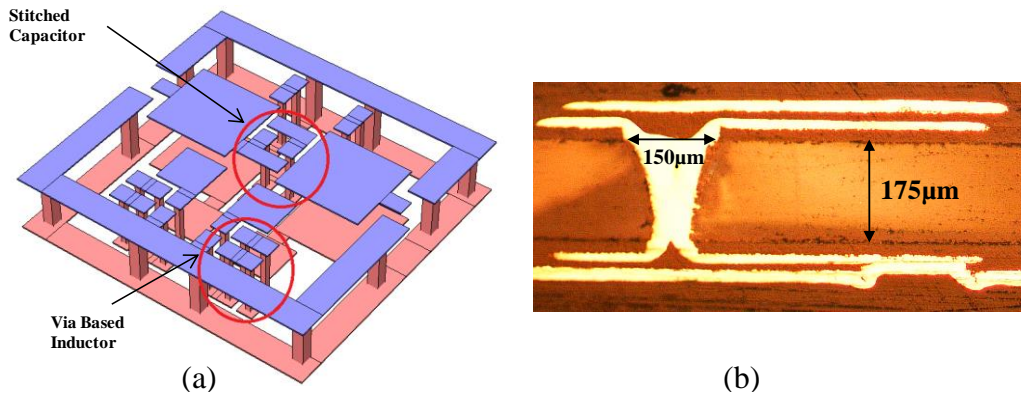


**Figure 21:** Band-pass filters on thin glass with TPVs: (a) Layout view, (b) cross-section of fabricated sample [12].

## EMI Shielding

Miniaturized multifunctional systems house several active and passive components in close proximity. All of them radiate electromagnetic (EM) fields of different strengths and frequencies. The region around an EM source is divided into near-field (distance  $< \lambda/2\pi$ ) and far-field (distance  $> \lambda/2\pi$ ). Considering that the typical distance of separation between components is around 2-6 mm, it can be concluded that all the components lie in the near-field region of each other even up to 8GHz . Additionally, the components also lie in the far-field region of external EM interference arising outside the package. Therefore, all components require electromagnetic interference (EMI) shields to prevent external interference from entering into the components, and also to suppress any radiation arising from the component. This section reviews the study of electromagnetic coupling between different package components. It, then, presents different approaches for electromagnetic shields.

### Electromagnetic Coupling between components

The typical methodology adopted in the EMI analysis of packages involves splitting a complex EM interference model into smaller models comprising the source, the path, and the victim [29]. Using such an approach, the radiation source, the mechanism of propagation, and the interference into a victim, can be decoupled from one another and analyzed individually. It is also critical to study the different sources of radiation in system-on-package (SOP) substrates from the point of view of RF, and digital signal and power integrity, as illustrated in Figure 22. To comprehensively address all these elements, this section is divided into three parts: a) Modeling EM radiation sources, b) EM coupling mechanisms, and c) Effects of EM interference.

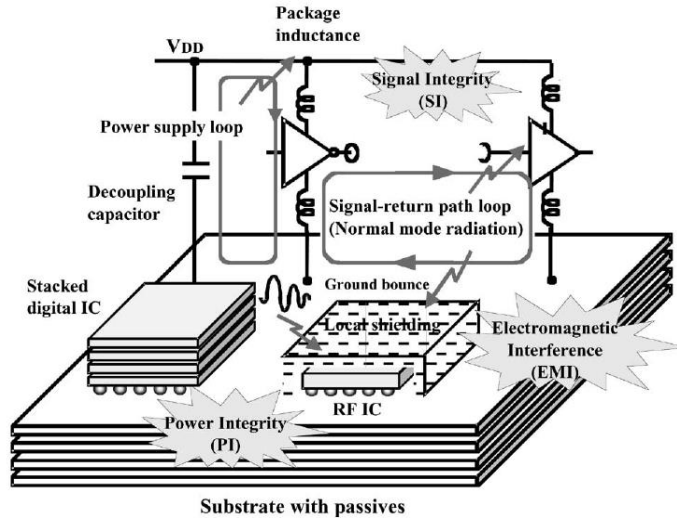


**Figure 22:** EM interference between various components in a SOP substrate.

### *Modeling EM radiation sources*

To model the radiation source at the package level, analytical models using an array of dipoles have been developed [30]. Additionally, the radiation from other sources such as chip-inductors, were modeled for different signal [31-33] and power levels [32]. A 3D inductor model and its current density on a solid plane shield and patterned plane shield are shown in Figure 23. It was concluded that, while on the one hand, patterned shields reduced the substrate losses without degrading the Q-factor of the inductors, the presence of patterned shields significantly increased the radiation above the inductor [32].

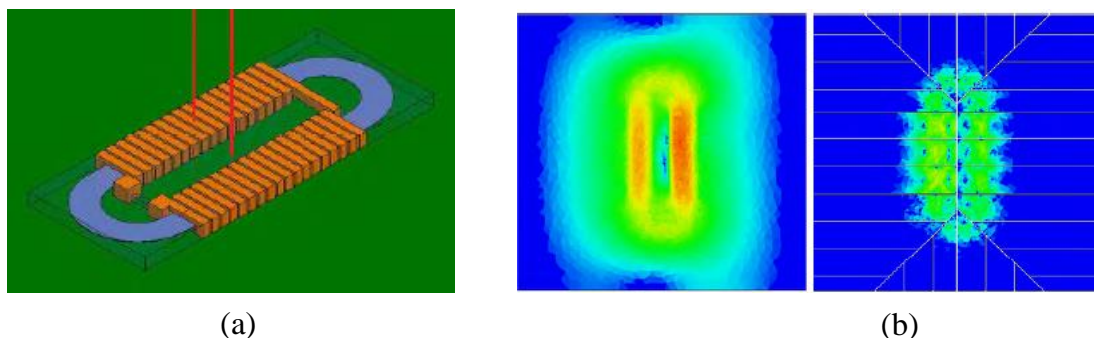


**Figure 23:** (a) 3D model of on-chip inductor, and (b) current density on the surface for various shields at 20MHz.

## EM coupling mechanisms

EM coupling mechanisms have been studied between components on a single substrate or between substrates. The coupling from radiated electromagnetic fields between components and other elements have been studied [19, 30, 31, 34-36] at the package level. One such schematic is depicted in Figure 24.

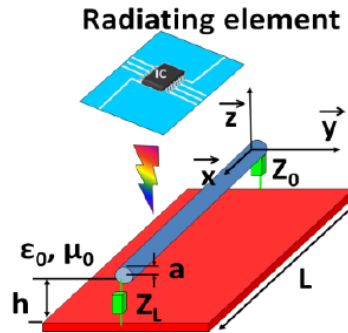


**Figure 24:** Coupling between a component and a transmission line.

In a study of the electromagnetic interference between LNA and PA CMOS dies, it was deduced through experiments that, when the dies are in a single-chip configuration (sharing a common silicon substrate), the primary source of EM interference was the silicon substrate coupling [37]. Further, when the dies are singulated to eliminate the effect of substrate coupling, the dominant interference phenomenon was magnetic coupling between on-chip inductors. It was also determined that at 5GHz, the total EM isolation degrades to lower than -50dB when two dies (LNA and PA) are spaced out by less than 0.4mm.

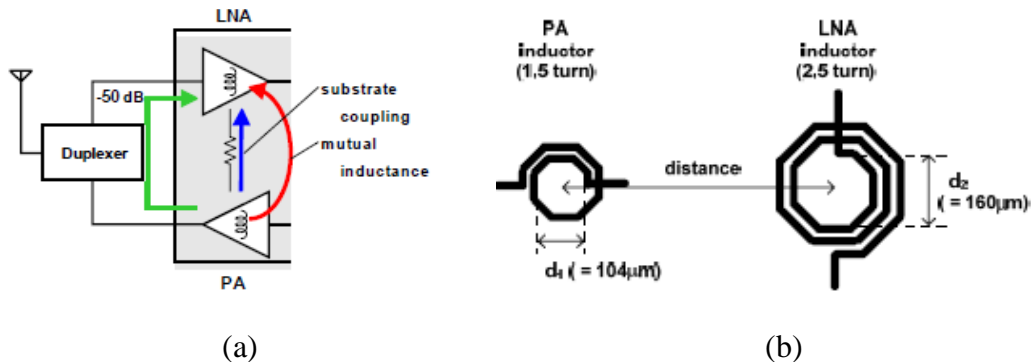


**Figure 25:** Coupling between PA and LNA dies: a) system-level schematic, (b) component-level schematic.

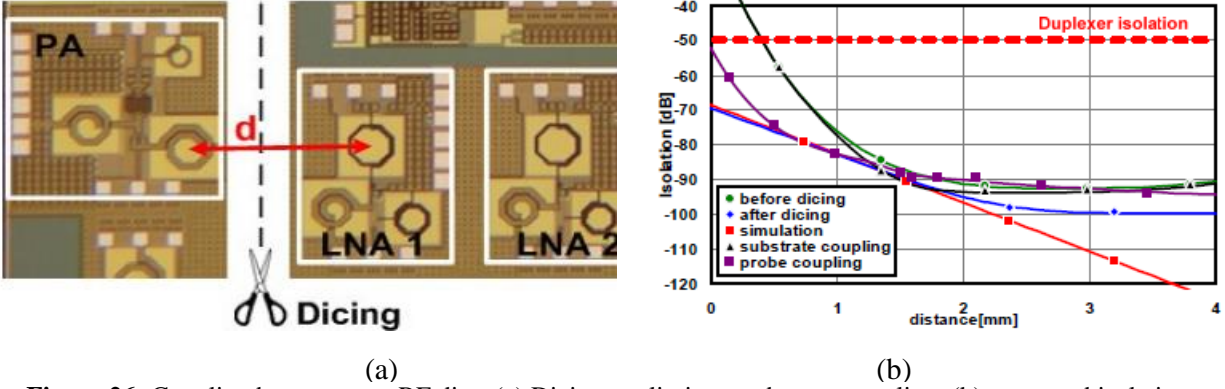


**Figure 26:** Coupling between two RF dies: (a) Dicing to eliminate substrate coupling, (b) measured isolation.

*Effects of EM interference*

The effect of EM coupling on the operation of a power amplifier die was modeled [38] [31]. Results suggest that a noise coupling of strength 50V/m through a slot length of 65mm, [38] can degrade the gain of the PA by up to 10dB as shown in Figure 27.

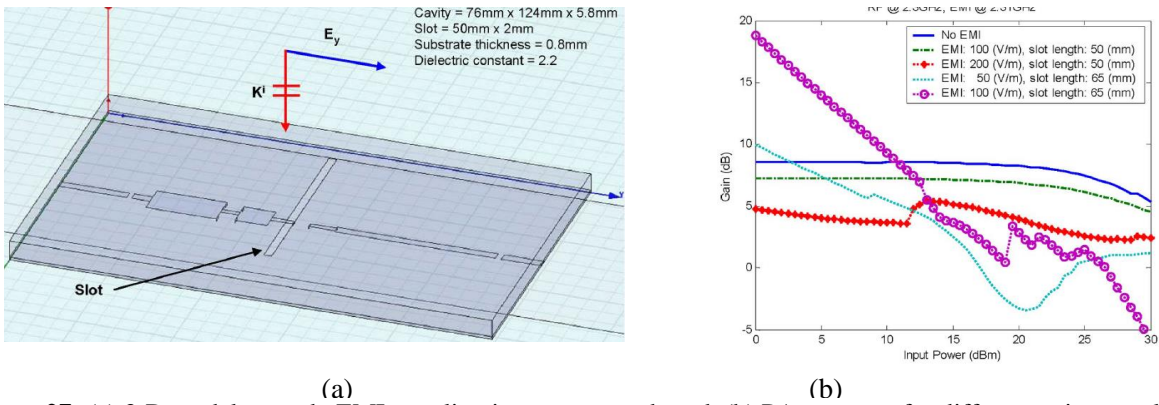


**Figure 27:** (a) 3-D model to study EMI coupling into trace on a board, (b) PA response for different noise coupling.

Further, the impact of digital noise coupling on the RF performance in mixed signal systems has been considered [19], and the effect of grounded via walls as a shield in such systems has been studied, as shown in Figure 28. The resulting EMI isolation from coupling was observed to be improved by more than -40dB, as depicted in Figure 29.

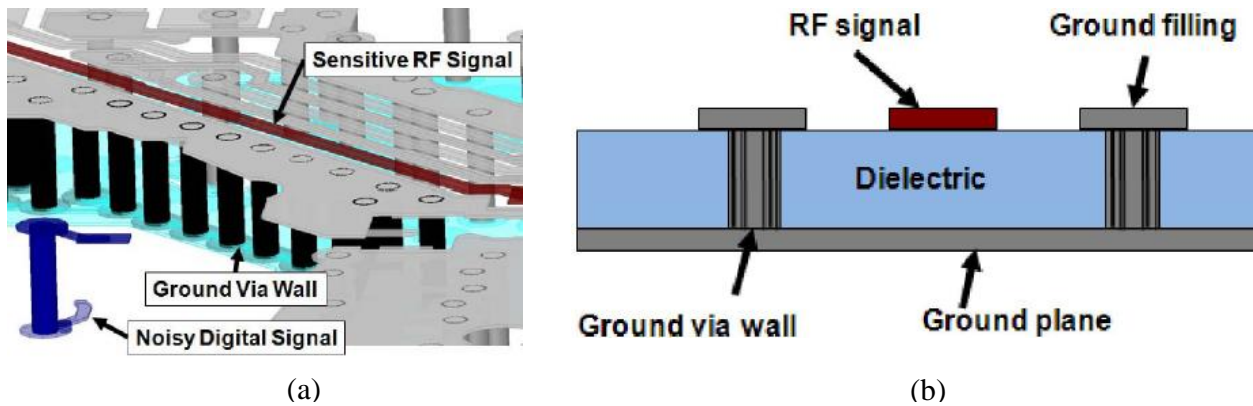


**Figure 28:** (a) Coupling between digital and RF signals in mixed-signal systems, (b) grounded via wall as a shield.

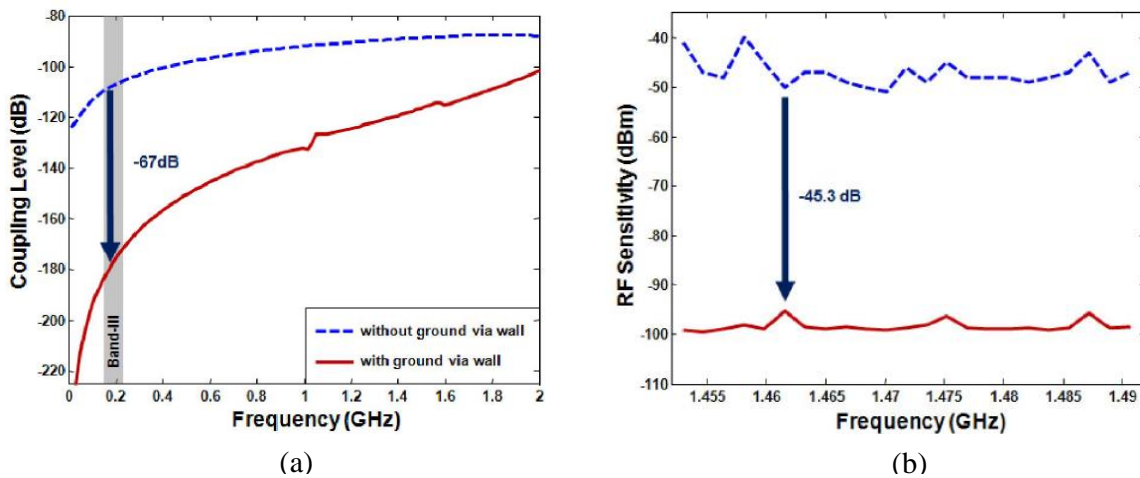


**Figure 29:** (a) Digital-RF Coupling and, (b) RF sensitivity improved through shield design techniques.

### EM shielding materials

Traditionally, EMI shielding has been implemented using metals that are inexpensive and can reflect and absorb EMI radiation. Such metals include copper, iron and aluminum [39]. Shielding from magnetic fields necessitated the use of magnetic materials such as nickel and stainless steel because they enable higher impedance compared to nonmagnetic materials. Using such magnetic materials, it is also possible to shield low-frequency magnetic radiation in the near-field by providing a low-reluctance path for the interfering magnetic fields, as shown in Figure 30.

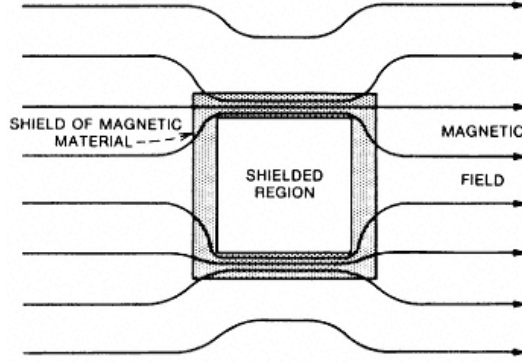
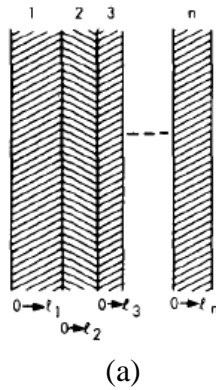


**Figure 30:** Magnetic field shielding by providing a low-reluctance path.

Shielding of magnetic fields using the low reluctance (magnetic resistance) of magnetic materials is necessary since the absorption and reflection losses are very low for near-field magnetic fields. However, for portable electronic systems, the size of the EM shield is constrained. Hence, there is a need for thinner shields that can effectively isolate strong near-field magnetic fields. A number of multi-layered shields, consisting of a combination of magnetic conductors, non-magnetic conductors, and insulators, have been developed. Such shields employ absorption and reflection losses to suppress electric, magnetic, and electromagnetic fields [40]. The shielding effectiveness of multiple metallic and non-metallic shield layers are quantitatively described in Figure 31.



(a)

$$S = -20 \log_{10} |T|$$

$$T = p[(1 - q_1 e^{-2\gamma_1 l_1})(1 - q_2 e^{-2\gamma_2 l_2})]^{-1} e^{-\gamma_1 l_1 - \gamma_2 l_2}$$

$$p = \frac{8\eta_0 \eta_1 \eta_2}{(Z_w + \eta_1)(\eta_1 + \eta_2)(\eta_2 + Z_w)} \quad q_1 = \frac{(\eta_1 - \eta_0)[\eta_1 - Z(l_1)]}{(\eta_1 + \eta_0)[\eta_1 + Z(l_1)]}$$

$$Z(l_1) = \eta_2 \frac{Z_w \cosh \gamma_2 l_2 + \eta_2 \sinh \gamma_2 l_2}{\eta_2 \cosh \gamma_2 l_2 + Z_w \sinh \gamma_2 l_2}, \quad q_2 = \frac{(\eta_2 - \eta_1)(\eta_2 - Z_w)}{(\eta_2 + \eta_1)(\eta_2 + Z_w)}$$

(b)

**Figure 31:** (a) Schematic of multiple layers, (b) equations for H-field shield effectiveness.

To shield electric fields, multi-layer stacks consisting of alternate layers of high-conductivity metals and magnetic metals or alloys have been developed [41]. The primary motivation to develop such layers is to shield the electric fields by trapping the interfering signals in a low-conductivity metallic layer that is sandwiched between two metallic layers having higher conductivity. Such a stack-up is shown in Figure 32. Additionally, a minimum thickness of a metal or alloy to effectively reflect incident EM waves has been identified [41].

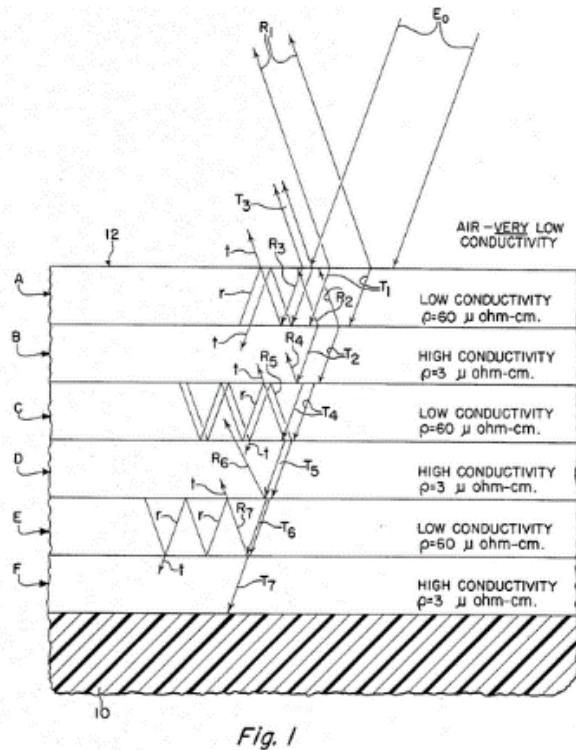


**Figure 32:** Multiple layers of magnetic and non-magnetic layers as EMI shield.

For near-field magnetic shielding in the MHz range, very-thin multi-layer stacks consisting of copper and high-permeability cobalt-niobium-zirconium (CoNbZr) was modeled, and characterized [42]. The multi-layer stack-up is shown in Figure 33, where the easy and hard axes are specified for the ferromagnetic layers. Such an anisotropy enhances permeability and frequency-stability of permeability, and is introduced by depositing magnetic layers in the presence of a strong magnetic field, the direction of which defines the easy axis.

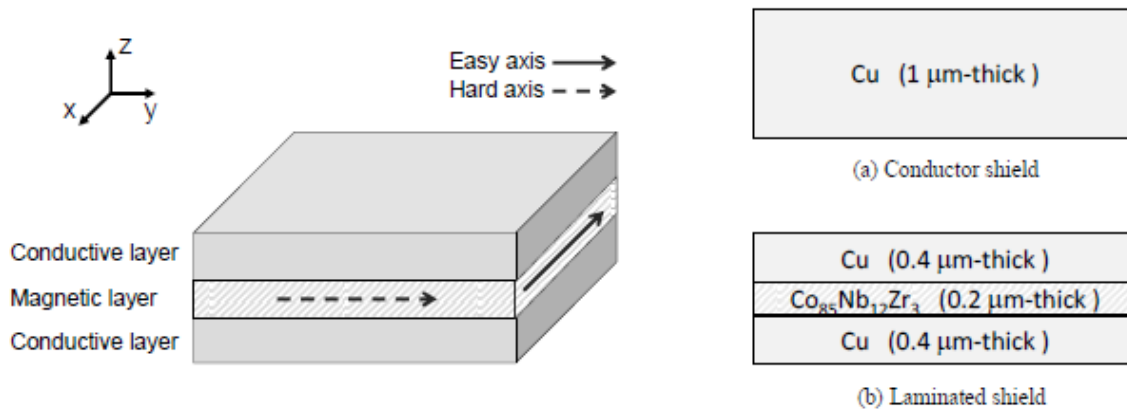


**Figure 33:** Thin multi-layer stack with high shielding effectiveness at frequencies close to the FMR (ferromagnetic resonance) frequency.

An experimental set-up was developed using a microstrip transmission line as the source of EM radiation and a magnetic probe to measure the radiated fields [42]. Good correlation was observed between the shield effectiveness obtained through analytical calculations using the material properties, and the 3-D EM models. The measured results also match the simulations. The experimental setup and the measured response are shown in Figure 34.

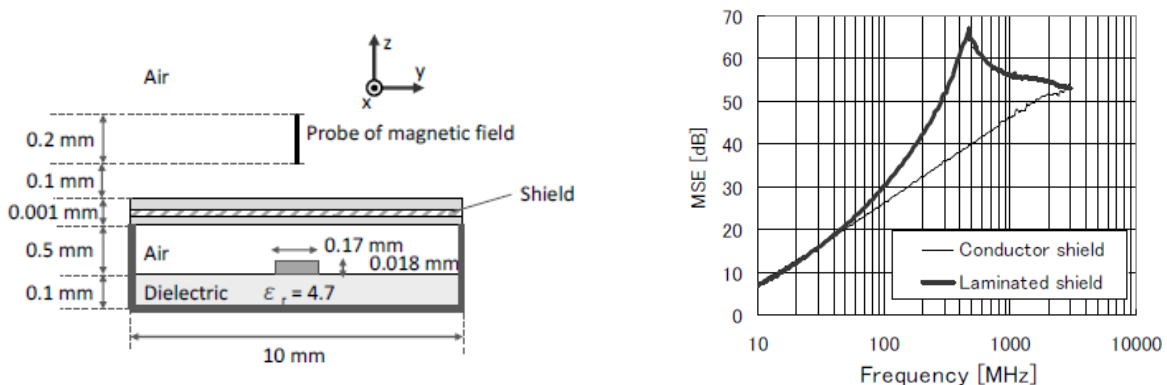


**Figure 34:** (a) 3-D EM and experimental set-up to measure shield effectiveness, (b) measured shielding effectiveness.

To shield near-field magnetic fields at higher frequencies, various metals and alloys have been developed based on electromagnetic shielding capabilities [41, 43]. Multiple layers of nickel-iron of thickness 10nm – 50μm, separated by acrylate, have been developed for shielding in 1-6 GHz [43]. The stack-up for such a multi-layer structure is shown in Figure 35, where the

layers indicated as '305' are the insulators, and the ones marked as '307' are the ferromagnetic layers.

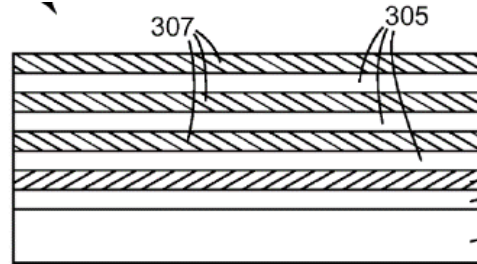


**Figure 35:** Multiple layers of NiFe and insulator used for shielding at high frequencies.

### EM shielding structures

EM shielding is required at different levels of system hierarchy. Traditional EM shielding was catered towards protecting RF devices from external EM interference and to prevent any radiation from the equipment, so as to comply with FCC regulations on electromagnetic interference. When components were large, they were packaged individually and assembled on a printed circuit board [14], as illustrated in Figure 36; where the EM shield is indicated as '58'.

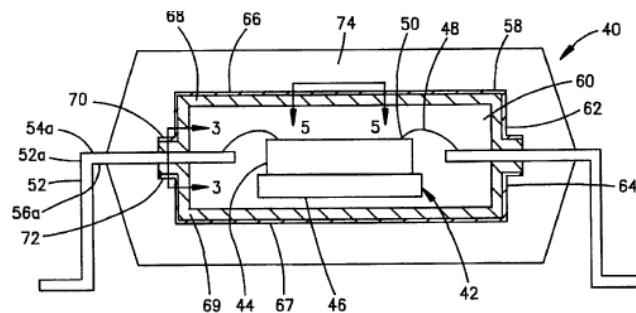


**Figure 36:** Single-component package with EM shield to suppress external interference.

As the size of systems scaled down, the modules needed to be assembled closer to one another. Further, because the individual component packages were not large enough, there was a need to shield one sub-module from another. For this purpose metallic cans were employed [15].

Such a package is shown in Figure 37. In such cases EM isolation between components was primarily achieved through spatial isolation.

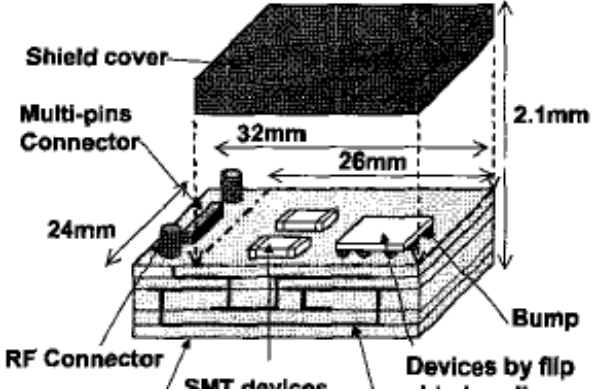


Figure 37: Metallic cans employed in EMI shielding [15].

Since metallic cans were bulky and caused detuning [16] of the devices that it enclosed, conformal coating on the over-mold compound was developed [17, 18]. Such packages are depicted in Figure 8 and Figure 9. Further, to isolate circuits on a die, metallic perforated shield on over-mold have been employed [44]. The die design and the proposed shielding structures are shown in Figure 40.

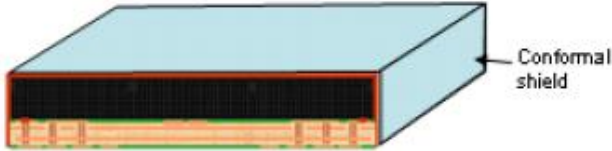


Figure 38: Conformally coated metallic shield for over-mold packages [17].

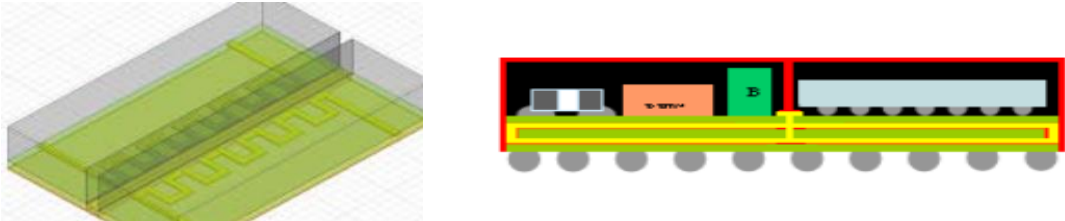
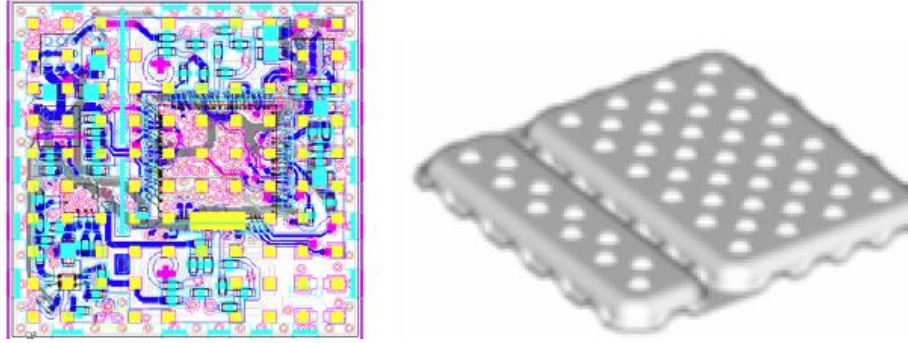
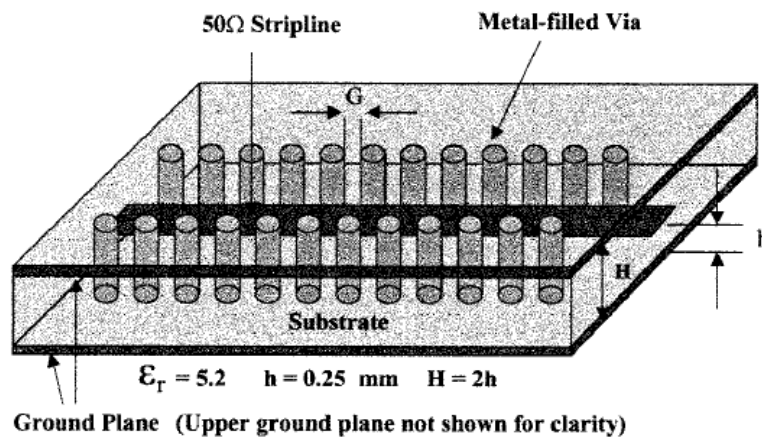


Figure 39: Compartment-based over-mold shielding [18].



**Figure 40:** (a) RF SiP design, and (b) shielding structure.

To shield the interference between other package elements such as transmission lines, via-based shield approaches have been explored [19-21] as shown in Figure 10. Extensive studies have been conducted on the performance of metal-filled vias in isolating striplines and microstrip lines [22]. It was observed that a continuous fence of vias was better than intermittent fence of vias since the latter increased the radiation loss and reflections by perturbing the propagating mode. Additionally, a distance of three times the substrate height was deduced to be the optimal spacing between a via fence and a transmission line. The vias were recommended to be drilled with the least possible spacing between each other. Further, via fences were found to be effective only if the via pads were shorted both on the top and the bottom.



**Figure 41:** Via-array based shield structures.

## RF Module Integration

A front-end RF module comprises of antennas, switch and duplexer banks, in conjunction with low-noise amplifiers and power amplifiers. In addition, several passives such as transmission lines, matching networks, filters, duplexers, shields etc. are necessary to support the active components. The System-on-Package paradigm, pioneered by Prof. Rao Tummala and team at GT-PRC since 1994, enables package-level high-density integration of such heterogeneous system components that are optimized for high performance and low cost [45]. Single-chip integration (or System-on-Chip) solutions are also being developed for partial integration of RF modules [2, 46]. Such an example of WLAN SOC is shown in Figure 42. However, the adaptability of SOC has been limited because of the lower performance of passives and high cost.

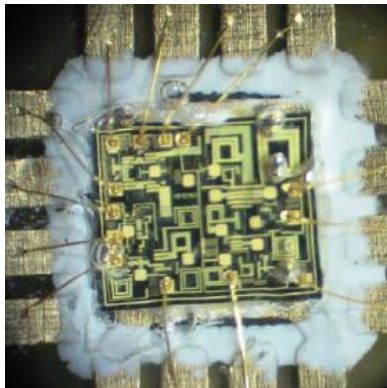


**Figure 42:** Single-chip WLAN 802.11b/g Front End Module [2].

### RF modules on LTCC substrates

Traditionally WLAN RF modules, with integrated high-performance actives and passives, were developed on Low Temperature Co-fired Ceramics (LTCC) substrates [47, 48], as shown in Figure 44. The primary motivation was the superior properties of LTCC such as low dielectric loss, low moisture absorption, high reliability based on the hermetic nature of ceramics, high-temperature stability, and the ability to form complex 3D multi-layered circuits. An example of LTCC-based WLAN modules integrating duplexers with actives is shown in

Figure 43. The LTCC-embedded diplexers were developed using both transmission-line based designs [49] and miniaturized lumped-element designs [46, 50].

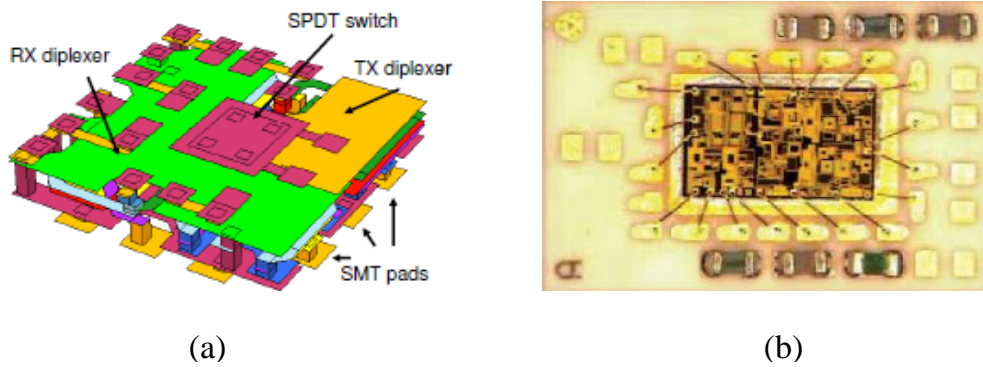


**Figure 43:** RF module with embedded planar diplexers on LTCC substrate: (a) Layout, (b) fabricated sample [46].

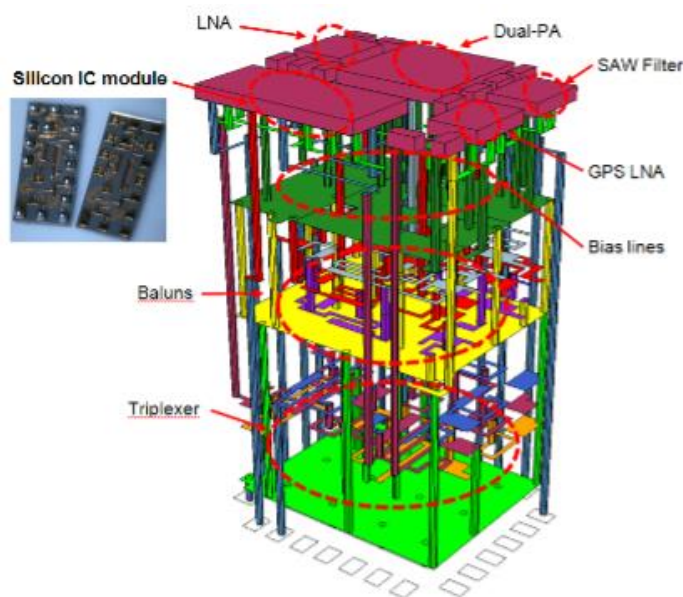


**Figure 44:** 3-D view of a LTCC front end module.

### RF modules on organic substrates

LTCC module technology eventually started to get replaced by organic laminate packaging because of lower cost and higher component densities. The high loss and moisture absorption with traditional organic laminates was addressed through RF integration on liquid crystal polymer (LCP) packages with surface-mounted actives [1], as shown in Figure 45.

Further, to address the requirement for low-profile form-factor and to improve RF performance, embedded die approaches such as chip-first fan-out wafer level packaging (FOWLP) [6, 51], Intel's chip-embedded substrates [8, 52] shown in Figure 46, and semiconductor embedded in substrate (SESUB) [53] have been pursued.

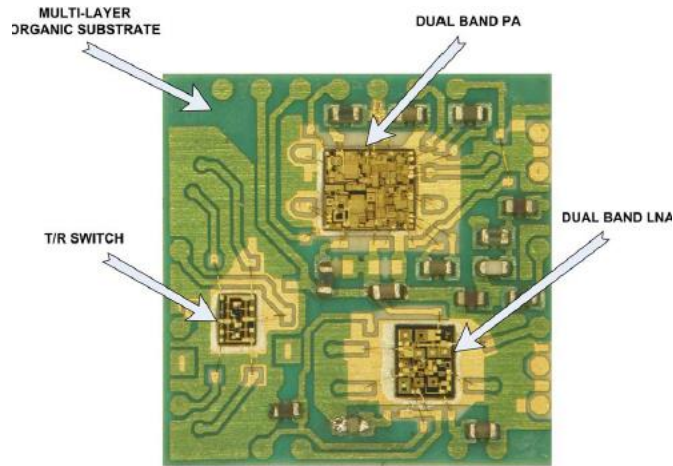


**Figure 45:** WLAN module on LCP substrate with embedded passives and surface mounted actives.

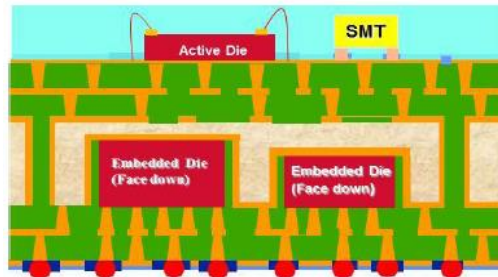


**Figure 46:** Embedded actives substrate for high-density integration.

However, chip-first embedded die approaches face the following barriers: 1) substrate yield loss issues after die embedding, 2) technical challenges associated with embedding multiple heterogeneous components having dissimilar thicknesses, and 3) thermal dissipation issues among densely integrated actives. To mitigate such concerns in miniaturizing high-performance modules, chip-last embedding was pioneered at Georgia Tech Packaging Research

Center (GT-PRC) [54]. A schematic of a substrate with chip-last embedded actives and embedded passives is illustrated in Figure 47.

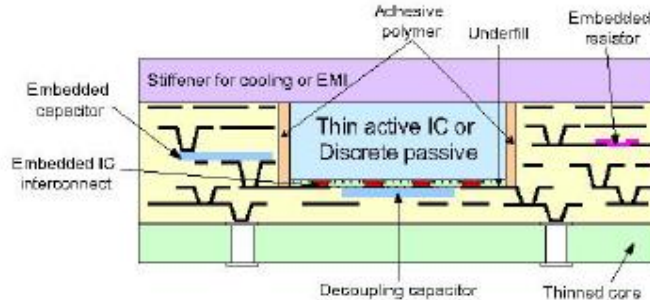


**Figure 47:** Schematic of chip-last embedded active substrate.

Chip-last embedding has six essential advantages over SOC and chip-first approaches: 1) ability to embed multiple heterogeneous actives, minimizing substrate yield-loss issues; 2) intermediate-testability of substrates and components before assembly; 3) shorter interconnections, enabling superior electrical performance; 4) accessibility of the die backside, facilitating improved thermal performance; 5) flexible choice of substrate materials to address the requirements of different components; and 6) low-cost manufacturability for market affordability. Using chip-last SOP, GT-PRC has demonstrated functional WLAN RF modules in ultra-thin six-metal-layer and three-metal-layer organic substrates [4, 55, 56]. A chip-last embedded WLAN RF receiver module with embedded BPF and chip-last embedded LNA dies is shown in Figure 48.

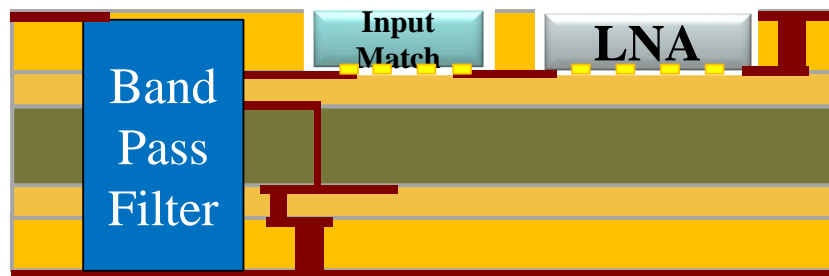


**Figure 48:** WLAN RF receiver module schematic cross-section.

## Glass as substrate material and 3DIPAC for RF modules

Development of ultra-miniaturized RF module requires high-density integration of multiple RF and power components on a package substrates. The desired material properties for RF passive applications include: stable high-frequency electrical performance [57], high resistivity for low signal loss, smooth surface profile for reduced conductor loss and precise lithography, dimensional stability to prevent frequency-shift, and low moisture uptake for high Q-factor. Over the years, RF actives and high-Q RF passives have been integrated at the package-level in ceramics, organic, and silicon substrates. However, each of these materials faces one or more barriers in performance, size, and cost.

Glass offers very low thickness for reduced form-factor, ability to define small features for high-density integration, mechanical stability for multi-component assembly, temperature coefficient of expansion (TCE) match with die and printed circuit board (PCB) materials for reduced thermo-mechanical stresses, and large-panel processability for low cost. However, the passive structures on glass, demonstrated earlier [5, 58] were limited to only one side of the substrate, as shown in Figure 50, because of the lack of ultra-small TPVs at small pitch. The illustration in Figure 49.explains how glass combines the advantages of other substrate materials, thus making it a high-performance and low-cost alternative for high-density integration [57].

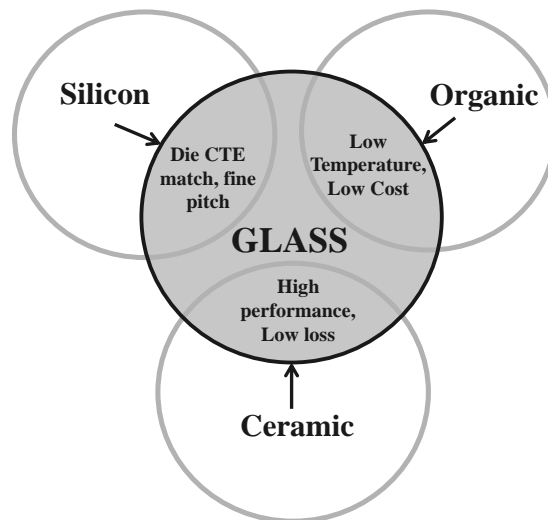


**Figure 49:** Glass provides the best combination of advantages from ceramic, organic and silicon.

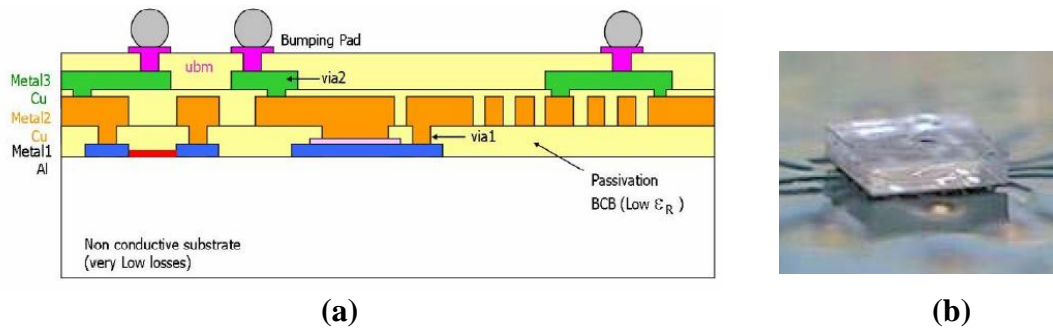


**Figure 50:** RF IPD on glass wafers - single-side processing; a) cross-section stack-up, b) assembled IPD component.

Recently, formation and metallization of through vias at fine pitch were demonstrated in thin glass interposers [59]. This is depicted in Figure 51. The ability to form such TPVs has facilitated ultra-short interconnections between components on either side of the glass interposer, enabling high-density 3D integration of passives and actives on glass with smallest interconnect losses.

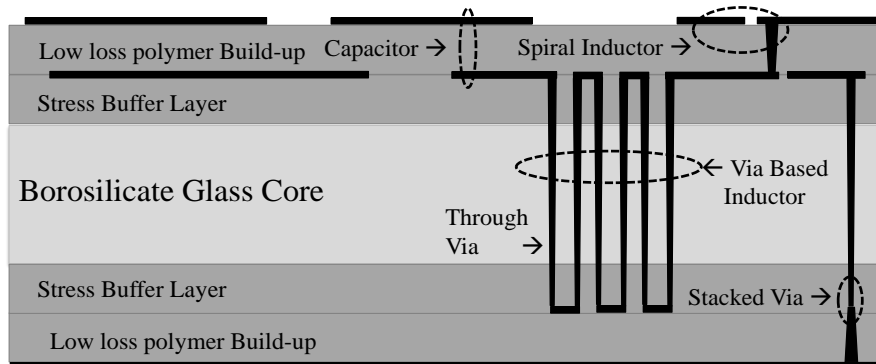


**Figure 51:** Stack-up cross-section of a 3D glass substrate.

### Summary and Thesis R&D Focus

In this chapter, advances in RF components and modules were reviewed in three categories: a) miniaturization of RF passives using filters and diplexers as examples, b) EMI shielding, and c) passive and active integration into modules. Advances in miniaturized planar passives with different substrate technologies were reviewed in the first section of the chapter.

While the progress of such passives from LTCC to organic substrates was driven by the need to reduce thickness and lower the cost, the subsequent migration from organic to glass substrates is driven by the need for: higher performance (low loss), improved dimensional stability, high-density integration of passives with actives, and lower cost. Currently, LTCC-based passives have a strong market presence because their superior properties and mature manufacturing infrastructure for high-volume production. However, glass panel-based 3D IPDs enable higher performance and better component integration at lower cost, and are expected to be more prevalent in the future. The key challenges that need to be addressed are: design of 3DIPD diplexers, double-side fabrication of glass substrate with through-vias, and development of low-cost panel-scalable processes. The modeling, design, fabrication and characterization of glass-based WLAN 3D IPDs diplexers forms the key focus of Task 1 in this thesis.

The need for higher component densities creates additional challenges from the electromagnetic interference between the components. The presence of inductors in RF actives and passives results in magnetic field radiation, which is difficult to shield at small distances from the source. Additionally, there is a need to shield multiple components from one another inside a single package. This is driving the trend towards thinner shields that can effectively provide EMI isolation without significantly increasing the package size. Multilayered metal nano-laminate shields are being explored to achieve this goal. The primary focus of Task 2 in this thesis will deal with shield material selection, followed by the development of component-level EM shields on glass substrates.

The demand for portable electronic systems is driving the need for high-performance, low-profile and very thin RF modules that occupy very less area on the board. LTCC substrates offer excellent RF performance and also enable area reduction by supporting multi-layer passives, and have, therefore, been the widely adapted for RF module integration. The need for miniaturization and cost reduction eventually led to the introduction of 2D RF modules on organic laminates with higher wiring densities. Further miniaturization has been achieved

through chip-first and chip-last embedding approaches, where, in addition to embedded thin-film passives, actives are also embedded in multi-layered organic substrates. Further development of miniaturized multi-functional RF modules requires low-loss, very thin, dimensionally-stable substrate materials that can also support realization of precision high-Q passives. Glass is a compelling substrate material as it satisfies all of these requirements, while also lowering processing and material costs. Innovative 3D glass package solutions are proposed to be developed for highly-integrated and miniaturized RF modules, as a part of Task 3.

## CHAPTER 3

### MINIATURIZATION OF WLAN DIPLEXER

The objective of this task is to model, design, fabricate, and characterize a high-performance and miniaturized WLAN diplexer. The circuit topology and layout of the filters play a key role in determining the performance and size of RF components. In addition, the Q-factor, and inductance and capacitance densities are critical, and are enabled by low-loss dielectric materials with high permittivity. As described in Chapter 1, 3D IPD concept with double-side thin-films on ultrathin glass substrates and through-vias meets both of these criteria to enable new breakthroughs in diplexer performance improvement and miniaturization. This chapter presents the development of such novel filter structures, their circuit topology and layout, fabrication and characterization. The chapter is organized into the following sub-sections: a) modeling and design of novel WLAN filters on glass substrates, b) fabrication and characterization of the WLAN filters, and c) design and demonstration of 3D IPD glass diplexers using these advanced filters.

#### Objectives

The objectives of the WLAN diplexer task are to model, design, fabricate and characterize miniaturized WLAN RF diplexers with the size and performance targets summarized in Table .

**Table 5**  
**Targets for Diplexer**

<b>Frequency</b>	2.4 GHz – 5 GHz	Enabling R&D Innovations: <ul style="list-style-type: none"><li>• Novel miniaturized resonator structures and filter layout.</li><li>• Low filter order and high attenuation.</li><li>• Double LC components on glass connected with through-vias</li><li>• Fabrication on ultra-thin 3D glass substrates using TPVs.</li></ul>
<b>Insertion Loss</b>	0.5 - 1 dB	
<b>Return Loss</b>	>15 dB	
<b>Adjacent Band Attenuation</b>	>15 dB	
<b>Dimensions</b>	1mm x 0.5mm x 0.15 $\mu$ m	

## Approach

A unique diplexer layout is developed that best utilizes the benefits of thin and low-loss substrate materials. A semi-lumped-element filter structure combining individual inductors and capacitors is proposed and developed as a key building block for the diplexers. Such a structure increases the volumetric density by eliminating the need for spatial isolation between inductors and capacitors as in traditional lumped element designs. The volume miniaturization is achieved by developing in-substrate embedded filters or through separate, testable and yieldable ultra-thin dual-band filters on glass with double-side thin-film passives and through-vias, referred to as 3D IPD diplexers. Glass, being a dimensionally stable material with excellent surface finish, just like silicon, enables fabrication of passives with fine features with good accuracy. Further, employing ultra-thin build-up polymers with low loss and high permittivity facilitates miniaturization of filters without compromising on performance. This chapter is divided into the following sections:

### Modeling and design of novel filters

Propose a novel filter schematic structure, extract its equivalent circuit using full-wave EM simulation and tune the structure to achieve the target filter characteristics.

### Fabrication and characterization of the filters

Fabricate the designed filters on ultra-thin 3D glass substrates with TPVs, characterize the filters, and correlate the measured RF performance with simulations.

### Design and demonstration of WLAN 3D IPD diplexer

Model and design a WLAN diplexer based on the novel filter concept to match the performance of commercial components. The 3D IPDs are then fabricated and characterized to compare their performance against that of commercial components.

## Modeling and design of novel filters

### Substrate stack-up and design rules

The material stack-up for the initial analysis and demonstration of the filter structure, shown in Figure 52 comprises of a 30 $\mu\text{m}$ -thin, low loss glass substrate laminated with a low-loss polymer on both sides. The glass has a dielectric constant ( $\epsilon_r$ ) of 6.7, and a loss-tangent ( $\tan \delta$ ) of 0.006. The dry-film polymer ( $\epsilon_r= 3$ ,  $\tan \delta= 0.005$ ) used in this study is available in different thicknesses (3-17 $\mu\text{m}$ ). The polymer helps to improve handling and metallization of the thin glass substrate. The polymer thickness for this demonstration was selected at 17 $\mu\text{m}$  thickness to facilitate easier handling of the ultra-thin glass. The minimum line width and spacing was 10 $\mu\text{m}$  and the TPV diameter was 30 $\mu\text{m}$ .

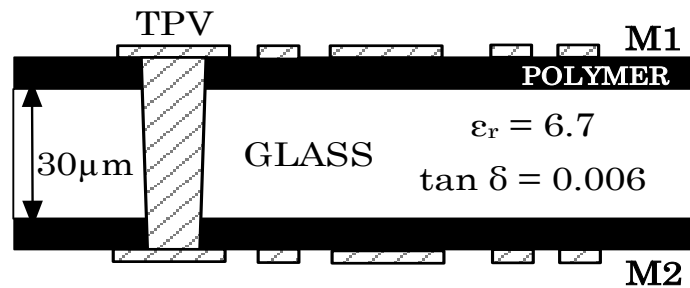


**Figure 52:** Stack-up of the glass substrate

### Description of the filter structure

The proposed filter structure employs a thin dielectric separation between its arms to increase the mutual inductance. The structure consists of two open-ended planar spirals separated by a thin dielectric, aligned with each other. In such a configuration, the pass-band response and transmission-zeros are achieved through resonance due to the inductance of both spirals and the capacitance between them through the substrate. Additionally, a metal patch is added to the center of each spiral to lower the resonance frequency. This is because the metal patches act as parallel-plate capacitors across the dielectric separation layer. Such an integrated structure combining parallel spirals with metal patches maximizes volume utilization through: a) compact

lateral arrangement of spiral inductors and planar capacitors, and b) vertical coupling between these structures across the thin dielectric. The perspective view of the proposed structure is shown in Figure 53.

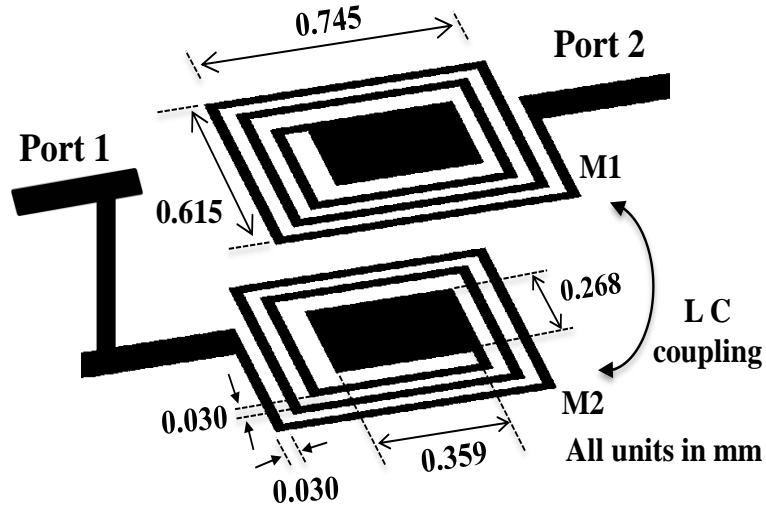


**Figure 53:** Perspective view of the innovative filter structure layout.

### EM Simulation and Modeling

The spiral and capacitor elements were individually simulated using full-wave EM solver (SONNET®). The simulated Q-factor for the capacitor was 200 and for the inductor spiral was 50. The complete structure was then simulated for two polymer thicknesses: 5 $\mu\text{m}$  and 17 $\mu\text{m}$ . The simulated responses of the filter are shown in Figure 54. It was observed that the pass-band center frequency for the 17 $\mu\text{m}$  polymer was 3.5 GHz, while that for the 5 $\mu\text{m}$  polymer was 2.5 GHz. This shift in the frequency response and the stop-band roll-off can be attributed to changes in capacitance and mutual inductance arising from the variation in dielectric thickness. For both cases, the simulated pass-band insertion loss was 0.7dB, with more than 20dB return loss, and more than 35dB attenuation at the transmission zero.

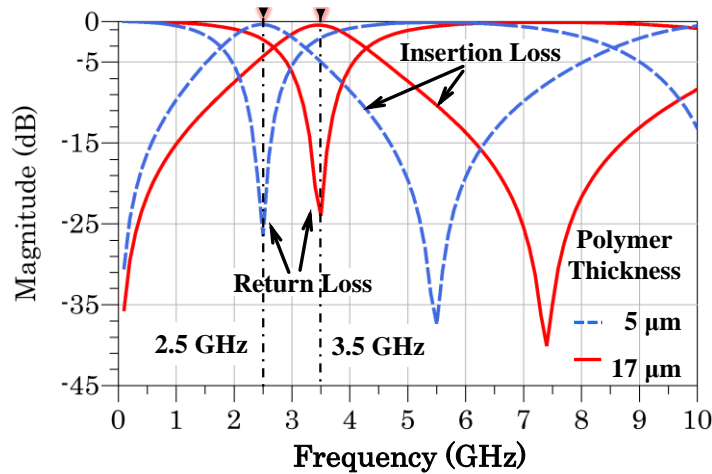


**Figure 54:** Simulated filter responses for two polymer thicknesses.

### Equivalent Circuit Schematic

A circuit model for the filter structure was developed using spice simulator (Agilent ADS) based on individually- simulated responses of the spiral and the capacitor elements. The schematic of such a structure is shown in Figure 55 in which ‘L1b’ and ‘L2b’ are the coupled inductor sections. The coupling factor ‘k’ along with ‘L1b’, ‘L2b’ controls the location of transmission zero and the pass-band. The coupling capacitor ‘C1’ can be tuned to vary the location of the transmission zero alone. However, all these values are interdependent and are a function of the dielectric thickness, the line width, line spacing, and number of turns of the spirals. The frequency of the transmission zero is less sensitive to variations in the inductance of the uncoupled inductor sections ‘L1a’ and ‘L2a’. Therefore, by varying ‘L1a’ and ‘L2a’, the center frequency can be shifted without significantly modifying the location of the transmission zero. ‘C2’ is the capacitance of the center patch. Varying ‘C2’ can change the pass-band and the transmission zero. However, the pass-band is shifted more than the transmission zeros. Hence, adding the central capacitor (C2) provides higher flexibility to modify the structure to obtain the desired frequency response. The component values of the schematic are specified in Table .

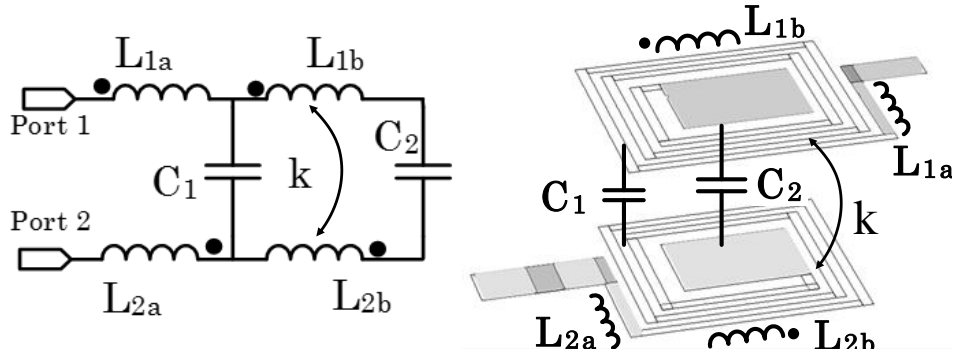


Figure 55: Equivalent circuit model of the proposed filter.

Table 6

Inductor and Capacitor values

L1a (nH)	L2a (nH)	L1b,L2b (nH)	C1 (pF)	C2 (pF)	K
0.44	0.25	8.05	0.059	0.198	-0.4

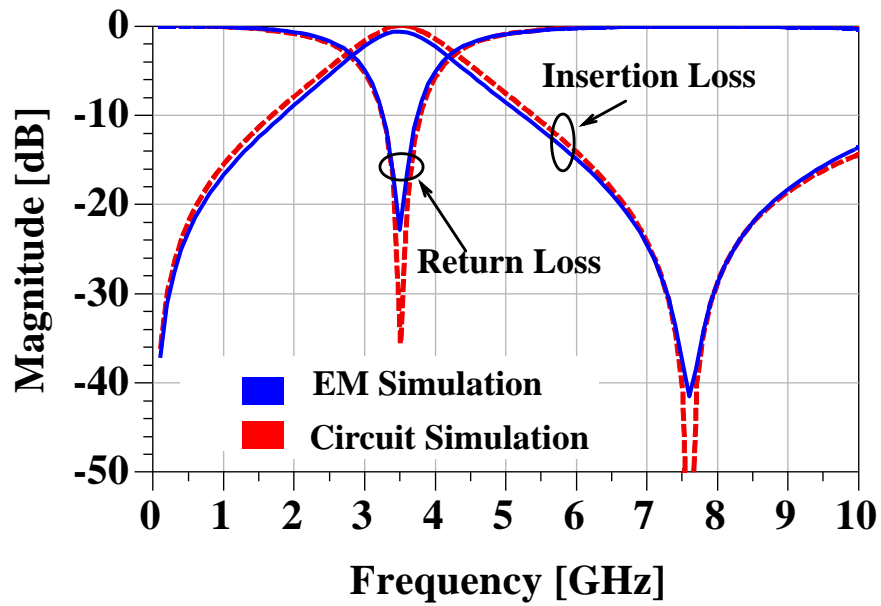


Figure 56: Correlating the EM and circuit simulation of the filter.

As can be observed from the Phase of insertion loss in Figure 57, the negative slope at the pass-band indicates electric coupling to be the dominant mechanism.

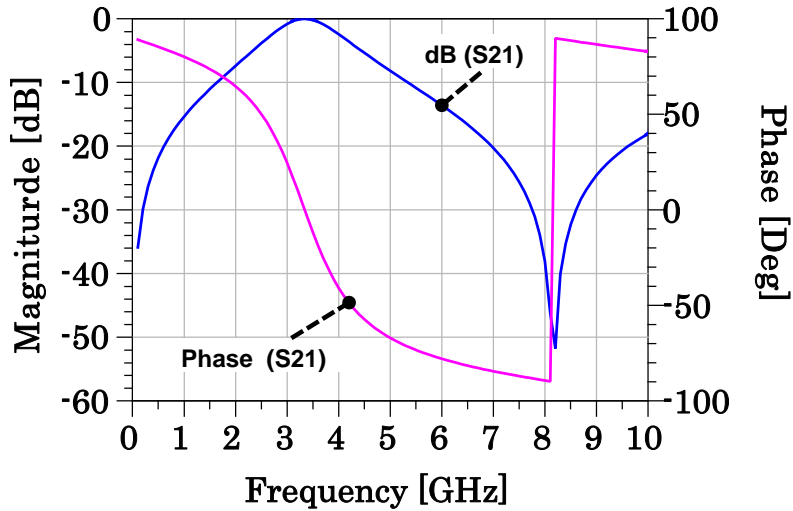


Figure 57: Magnitude and phase of insertion loss.

Further, from the plot of the group delay shown in Figure 58, it can be observed that the pass-band delay of this filter is only about 0.2ns, which is quite low, due to the low filter order.

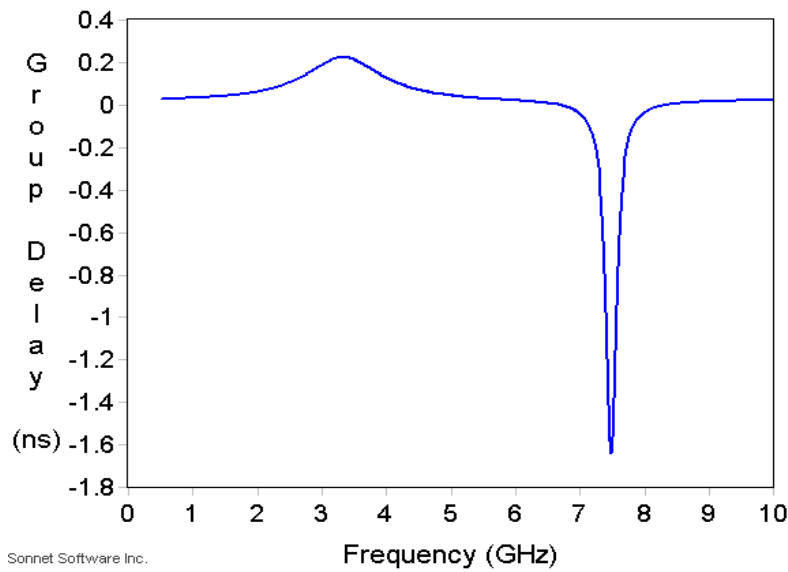


Figure 58: Group-delay through the filter.

### Parametric variations

The filter structure was modified to study the effect of process-variations on the filter performance. The modifications include changes in line width and spacing, polymer thickness, and X-Y alignment. The simulations were performed using EM simulations tools Sonnet EM Suite and HFSS. The results from studying these variations can directly help in the process of layout-level optimization which is the ultimate process that is closest to the measured performance.

#### *Line width and spacing variations*

The line width and spacing of the filter design were  $30\mu\text{m}$ . Keeping the pitch between two lines of the spiral at  $60\mu\text{m}$ , the line width was varied from  $20\mu\text{m}$  to  $45\mu\text{m}$ . The resulting variation in the filter response was studied. The variation in the pass-band center frequency and insertion loss is shown in Figure 59. As the line width increased from  $20\mu\text{m}$  to  $45\mu\text{m}$ , the center frequency increased, whereas the insertion loss decreased. When the line width is increased, although the capacitance between the spirals increases, the inductance of the spirals reduces. Since the resonant frequency depends on both inductance and capacitance, it can be deduced that the increase in capacitance is not as much as the reduction in inductance, resulting in increase of the resonant frequency. Further, since the primary pass-band mechanism is electric-field coupling, the insertion loss decreases with higher capacitance.

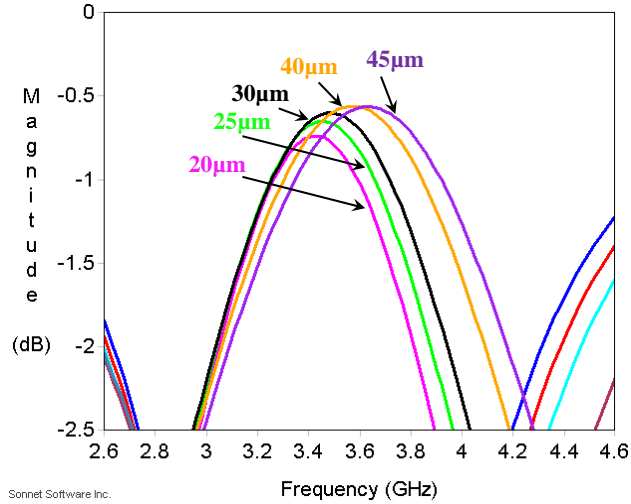


**Figure 59:** Simulated filter pass-band insertion loss for different line widths.

The variation in the transmission zero insertion loss of the filter for different line widths is shown in Figure 60. As the line width increases, the frequency of the transmission zero decreases, until 30µm. After that, the frequency of the transmission zero increases. It can also be observed that the attenuation reduces with increasing line width.

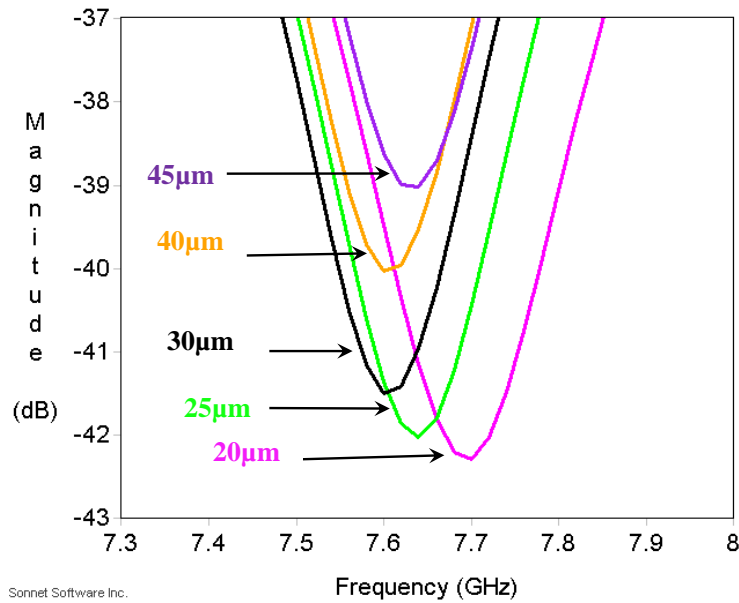


**Figure 60:** Simulated filter transmission zero for different line widths.

### Variation in polymer thickness and spiral lengths

The center-frequency of the pass-band is plotted in Figure 61a for different polymer thicknesses from 3 $\mu\text{m}$  to 17 $\mu\text{m}$ . It was observed that as the polymer thickness increased, the resonant frequency increases linearly. This is attributed to the reduction in the capacitance between the two metal layers and also to the smaller coupling between the inductors. In addition, the center frequency can be altered through the increase or decrease of the spiral length. The variation in the performance for the original design consisting of 2.5 turns and a modified design with 1.5 turns is shown in Figure 61b.

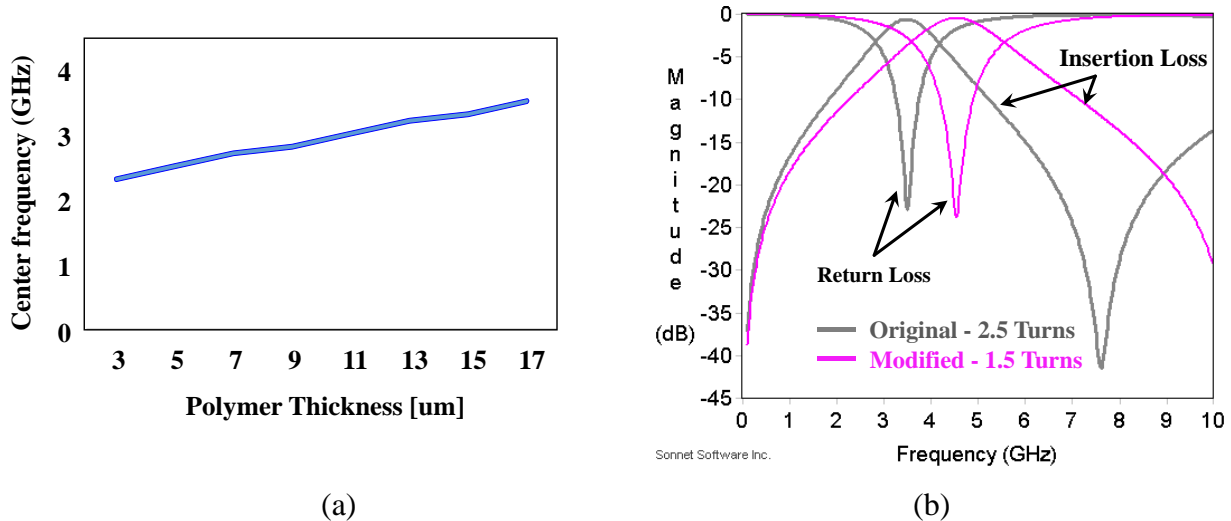


**Figure 61:** Variation in pass-band center frequency for different (a) polymer thicknesses, (b) spiral lengths.

### Variation in X-Y alignment

When fabricating multi-layer substrates, misalignment between successive layers is a common issue that arises from lithography processes and is attributed to tool limitations, material shrinkage (in organics), and positional tolerance of vias. Hence, it is useful to study the effect of such misalignment on the performance of the proposed filter. It can be seen from Figure 62 that, for X-Y misalignment of up to 30 $\mu\text{m}$ , the filter pass-band does not shift, whereas the transmission zero shifts by 300 MHz.

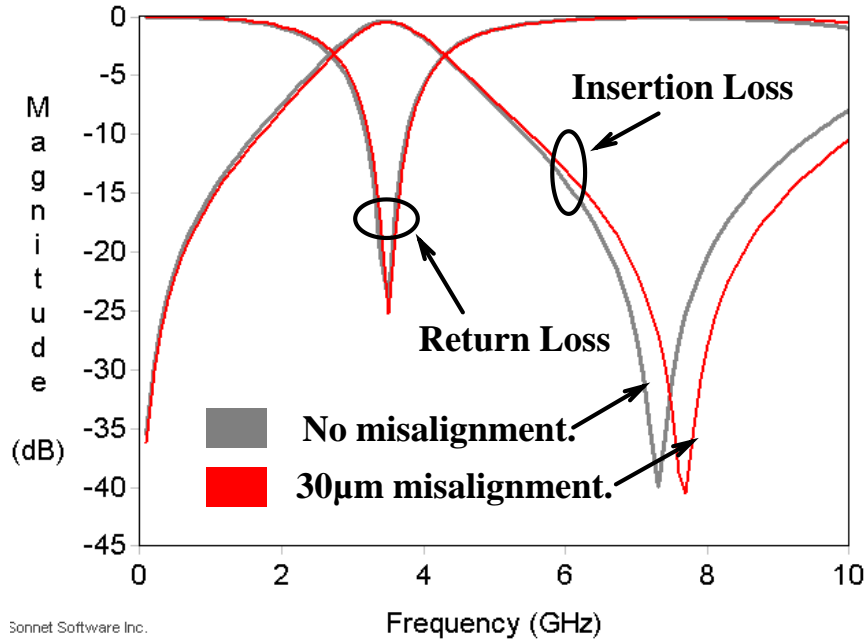


**Figure 62:** Simulated filter responses for X-Y misalignment between the metal layers.

### Modifications to improve the filter performance

To improve the filter performance, structural modifications were performed on the basic filter structure presented in Figure 53. The following modifications were analyzed: a) secondary spirals, b) grounded spirals, and c) ground capacitors.

#### *Addition of secondary spirals and capacitors*

Secondary spirals were added to the spirals on each layer, at a particular ‘point of tap’, as shown in Figure 63. The addition of such spirals increased the capacitance and the inductance in the primary spirals, thereby lowering the pass-band frequency and the transmission-zero frequency. From Figure 64, it can be observed that the frequency of the transmission zero shifts more than that of the pass-band. Small variations in the location of the ‘point of tap’ or the size of the secondary spirals will result in a small change to the pass-band but a larger shift in the transmission zero. Further, the addition of a capacitor plate in place of the secondary spiral results in a similar shift in the pass-band, but smaller shift in the transmission zero.

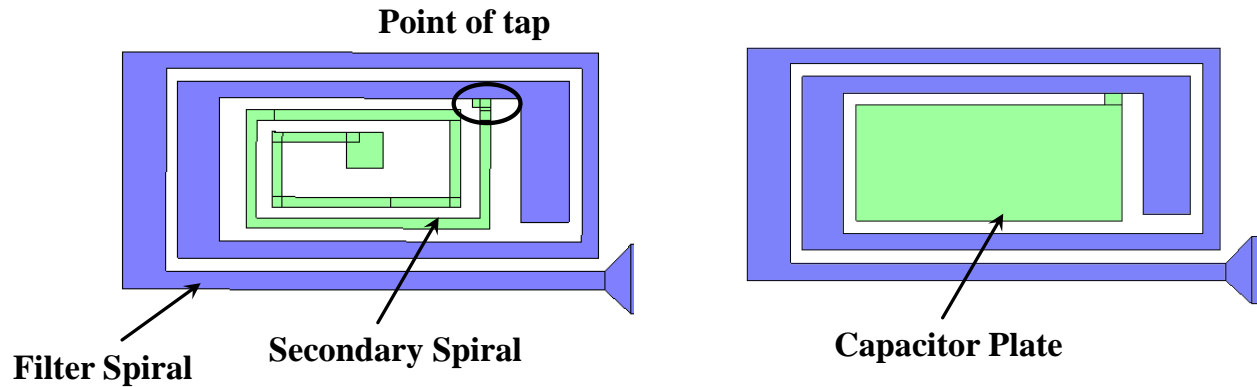


**Figure 63:** Top-view of the filter layout with secondary spiral and capacitor plate.

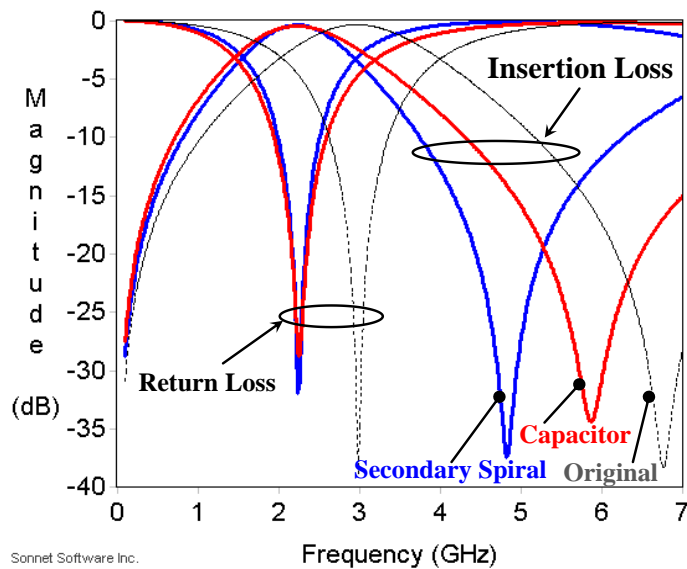


**Figure 64:** Simulated filter responses of the filter with and without secondary spirals.

### *Addition of grounded spirals*

To increase the attenuation characteristics of the filter, grounded spirals were introduced between the spirals as shown in Figure 65. The grounded spirals attenuate a wider range of frequencies compared to having just a single transmission zero for attenuation. The other advantage of such ground spirals is that they do not increase the area of the filter significantly. The frequency response of a 2.4GHz filter with and without ground spirals is shown in Figure 66.

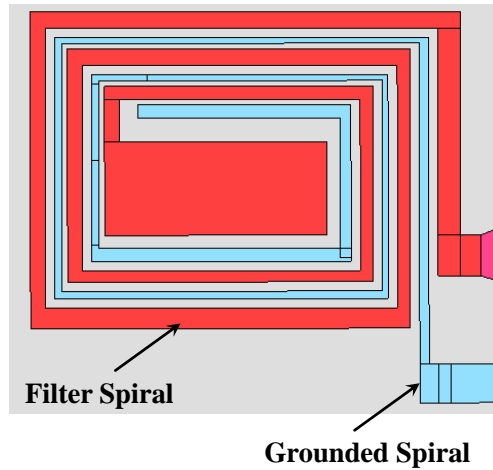


**Figure 65:** Top-view of the filter layout with grounded spirals.

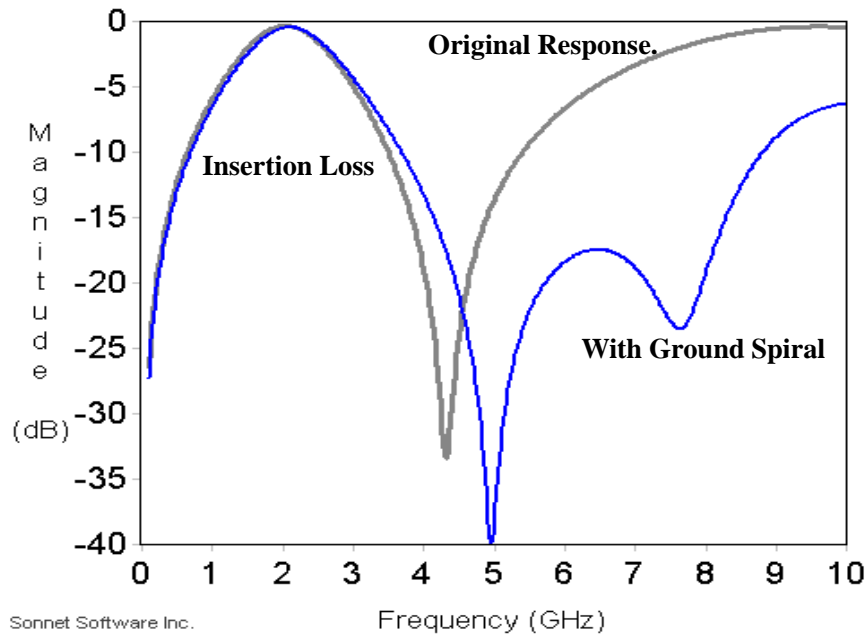


**Figure 66:** Simulated filter responses with and without ground spirals.

*Effect of adding ground capacitors*

Similar to the addition of grounded spirals, the introduction of capacitors to ground improves the attenuation in the upper stop-band. The top-view of the filter layout with the ground capacitor is shown in Figure 67. The corresponding simulated frequency response with and without the ground capacitor is shown in Figure 68.

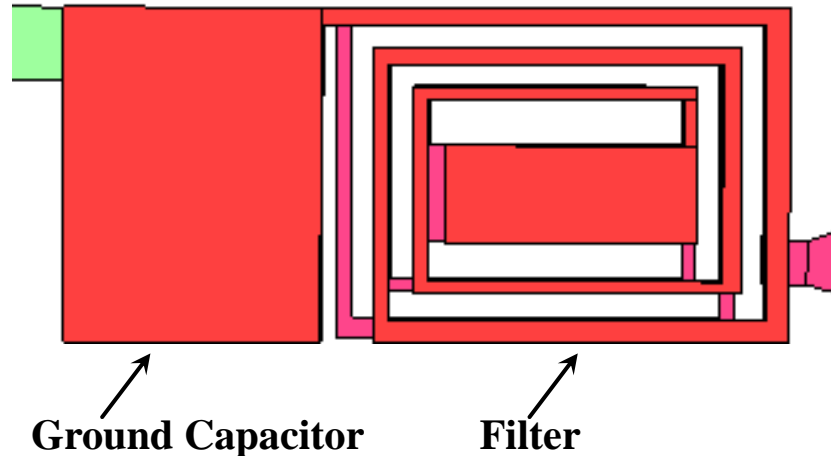
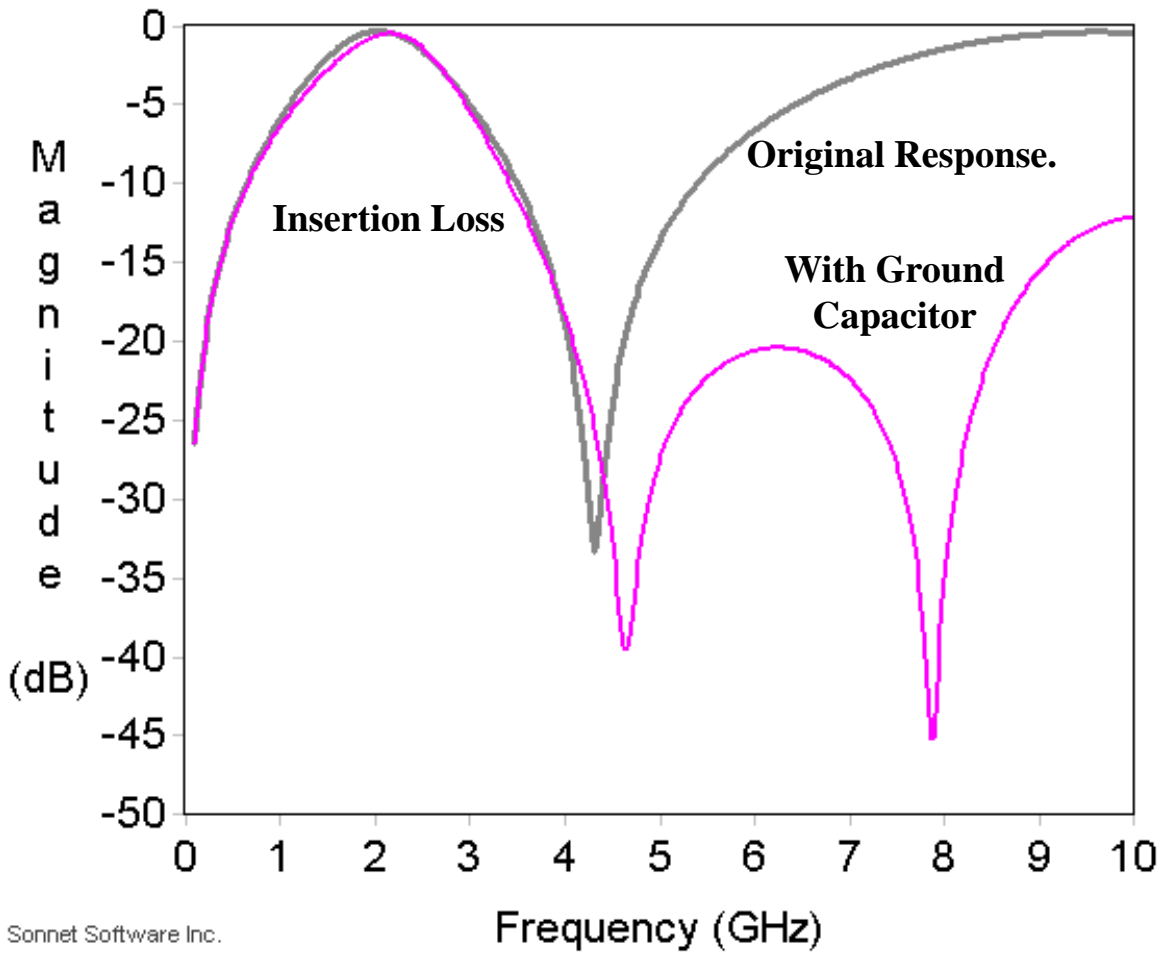


**Figure 67:** Top-view of the filter layout with grounded capacitor.



Sonnet Software Inc.

**Figure 68:** Simulated filter responses with and without ground capacitors.

## Fabrication and characterization of filters

### Fabrication process for glass substrates

A pictorial representation of the key process steps in fabricating a two-metal-layer glass-substrate with TPVs is shown in Figure 69. A borosilicate glass substrate having a thickness of 30  $\mu\text{m}$  - 100  $\mu\text{m}$  was used as the RF module substrate. Firstly, the glass surface was cleaned using organic solvents (acetone, methanol and Isopropyl alcohol (IPA)), to remove residue and impurities from the surface. Following this, thin dry-film polymer with a thickness of 3  $\mu\text{m}$  - 17  $\mu\text{m}$ , was laminated on both sides of the glass substrate using hot-press lamination process. TPVs were formed in the polymer-laminated glass substrate using UV-laser ablation. Electro-less copper deposition process was used to achieve a conformal seed layer. Lithography was performed on the seeded samples, and a semi-additive plating (SAP) process was used to further metallize the TPVs and to achieve the redistribution layer (RDL) patterns on both sides.

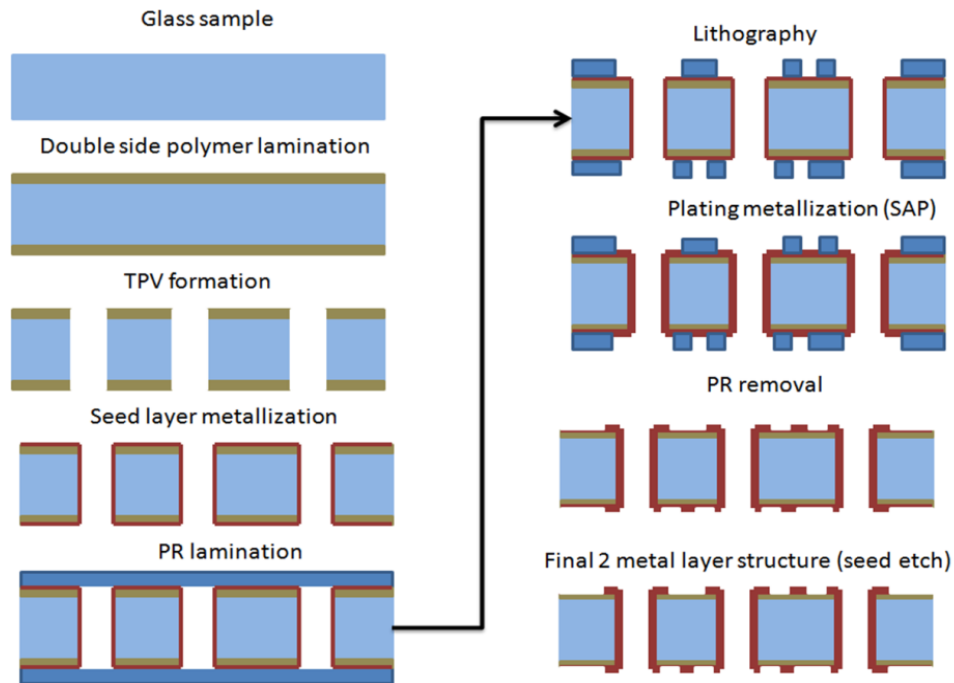


**Figure 69:** Process flow for the fabrication of the ultra-thin glass substrate with TPVs [57] .

### Fabrication of the filters

The BPF was fabricated on ultra-thin glass substrate (D263® – from SCHOTT glass) having a thickness of 30 $\mu\text{m}$ , using a panel-based double-side thin-film wiring process. The use of thin polymer layers on glass interposers have been shown to facilitate handling and plating metallization [23]. A thin dry-film polymer was laminated on both sides of the thin glass. The copper thickness was 8 $\mu\text{m}$ . The top view image of the fabricated structure and the characterization setup are shown in Figure 70.

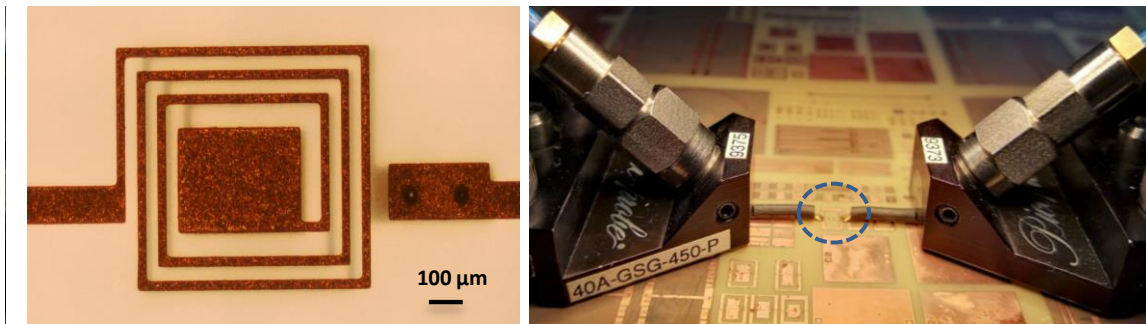


**Figure 70:** Measurement and top view optical image of fabricated BPF structure on 30 $\mu\text{m}$  thin glass.

### Characterization of the filters

The frequency response of the fabricated structure was obtained through S-parameter characterization using a vector network analyzer (VNA). A short open load thru (SOLT) calibration was performed prior to the measurements. As shown in Figure 71, very good correlation between the measurements and simulations was observed for the pass-band insertion loss and return loss.

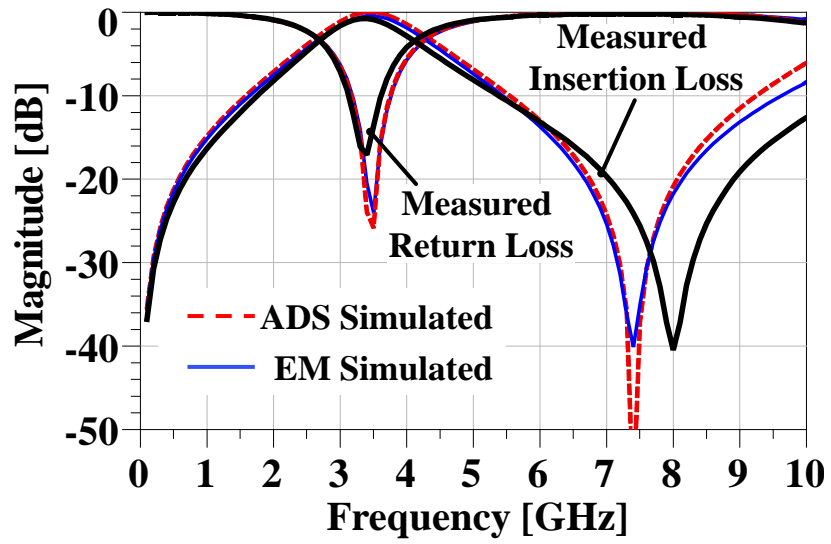


Figure 71: Simulation-Measurement performance correlation of the filter.

## Design and demonstration of 3D IPD diplexer

A diplexer is a passive filtering component that guides incoming signals to two different output ports depending on their frequency. Diplexers are typically employed in dual-band modules where a single antenna has to support front-end modules operating in two frequency bands. A diplexer is composed of two filters, one operating in the high frequency band, and the other in the low frequency band. These filters could be low-pass, high-pass or band-pass. In this design and demonstration, both were realized as band-pass filters. There were two design iterations. The substrate stack-up were also different for each iteration. The details of the design, fabrication and characterization of the diplexers are detailed in this section. The specifications based on a commercial ceramic chip-type diplexer are as shown in Table .

**Table 7**  
**Performance Specifications of the WLAN Diplexer**

Low-Band			High-Band		
Parameter	Freq. (GHz)	Spec (dB)	Parameter	Freq. (GHz)	Spec (dB)
Insertion loss	2.4-2.5	0.5	Insertion loss	4.9-5.95	0.5
Attenuation	4.8-6	25		Attenuation	0.03-2.4
	7.2-7.5	23	2.4-2.5		30
Return Loss	2.4-2.5	10	2.5-2.69		24
			9.8-11.9		20
Common Port			Return Loss	4.9-5.95	10
Parameter	Freq (GHz)	Spec (dB)			
Return Loss	2.4-2.5	10			
Return Loss	4.9-5.95	10			

### Initial diplexer design

The proposed filter structure demonstrated in the previous sections was tuned with ADS and optimized in sonnet to design a WLAN diplexer. A 4-metal-layer diplexer was designed targeting the specifications of a commercial diplexer.

### Substrate-stack up and design rules

The substrate stack-up and design rules depicted in Figure 72 were employed in the design and fabrication of the diplexer. The substrate core was glass of thickness 100  $\mu\text{m}$ , laminated with a 22 $\mu\text{m}$ -thick polymer. The build-up layer consisted of a polymer layer having a thickness of 22  $\mu\text{m}$ . The diameter of the TPVs was 100  $\mu\text{m}$ , and that of the blind vias was 45  $\mu\text{m}$ . The minimum line width and spacing was 20  $\mu\text{m}$ , with the metal thickness on each layer being 10  $\mu\text{m}$ .

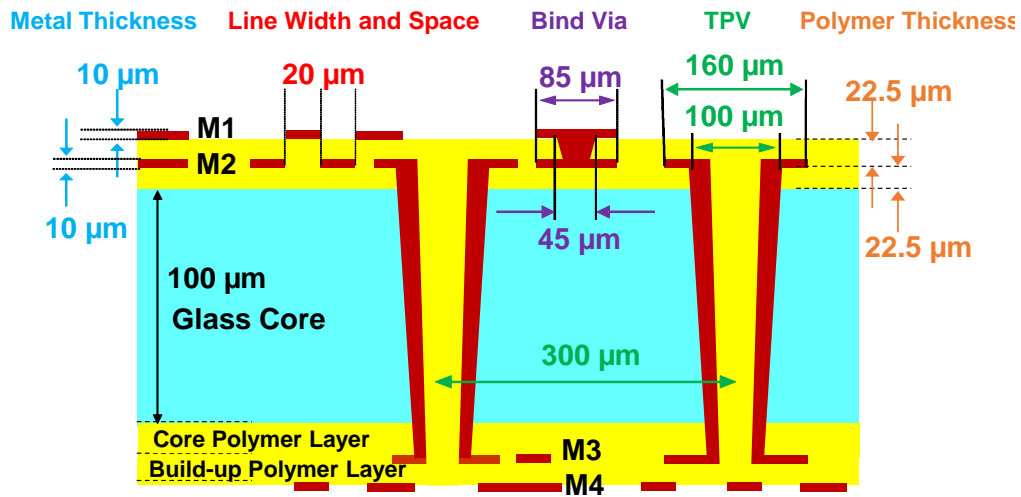
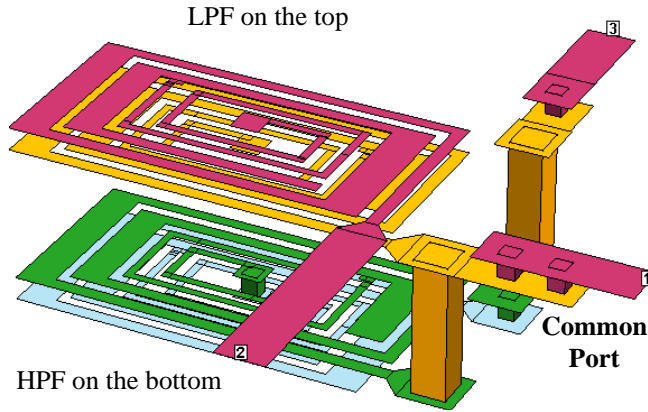


Figure 72: Substrate stack-up and design rules for 4ML diplexer fabrication.

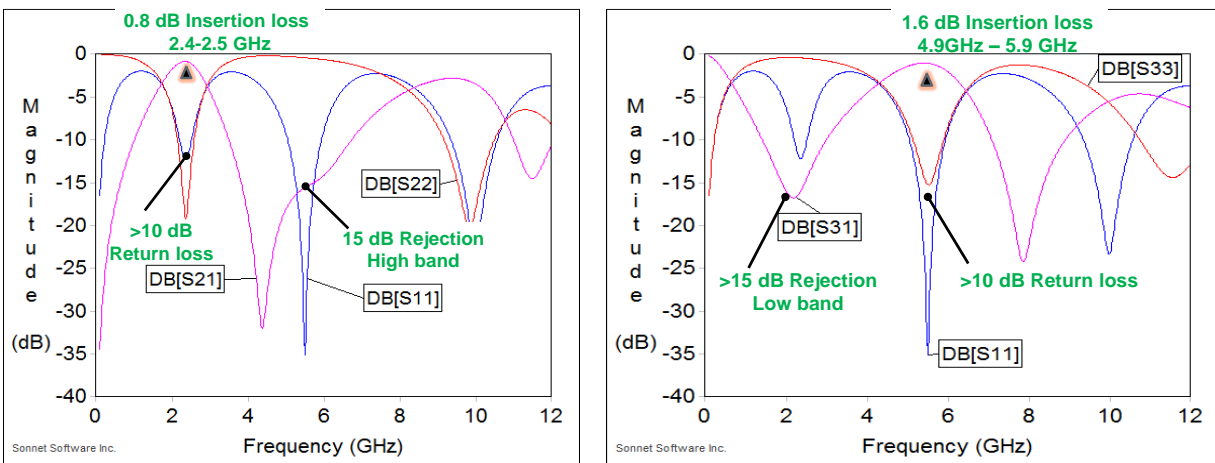
### Diplexer design and layout

The diplexer low-band and high-band filters were designed based on the filter designs and parametric variations presented in the previous sections. The design utilized four metal layers, two for each filter. TPVs were employed to connect the filters on either side of the glass substrate. To reduce the insertion loss, varying line widths were employed and, secondary spirals were employed to tune the transmission zeros. The dimensions were 1.3mm x 0.8mm x 0.2mm. This design was simulated in a full-wave electromagnetic simulator (SONNET) and the

simulated response showed ~1dB insertion loss and more than 10dB return loss, with 15dB rejection in the adjacent band as shown in Figure 74.



**Figure 73:** 3D view of the initial diplexer design



(a) (b)

**Figure 74:** Simulated response of (a) low-band filter, (b) high-band filter.

### *Fabrication and characterization*

The process for the fabrication of the diplexers was similar to the two-metal-layer substrate processes depicted in Figure 69. For the four-metal-layer fabrication, the process was continued by laminating another polymer build-up layer on each side of the two-metal-layer

substrate. To electrically connect the metal layers on the inner layers to those on the surface, micro-vias were formed on the build-up polymer using UV lasers and metallized. A semi-additive plating approach was used to metallize and pattern the surface metal layers. The designs were fabricated with four-metal layers on glass substrate as shown in Figure 75. Further, the measured responses of the filters are shown in Figure 76.

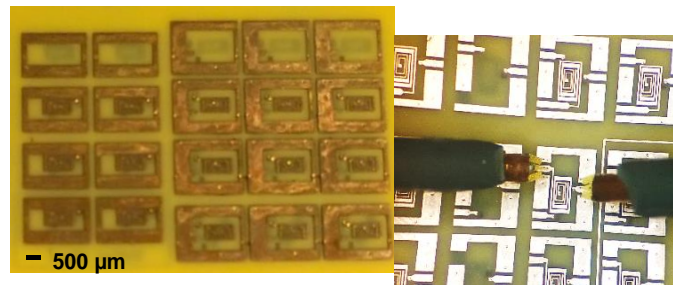


**Figure 75:** (a) Fabricated Diplexer substrate, (b) RF Probing of diplexer

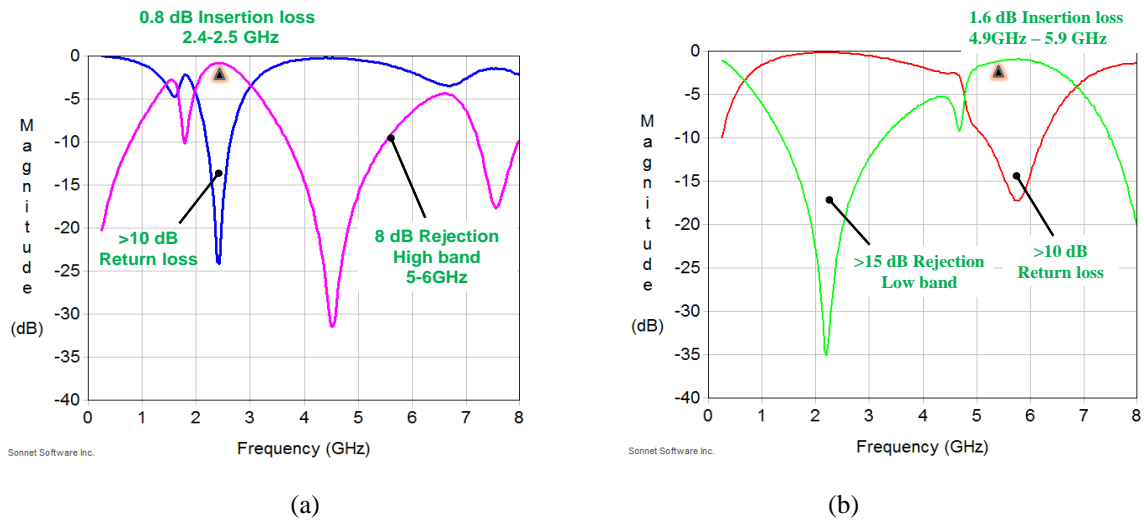


**Figure 76:** Diplexer measurement results: (a) Low-Band (b) High-band.

From these responses it can be seen that while the pass-band insertion loss and return loss were good, the out-of-band attenuation did not meet the specifications. Hence, the diplexer design was revised to improve the performance so as to meet the specifications.

## Revised diplexer design, fabrication and characterization

### *Modified substrate-stack up and design rules*

The substrate stack-up and design rules were revised, as depicted in Figure 77 were employed in the design and fabrication of the diplexer. The substrate core was glass of thickness 100  $\mu\text{m}$ , laminated with a 20.5  $\mu\text{m}$ -thick polymer. The build-up consisted of a polymer layer having a thickness of 17.5  $\mu\text{m}$ . The diameter of the TPVs was 100  $\mu\text{m}$ , and that of the blind vias was 45  $\mu\text{m}$ . The minimum line width and spacing was 20  $\mu\text{m}$ , with the metal thicknesses on each layer were 8  $\mu\text{m}$ .

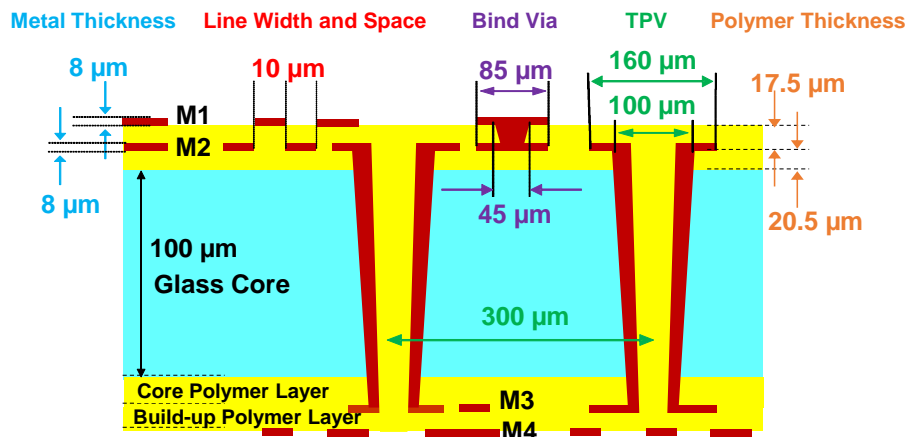


**Figure 77:** Modified substrate stack-up and design rules for 4ML diplexer fabrication.

### *Modified Diplexer design and layout*

The diplexer design was modified to reduce the physical dimensions and improve the performance. This was enabled by the thinner (17.5  $\mu\text{m}$ ) build-up polymer, and by employing additional ground capacitors. The four-metal layer layout of the revised diplexer is shown in Figure 79.

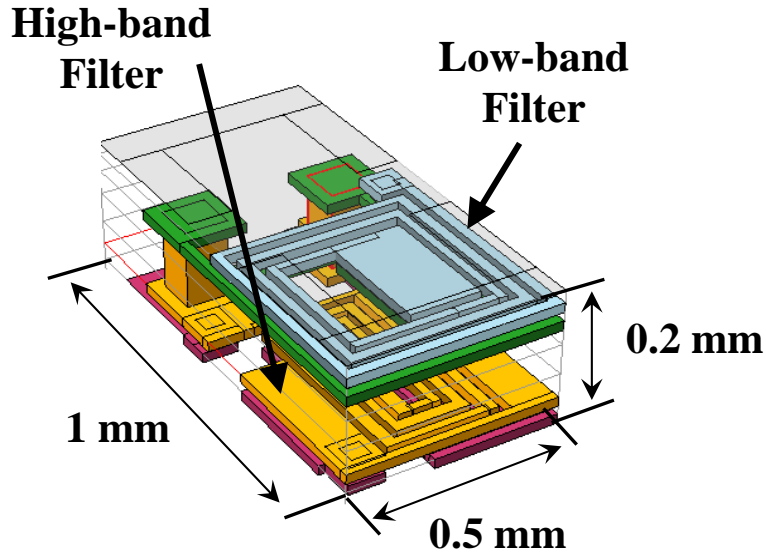


Figure 78: 3D view of the initial diplexer design

This design was simulated in a full-wave electromagnetic simulator (SONNET) and the simulated response showed ~1dB insertion loss and more than 10dB return loss, with close to 12 dB rejection in the adjacent band as shown in Figure 74.

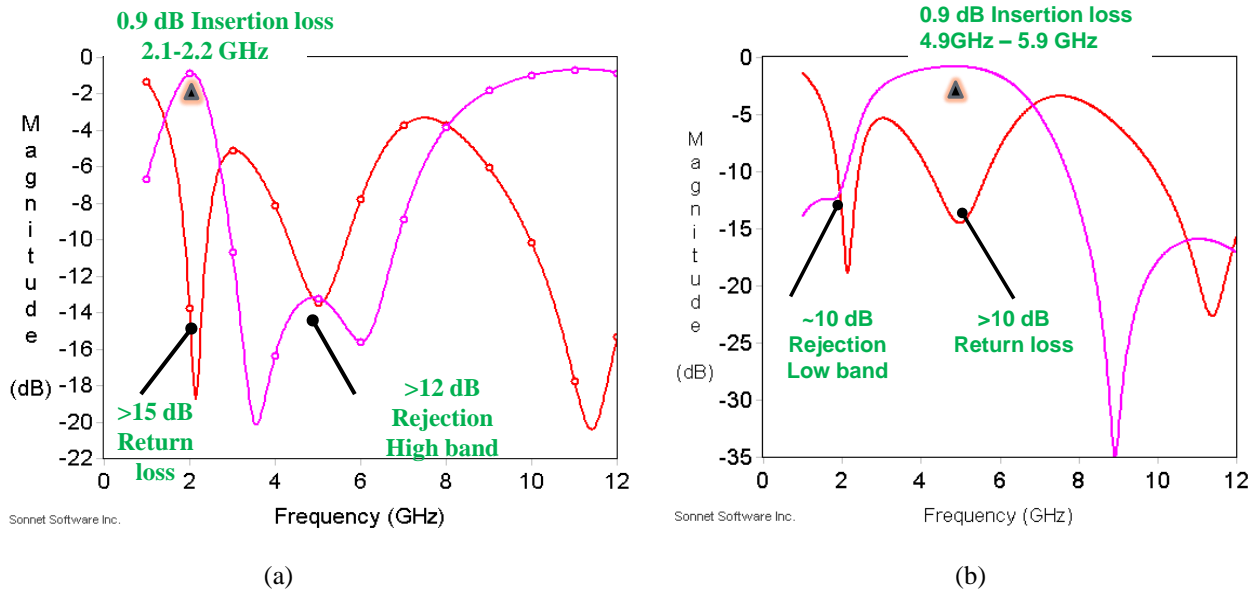
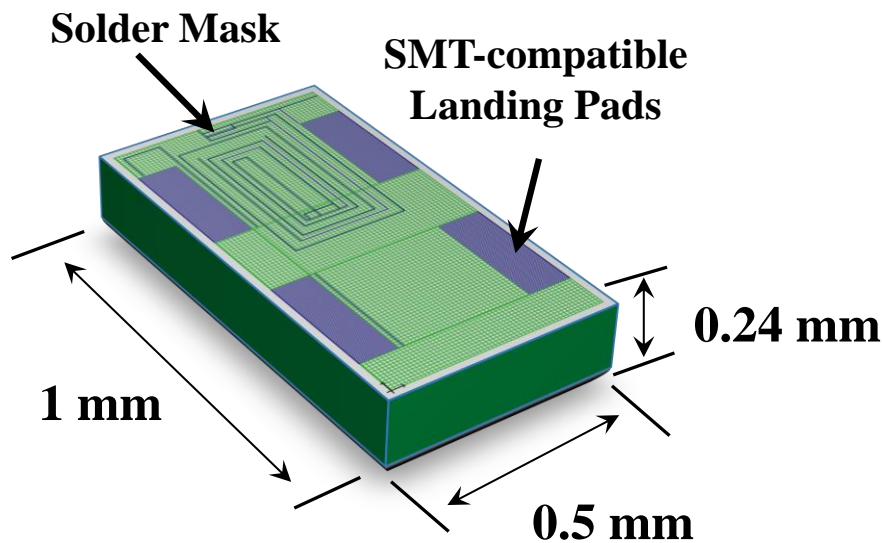


Figure 79: Simulated response of (a) low-band filter, (b) high-band filter.

To demonstrate the feasibility of a 3D IPD diplexer component, the diplexer design was also optimized keeping the footprint of the resulting component in mind. One key aspect of the design involved integrating the input and output SMT landing pads as capacitors in the design. This helps in accounting for the parasitics of the pads and also to miniaturize the component. A conceptual view of the resulting 3D IPD component is shown in Figure 80.



**Figure 80:** Conceptual 3D view of a 3DIPD WLAN diplexer component.

### *Revised Low-band design*

A revised version of the low-band filter, with slightly larger dimensions was designed with both ground capacitors and grounded spirals. The layout and simulated response is shown in Figure 81. The simulated response is shown in Figure 82. The insertion loss was 0.9dB with more than 25dB high-band rejection up to 8GHz.

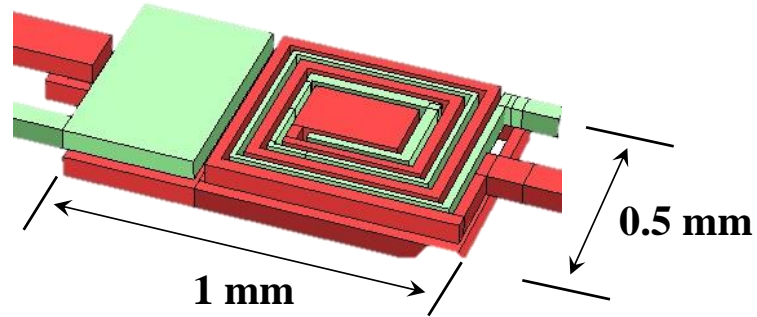


**Figure 81:** 3D view of the revised low-band filter design

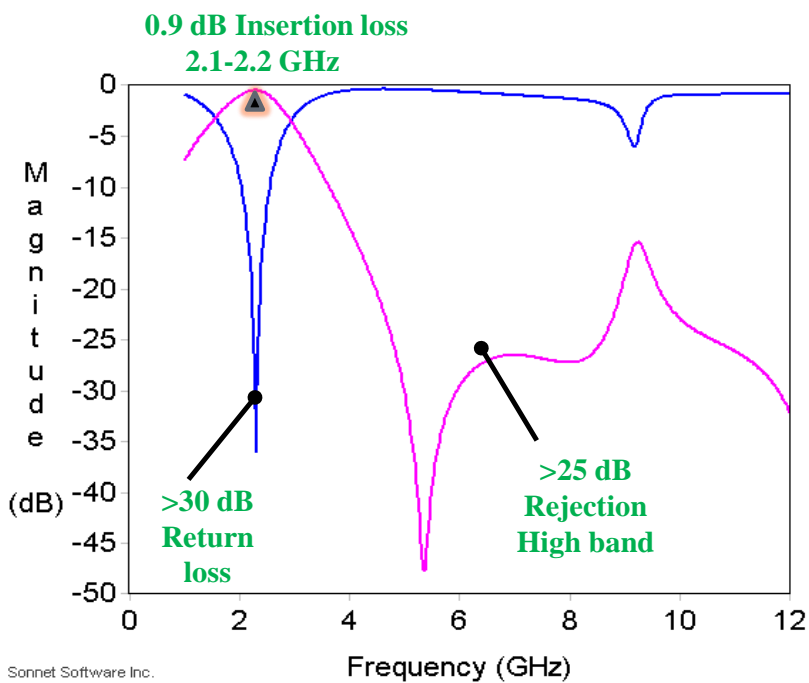


**Figure 82:** Simulated response of the revised low-band filter.

### *Fabrication with the revised designs and characterization*

The revised low-band design was fabricated on two-metal-layer glass substrates. The fabricated sample and the measured responses of the low-band filter are shown in Figure 83 and Figure 84. It can be seen that the insertion loss was 0.6dB, which is close to the target specification of 0.5dB. The high-band rejection was more than 25dB from 5.5 GHz up to 9.5 GHz. Over all, the frequency response was shifted from the design target by about 200MHz in

the pass-band and 500MHz in the rejection band. This is a result of process variations and can easily be rectified through subsequent optimization of the design to account for process variations.

**Figure 83:** Top-view of the fabricated revised low-band design.

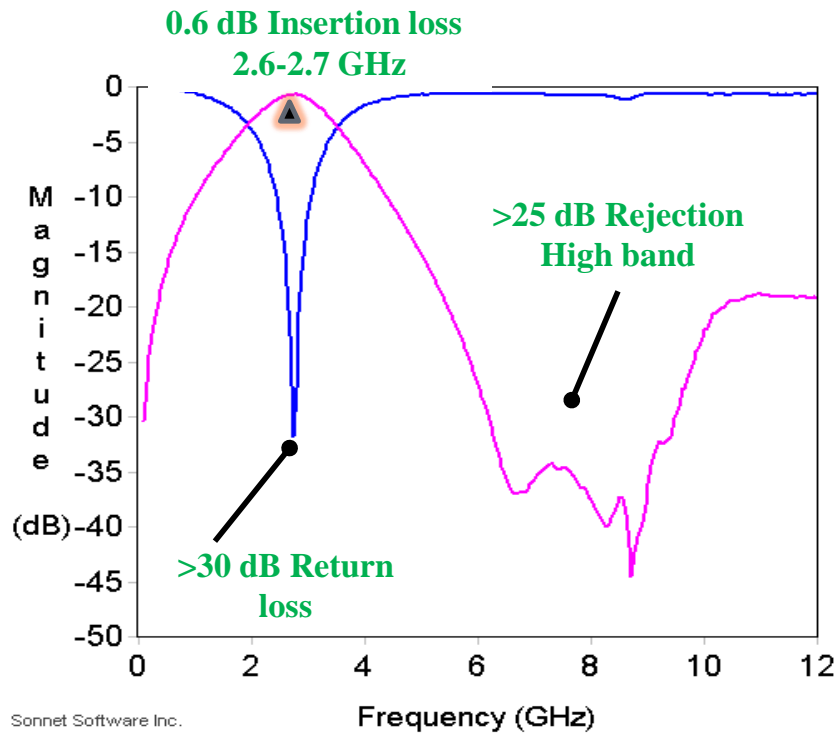


**Figure 84:** Measured performance of the revised low-band design.

### Summary

Next-generation RF systems require miniaturized ultra-thin passives that can be surface-assembled as ultra-thin devices or embedded in the substrate. In lieu of these requirements, this chapter discussed the modeling, design, fabrication, and characterization, of an innovative high-performance and ultra-thin WLAN diplexer. A novel ultra-thin glass-based band-pass filter structure was proposed and a corresponding lumped-element circuit schematic was developed.

The equivalent circuit was verified with full-wave EM simulations. Further, the mechanism of coupling in the structure was determined to be electric, and the simulated group-delay was found to be very less, at 0.2ns in the pass-band. Parametric variations were performed on the layout of the filter and the effect on the performance of the filter was studied. These included variations in the line width, polymer thickness and X-Y alignment. In addition, the filter structure was modified to study the subsequent effect in performance. The different modifications consisted of the addition of secondary spirals, grounded spirals, and ground capacitors. The basic filter structure was fabricated on ultra-thin glass substrate of thickness 30  $\mu\text{m}$ , and measured to obtain the S-parameter response. The measurement showed good correlation with the simulated performance.

Based on the proposed filter layout and the modifications, a WLAN diplexer was then designed, fabricated and characterized on a four-metal layer substrate consisting of a 100  $\mu\text{m}$  –thick glass core. The X-Y dimensions of this diplexer design were 1.3mm x 0.8mm. The measured pass-band insertion loss of 0.8-1.6dB was achieved in the low and high band, along with 10dB adjacent-band attenuation. Subsequent design improvements were targeted to enhance the adjacent-band rejection and miniaturization. A miniaturized diplexer with dimensions 1mm x 0.5mm x 0.2mm was designed with 0.9dB insertion loss and 12dB rejection. The low-band filter design of the diplexer was further improved using grounded spirals and ground capacitor. This revised design with dimensions of 1mm x 0.5mm was fabricated on a two-metal layer substrate with a polymer of thickness 17.5  $\mu\text{m}$  between the spirals. The measured insertion loss was 0.6dB and high-band rejection was more than 25dB. This revised design matched the target specifications reasonably well. Thus, the capability of the proposed filter design to achieve high performance and miniaturized 3D IPD diplexer components was demonstrated on ultra-thin glass substrates.

## CHAPTER 4

### MINIATURIZED COMPONENT-LEVEL EMI SHIELDING

The objective of this task is to develop component-level shielding for miniaturized RF modules, providing up to 60dB electromagnetic (EM) isolation at distances less than 100  $\mu\text{m}$ , in 1-20GHz frequency range. Miniaturization of multi-functional RF modules requires high component densities. The electromagnetic interference between components increases with higher functional density or reduced inter-component distance. Hence, there is a need to shield components from one another in miniaturized RF modules. An integrated EM shielding is implemented between components or transmission lines that interfere with one another, using metallized trenches in the organic build-up layers. This involves four key advances, which also form the key sub-sections of the chapter: a.)Modeling of EM radiation in RF modules, b.)Analytical modeling – Material and multi-layer stack-up design, c.)Modeling and design of component-level EMI shields, d.)Fabrication and characterization of EMI shields.

#### Objectives

The objectives of this section are to model, design, fabricate and characterize miniaturized component-level EM shields for RF modules with the size and performance objectives as summarized in Table .

**Table 8**

**Targets for EMI shielding**

<b>EM Isolation</b>	30 – 60 dB	Enabling R&D Innovations: <ul style="list-style-type: none"><li>• Materials and structures with enhanced shield-effectiveness</li><li>• Integrated EM isolation shields using trench structures on dielectric build-up layers;</li></ul>
<b>Frequency</b>	1 GHz - 20 GHz	
<b>Distance from components</b>	< 100 $\mu\text{m}$	
<b>Integrated Shield Thickness</b>	< 100 $\mu\text{m}$	
<b>Shield Metal Thickness</b>	< 10 $\mu\text{m}$	

## **Approach**

To address the issue of EM interference between components that are integrated in close proximity to one another, four challenges need to be addressed: a) Identifying the sources of radiation and the coupling between components, b) selecting the right material for the particular application, c) identifying the effective shield structure through modeling and simulations, and d) fabrication and characterization of the shield structures. Four sub-tasks are proposed to address these challenges:

### Modeling of EM radiation in RF modules

Model the electromagnetic propagation and interference between different elements such as passives, actives and interconnections of typical RF modules using electromagnetic simulations. From these simulations, guidelines will be developed for placement of these elements in a miniaturized RF module.

### Analytical modeling - Material and multi-layer stack-up design

Model the shield effectiveness of different materials and material combinations through analytical modeling, and develop a novel material stack that is significantly better than traditional single-layer shields.

### Modeling and design of component-level EMI shields

Propose component-level shielding structures and study their shield effectiveness through 3D EM simulations.

### Fabrication and characterization of EMI shields

Demonstrate the effectiveness of the proposed shield structure through fabrication and characterization.

## **Modeling EM Radiation in RF modules**

### Full-wave 3D EM Simulation Setup

In order to study the coupling between package elements, simulations were performed using HFSS – a full-wave 3D EM tool. The geometries and metal thicknesses of the different elements were constructed based on the design rules. The inductors had a line width and spacing of 50 $\mu\text{m}$  with overall dimensions of 0.5mm x 0.6mm. The dimensions of the capacitor plates were 0.5mm x 0.6mm, with a dielectric thickness of 7 $\mu\text{m}$  between the plates. The TPV diameter was 60 $\mu\text{m}$  with the capture pad dimension of 180 $\mu\text{m}$ . A microstrip type transmission line with width of 20 $\mu\text{m}$  and length 2mm was used. The transmission line was not matched to 50 $\Omega$  to facilitate increased radiation due to the impedance mismatch. This would in turn help study the worst-case EM interference scenario.

To study the coupling between these elements, two of these elements were integrated into a 3D EM model, assuming 400 $\mu\text{m}$  of separation between the elements. The “Solution set-up” was set as “driven-terminal” type. “Lumped ports” were employed to excite the structures. The far-end cross-talk between these elements was used to study the induced interference. The simulation was performed from 100MHz to 20GHz, in steps of 100MHz. The top view of the typical simulation set-up consisting of a TPV, a capacitor, an inductor and a transmission line (TL) is shown in Figure 85.

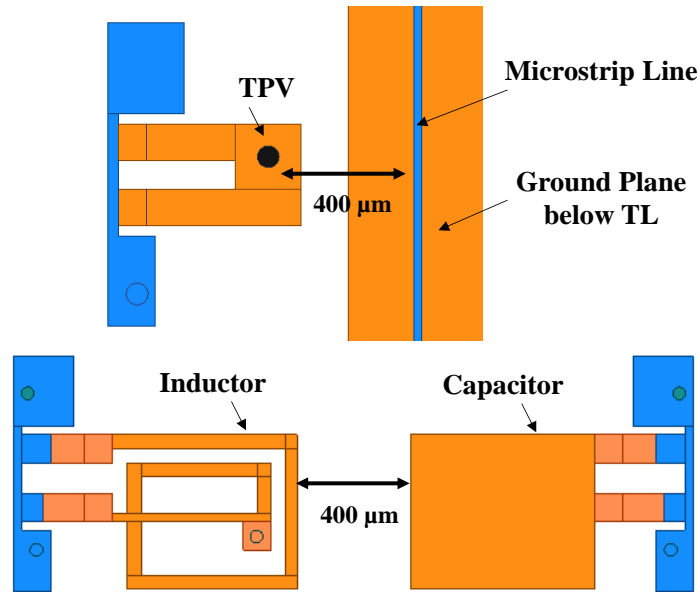


**Figure 85.** Top view of the typical simulation setup.

### Simulation results and analysis

The lateral coupling between different elements are compared in Figure 86. It can be observed that the coupling is highest between the unmatched transmission lines with a common ground plane. The next highest coupling is between inductors as they do not have a tightly coupled ground reference. Further, since inductors and TPVs are current-based elements, the coupling onto an inductor from a TPV was observed to be higher than that from a capacitor, which is a voltage-based structure. Capacitors are coupled structures and hence the EM coupling into a capacitor was lower than that for inductors and TPVs. As can be expected, the coupling between capacitors was the least compared to inductors and TPVs. As microstrip transmission lines are always referenced to a ground plane, it was observed that the coupling between microstrip lines and other elements was the least. While transmission lines may be the least susceptible to lateral EM interference from other package elements, it is essential to shield two microstrip lines from each other as the coupling between them is significant.

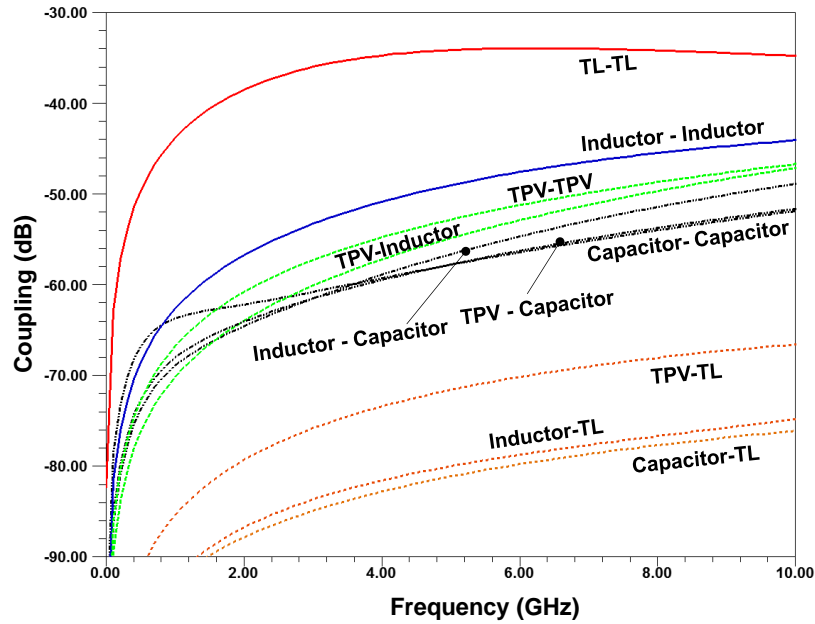


**Figure 86.** EM coupling between package elements.

Based on these simulations a basic set of guidelines are defined for the placement of these passives:

- The layout procedure must begin with the placement of inductors and TPVs so that they can be spatially isolated as much as possible.
- The distance of separation between capacitors and transmission lines may be lower than that between inductors and TPVs.
- Transmission lines can be routed closest to other structures.
- Parallel place capacitors may be safely placed closer to each other or to other passives.

## Analytical material modeling - Material and multi-layer stack-up design

### Need for EM Shielding

Depending on the frequency of radiation, the region around a source of EM radiation is divided into near-field and far-field, as shown in Figure 87. The far-field distance is given by:

$$\text{Far-field region} > \lambda/2\pi, \quad (1a)$$

where  $\lambda$  is the wavelength of the radiation.

In the far-field region, the radiated wave is electromagnetic in nature, which means that the electric and magnetic fields are coupled and have the same wave impedance. The near-field distance is given by:

$$\text{Near-field region} < \lambda/2\pi \quad (1b)$$

In the near-field region, the electric and magnetic fields are decoupled and have different wave impedances. This causes the electric and magnetic fields to exhibit different shielding characteristics in the near field.

A miniaturized multifunctional system houses several active and passive components in close proximity. All of them radiate electromagnetic (EM) fields of different strengths and frequencies. The typical separation distance between components is around 2-6 mm. This means the components lie in the near-field region of each other even up to 8 GHz. Additionally, the components also lie in the far-field region of external EM interference arising outside the package. Therefore, all components require electromagnetic interference (EMI) shields to prevent external interference from entering into the components, and also to suppress any radiation arising from the component. To this end, sputtered magnetic and non-magnetic thin-

films provide the ability to design and create unique EMI isolation layers instead of the metallic cans made from thick materials[13] or expensive spray-coated paints [17].

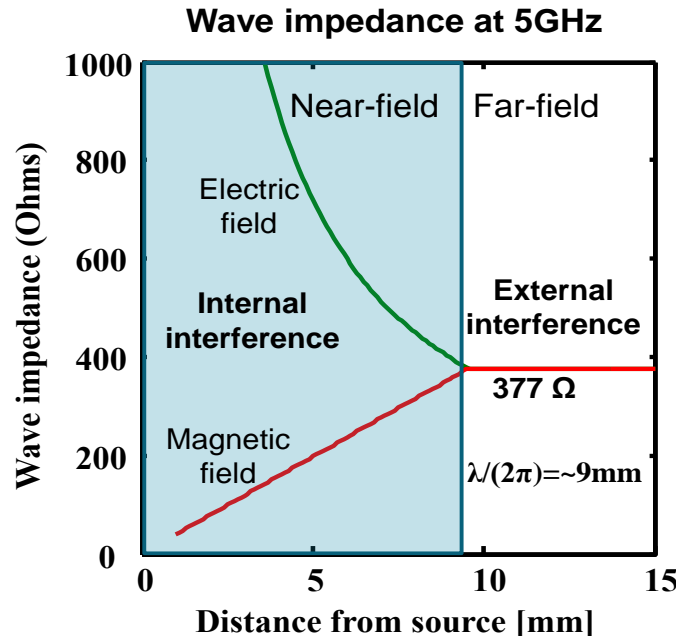


**Figure 87.** Wave impedance with varying distance from an EM source radiating at 5GHz.

### Mechanism of EM Shielding

Fundamentally, EM shielding is effected through the following mechanisms[39] as depicted in Figure 88:

1.) Reflection loss – An interfacial phenomenon arising because of the difference in the impedance between the medium around the shield and the shield material. The reflection loss is different for far-field and near-field regions. In the near-field region, it is higher for electric than for magnetic fields. The expression for near-field magnetic field reflection loss is given by:

$$R_m = 20 \log \left( \frac{Z_w}{4|Z_s|} \right) \text{ dB.} \quad (2)$$

‘ $Z_s$ ’ is the impedance of the shield metal in ohms, defined as:

$$Z_s = \sqrt{\frac{\omega \mu_m}{\sigma}}, \quad (3a)$$

where ‘ $\omega$ ’ is the angular frequency given by ‘ $2\pi f$ ’; ‘ $\mu_m$ ’ is the permeability of the shield metal, and ‘ $\sigma$ ’ is the conductivity of the shield metal specified in mhos/meter. ‘ $Z_w$ ’ is the near-field wave impedance (unit ohms) of magnetic fields given by:

$$Z_w = 2\pi f \mu_w r, \quad (3b)$$

where ‘ $f$ ’ is the frequency of radiation, ‘ $\mu_w$ ’ is the permeability of the material surrounding the shield, ‘ $r$ ’ is the distance from source to shield.

2.) Absorption loss – Effected in the bulk of the material, absorption loss occurs because of the EM waves getting attenuated inside the metal. Absorption loss is defined as:

$$A = 15.6t \sqrt{f \mu \sigma} \text{ dB}, \quad (4)$$

where ‘ $t$ ’ is the thickness and ‘ $\mu$ ’ is the permeability of the shield metal, and ‘ $\sigma$ ’ is the conductivity of the shield metal specified in mhos/meter.

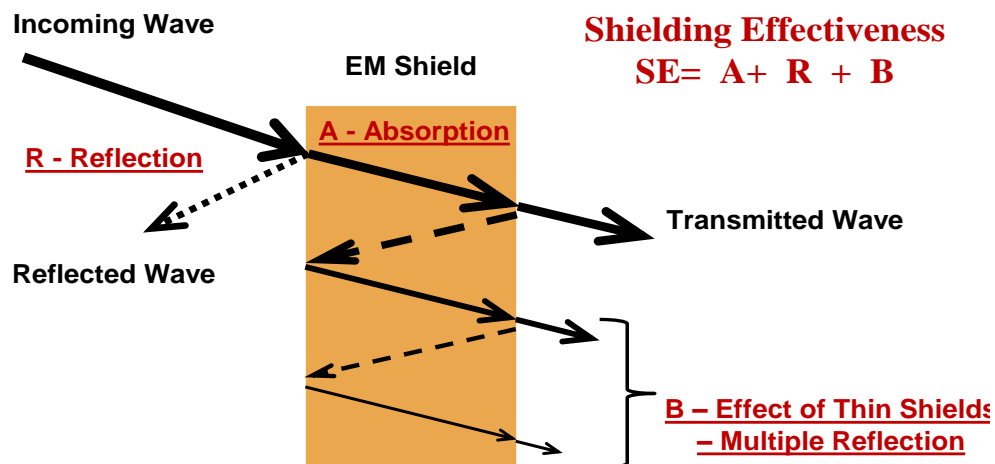


Figure 88. The various mechanisms associated with EM shielding.

Unlike electric fields, the low wave-impedance of magnetic fields in the near-field region makes it difficult to shield them through reflection loss. Usually, a shield with high absorption loss is used – which can be achieved through one of the following properties: large shield thickness, high conductivity, or high permeability. However, in ultra-miniaturized systems the metal thickness cannot be high enough, resulting in low absorption loss. In addition, magnetic materials exhibit high permeability only up to a particular frequency, defined by the material properties. These lead to additional phenomena that need to be considered:

1.) When the metal thickness is less than one skin depth, the wave attenuation due to absorption loss is very less. As a result, the EM waves are strong enough to undergo multiple reflections inside the thin shield layer and produce secondary and tertiary emissions. This essentially reduces the shield effectiveness. This effect is quantified as[40]:

$$B = 20 \log_{10} \left( 1 - q e^{-\frac{2t}{\delta}} \right) \text{ dB} \quad , \quad (5a)$$

where ‘t’ is the thickness, ‘δ’ is the skin depth of the shield metal, in meters and ‘q’ is the ratio between impedance of the shield ( $Z_m$ ) and wave impedance ( $Z_w$ ), defined by:

$$q = \frac{(Z_w - Z_m)^2}{(Z_w + Z_m)^2} \quad (5b)$$

2.) With magnetic materials, the frequency stability of the permeability determines the applicability of the material, and is dictated by the FMR (ferromagnetic resonance) frequency. Because of the above-described phenomena of absorption loss, for a material to act as a shield, the FMR has to be higher than the frequency of interest. The FMR is related to the effective field anisotropy, and is written as:

$$F_{FMR} = \frac{\gamma}{2\pi} H_{Eff} \quad (6)$$

For a thin film with magnetic anisotropy, this resonance frequency is given by:

$$\frac{\omega_{FMR}}{\gamma} = \sqrt{(4\pi M_s + H)H}, \quad (7)$$

Where H is the applied field or the anisotropy field  $H_k$  (in Oe), ' $4\pi M_s$ ' is the saturation magnetization (in Gauss) and ' $\gamma$ ' is the gyromagnetic ratio ( $2.31 \times 10^8$  m/kAs). The equation can be further simplified as

$$FMR (MHz) \sim 2.8 \sqrt{(Sat. Magnetization)H_k} \quad (8)$$

The structure, composition and magnetic anisotropy can be designed to tune the FMR, resistivity and permeability in order to create EMI isolation in the target frequency band. For materials with uniaxial anisotropy, the inherent frequency-stability and magnetic loss are governed by the saturation magnetization ( $M_s$ ) and field anisotropy ( $H_k$ ). Therefore, materials with high  $M_s$  and  $H_k$  are critical for high-frequency (GHz range) EMI shielding with reflection and absorption losses. However, it is important to note that the FMR itself can cause shielding because of its resonance-assisted microwave absorption.

#### Analytical simulations for material selection

To determine the material that is most suited for the shielding application under consideration, the shield effectiveness of different metals and metal alloys were analytically modeled using the material properties such as resistivity, permeability, and FMR. Substrate-compatible metals such as copper, nickel, and aluminum were considered for this analysis, along with nickel-iron (NiFe) and cobalt-zirconium (CoZr). The properties of NiFe and CoZr measured by [16-18] are considered as guidelines. The different material properties are summarized in Table . Magnetic materials lose their magnetic properties (permeability becomes unity) beyond a certain frequency that is specific to each material. This frequency is known as the ferromagnetic resonance (FMR) frequency. Above its FMR frequency, a magnetic material absorbs the

radiation incident on it. The absorption due to ferromagnetic resonance needs to be determined through experimental characterization, and hence was not accounted for in the simulations.

**Table 9**

**List of Material Properties**

<b>Material</b>	<b>Resistivity (<math>\mu\text{ohm-cm}</math>)</b>	<b>Permeability</b>	<b>FMR</b>
Copper	1.68	1	-
Aluminum	2.8	1	-
Nickel	6.99	100	20MHz
CoZr	100	200	3 GHz
NiFe	50	400	1 GHz

Analytical calculations (without FMR effects) were performed to estimate the shield effectiveness of the materials, assuming a distance between source and shield of 0.5mm – the typical separation between components in a miniaturized sub-system. The simulation considers 0.5GHz - 20GHz since this covers the operating frequencies of WLAN and cellular RF modules, including three harmonics. The impact of thickness on shield effectiveness is also studied by varying the metal thickness from 1 $\mu\text{m}$  up to 5 $\mu\text{m}$ . The assumptions for the analytical model include the following:

- Only material properties are compared. Hence the computed shield effectiveness is ideal and independent of the structural effects. When the structural effects are taken into account, the actual shield effectiveness is expected to be lower.
- The EM noise is assumed to be at low power levels, below the saturation limits of the magnetic materials.

Comparison of shielding effectiveness of single-layer shields

The comparison of shield effectiveness between the different materials is shown in Figure 89. It can be observed that copper has the best shield effectiveness because of its low resistivity, followed by aluminum. Nickel and nickel-iron show low shield effectiveness since the frequency-range under consideration is already past their FMR. However, for cobalt

zirconium, since the FMR occurs only at 3GHz, it can be seen that till 3GHz its shield effectiveness is as good as that of aluminum. This effect of reduced permeability beyond FMR can be observed in Figure 89. Since shielding due to FMR is not captured in this analytical model, the actual shielding effectiveness is expected to be higher for Ni, NiFe and CoZr. The effect of metal thickness on shield effectiveness for copper is depicted in Figure 90. It can be seen that the shield effectiveness increases with increasing metal thickness since the dominant shielding phenomenon at these frequencies is absorption loss which depends on the thickness of the shield metal.

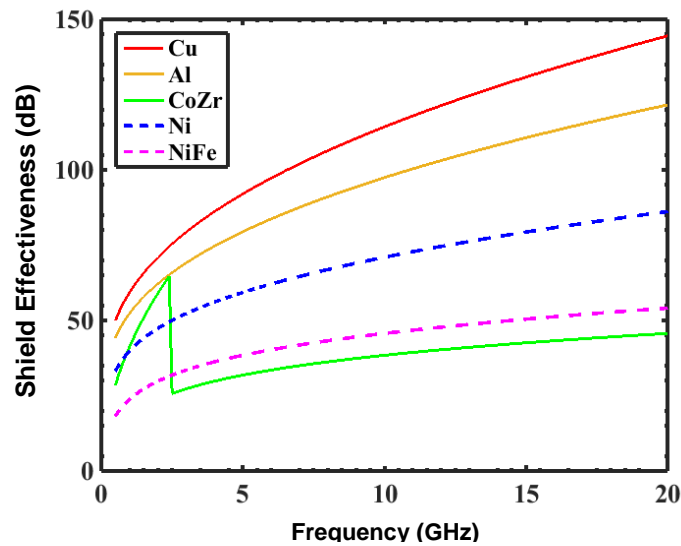


Figure 89. Comparison of shielding effectiveness of different materials.

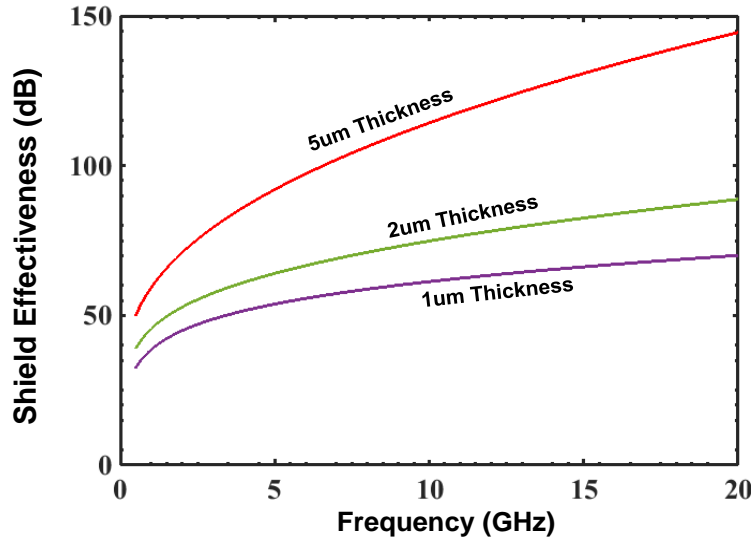
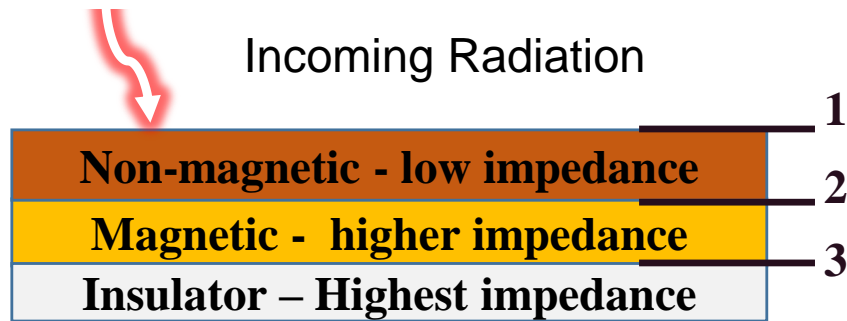


Figure 90. Shield effectiveness with varying thickness of the shield metal.

### Novel multi-layer shield

#### *Stack-up description*

To achieve higher shielding effectiveness using very thin films, a novel material stack-up was developed using a combination of magnetic, non-magnetic and insulating thin-films. The unit stack-up is shown in Figure 91. This unit stack is repeated. From Equation 3a, it can be seen that as the conductivity increases, the shield impedance decreases and as the permeability increases, the shield impedance also increases. Copper has the highest conductivity among the metals in consideration and hence has the lowest shield impedance. NiFe and CoZr have higher permeability and lower conductivity, and hence have higher impedance. The near-field wave impedance of insulators is defined by Equation 3b. Insulators have higher impedance than metals. However, as depicted in Figure 87, the wave impedance of magnetic fields in the near-field is lower than that of electric fields, and also lower than the far-field electromagnetic wave impedance.



**Figure 91.** Proposed unit stack-up.

### *Mechanism of shielding*

Understanding the mechanism of shielding begins with considering an incoming near-field magnetic wave that impinges the shield at Interface ‘1’, as indicated in Figure 91. This wave gets attenuated due to absorption loss in the non-magnetic layer. Since magnetic fields get reflected only when propagating from a low-impedance medium into a high-impedance medium, this magnetic field wave gets reflected only at Interface ‘2’, and not at Interface ‘1’. The reflection can be estimated from the shield impedances for the magnetic and non-magnetic layers, using Equation 2. Upon reflection at Interface ‘2’, a part of the wave continues to propagate further inside the shield. This component, in addition to the attenuation due to absorption loss as it traverses through the magnetic layer; undergoes a reflection at interface ‘3’ between the magnetic layer and the insulator. The advantage of this multi-layer stack is its ability to minimize the effect of multiple reflections that was described using Equation 5a. To understand this effect, an outgoing magnetic field wave is considered after the incoming wave is reflected at Interface ‘3’. This wave does not get reflected at Interface ‘2’ since the impedance of the insulator layer is higher than that of the magnetic layer. Instead, the outgoing wave reflected from Interface ‘3’ experiences the first reflection only at Interface ‘1’ as it propagates from the low-impedance non-magnetic layer into the air medium outside the shield. Thus the presence of non-magnetic layer helps eliminate the effect of multiple reflections in the thin magnetic layer. Further the part of the wave that gets reflected inside at Interface ‘1’ tries to enter the shield

again, but it gets reflected at Interface '2' and then at Interface '3', in addition to getting absorbed in the non-magnetic and the magnetic layers. Hence, reflected waves that re-enter the shield and could potentially manifest as secondary and tertiary emissions out of the shield; are attenuated by a series of absorption and reflection losses. This mechanism is depicted in Figure 92.

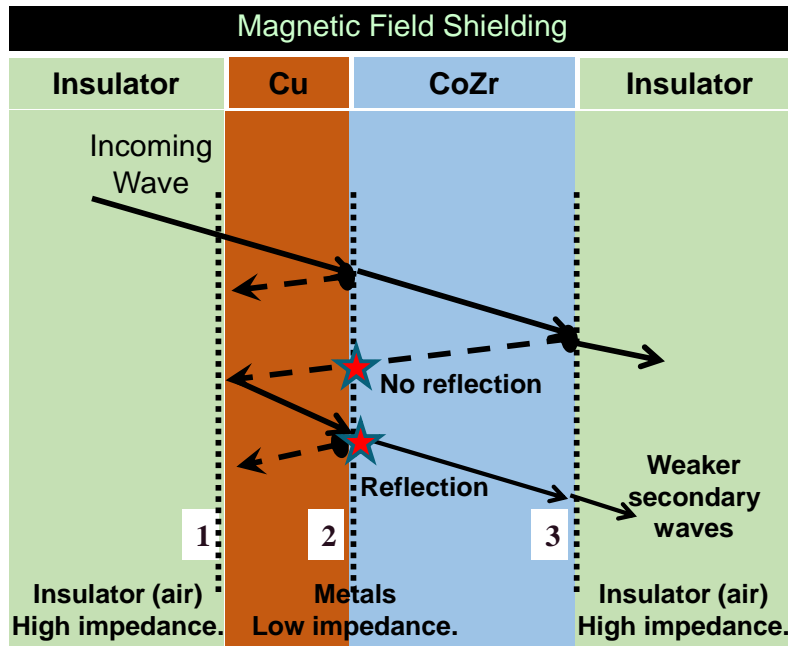


**Figure 92.** Mechanism of EM shielding in the proposed multi-layer stack.

The optimized unit stack consisted of 200nm-thick copper as the non-magnetic layer, 200nm-thick CoZr as the magnetic layer, and 20nm-thick alumina as the insulator. This unit stack was repeated four times, separated by 20nm-thick insulator. The shield effectiveness of this multi-layer stack was simulated using the equations [40] in Figure 31, from chapter 2, and compared with different thicknesses of copper. The simulation result is shown in Figure 93. Here the simulation is shown only till 3GHz since CoZr has a FMR at 3GHz. Beyond this frequency, the FMR absorption would contribute to the shielding performance.

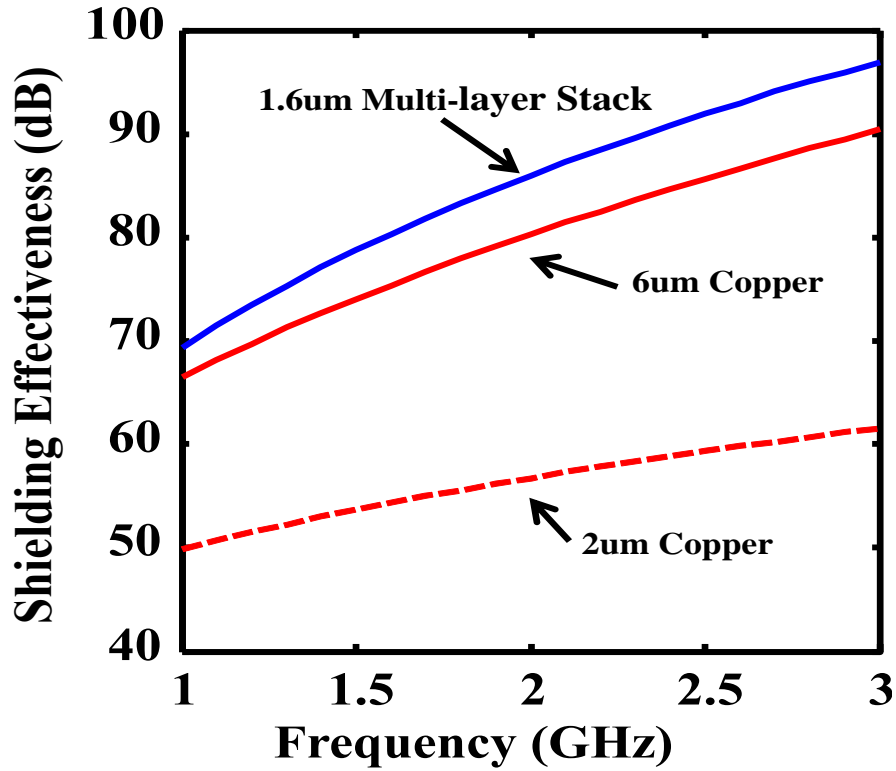


**Figure 93.** Comparison of simulated shield effectiveness of the proposed multi-layer stack and single-layer copper.

Among the various shield material combinations, the most effective and stable choice is copper as it does not have frequency limitations and is compatible with standard substrate fabrication processes. However, a combination of the proposed multi-layer stack and single-layered copper could potentially offer enhanced shielding in 1-3GHz frequency band, and sufficient shielding thereafter, up to 20GHz.

## Modeling and Design of component-level EMI shields

The type of structure that is employed for shielding is an important consideration in shield design. It is also important that the structure is compatible with the fabrication process for easy integration with the rest of the sub-system. In this regard, two types of structures were identified – vias and trenches. The shielding effectiveness of via array is compared with that of trenches, in a multi-layer package substrate through full-wave EM simulations. Transmission lines were used to study the effectiveness of the different shield structures.

### Design rules for via and trenches, Metal thicknesses

The design rules of the substrate under consideration are tabulated in Table .

**Table 10**

**Design Rules for the shield structure**

Parameter	Dimension
Micro-Via diameter, Trench diameter	45 $\mu\text{m}$
Metal thickness	6 $\mu\text{m}$
Dielectric thickness	15 $\mu\text{m}$

### Full-wave EM Simulation setup

The simulations to study the shield effectiveness of structures were performed using HFSS– a full-wave 3D EM simulator, and Sonnet – a full-wave planar EM simulator. The geometries and metal thicknesses of the different elements were constructed based on the design rules mentioned in Table . To study the shield effectiveness, a pair of microstrip transmission lines of length 15mm separated by 180 microns, were considered and the required shield structure was integrated between them. The far-end crosstalk between these lines was employed to compare the shield effectiveness of the shield structures. The set-up is depicted in Figure 94, where each transmission line is terminated with 50-ohms on one end and probed at the other.

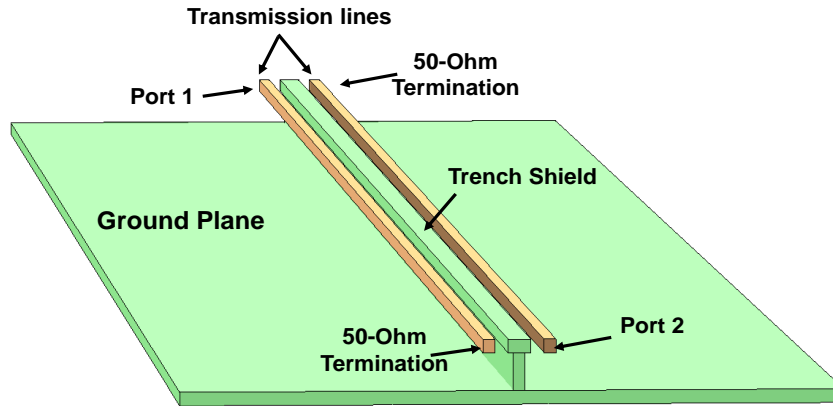


**Figure 94.** Simulation set-up showing transmission lines separated by a trench-based shield.

Simulation results and analysis

The EMI isolation for the via-array and trench were simulated and the comparison of their shield effectiveness is shown in Figure 8. The shield effectiveness of the trench structure was more than that of the via-array, with the highest simulated EM coupling between the transmission lines being 20dB for the via-array and 25dB for the trench.

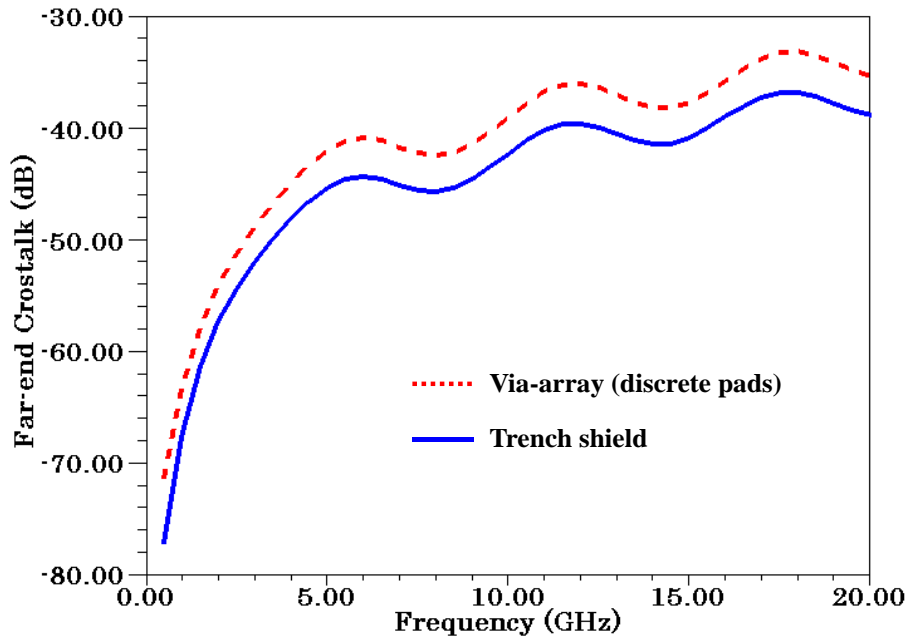


**Figure 95.** Comparison of TL-TL coupling in presence of via-arrays and trenches.

### Via-array shields with continuous via pad

When the via pads on the upper metal layer were merged, as mentioned in [22], it was observed that the shielding effectiveness matched that of trench-based shields. The 3D view of the via-array shields with continuous and discrete pads, is shown in Figure 96. The simulation results of these cases are compared with that of continuous trench, in Figure 97.

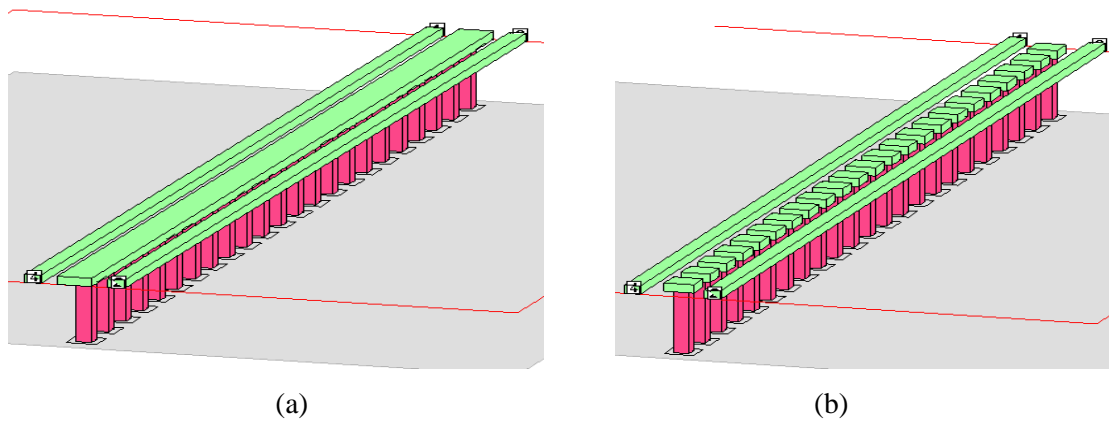


**Figure 96.** Simulation setup of the via-array shields, (a) with continuous via pad, and (b) discrete via pads.

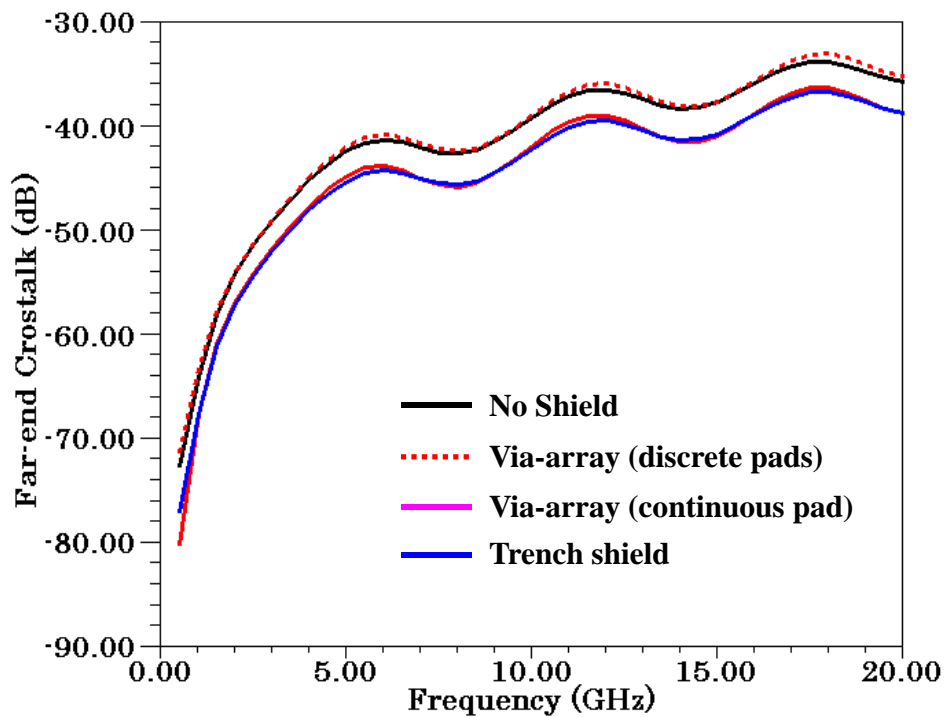


**Figure 97.** Comparison of TL-TL coupling in presence of trenches and different via-arrays configurations.

Figure 97 indicates that a via-array shield with discrete pads does not reduce the coupling between the transmission lines. Alternatively, when the pads are merged, the reduction in coupling due to via-array shield is the same as that due to a trench-based shield. This is explained in Figure 98. Since the lowest frequency of propagation depends on the largest aperture, the small aperture in the via-array with the continuous pad prevents the frequencies in 1-20GHz from propagating through the shield; whereas, in case of the via-array with discrete pads, the unbounded aperture allows all frequencies to pass through.

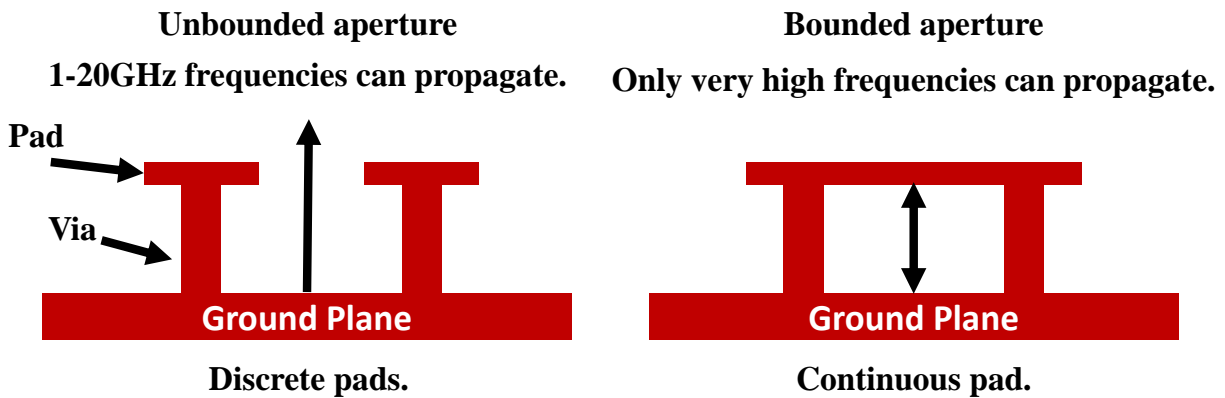


**Figure 98.** Lateral view of via-array shields to compare the aperture for different scenarios.

*Extended trench-based shields*

The coupling between two microstrip transmission lines was also simulated with the trench-based shield extended vertically upwards such that it was taller than the transmission lines. The height of the trench above the transmission line was set at 20 $\mu$ m and 40 $\mu$ m, and the couplings between the transmission lines were studied. Since microstrip transmission lines are referenced to a ground plane only on the bottom, they radiate more above the plane containing the signal lines. The presence of a trench shield above the plane of the transmission line was found to improve the shielding between the transmission lines. The 3D view of the trench-based shield extending above the plane of the signal lines is shown in Figure 99. The couplings

between the transmission lines for both vertical heights were compared through simulations and are shown in Figure 100. It can be seen from Figure 100 that, as the height of the trench above the transmission line increases by 20 $\mu\text{m}$ , the coupling reduces by 3dB. Typical tradeoff while employing such trenches would involve a compromise between the shield effectiveness and the maximum thickness of trench that can be fabricated above the plane of a transmission line.

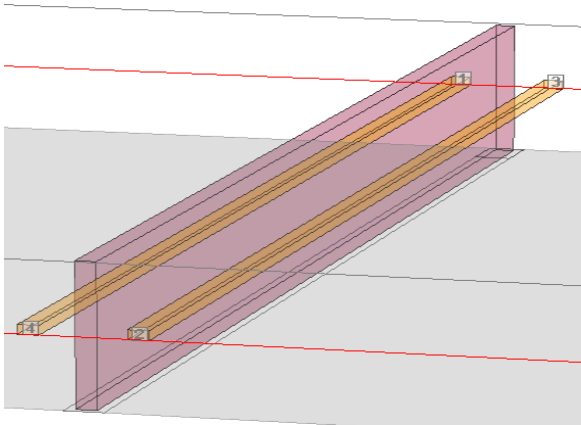


**Figure 99.** 3D view of the trench-based shield extending above the plane of the signal lines.

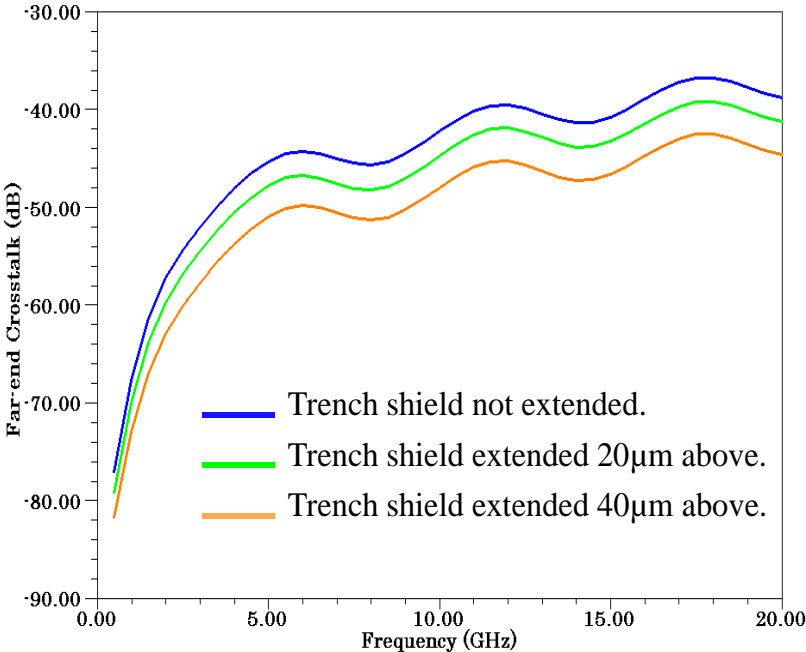


**Figure 100.** Comparison of TL-TL coupling for different trench configurations.

## Fabrication and characterization of EMI shields

A layout of the transmission lines was designed as per the simulation set-up, and fabricated on a glass substrate. The advantage of the proposed trench structure is its ability to be integrated into standard substrate fabrication processes without increasing the process steps [19]. The first step in the fabrication involves cleaning of the glass followed by polymer lamination. Next, through package vias (TPVs) are formed using laser ablation. After the TPVs are formed, using a double-side wet metallization process, the core and TPVs are metallized and patterned. Following this, the build-up polymer was laminated on both sides of the substrate. The shielding trenches and the micro vias were simultaneously formed on the build-up through laser ablation using ultraviolet laser. The top-view of the substrate, after the micro vias and the trenches are formed, is shown in Figure 101. The metallization of the trenches was carried out along with the metallization of the micro via and the build-up metal pattern. The process flow of the fabrication is depicted in Figure 102. An image of the fabricated structures is shown in Figure 103.

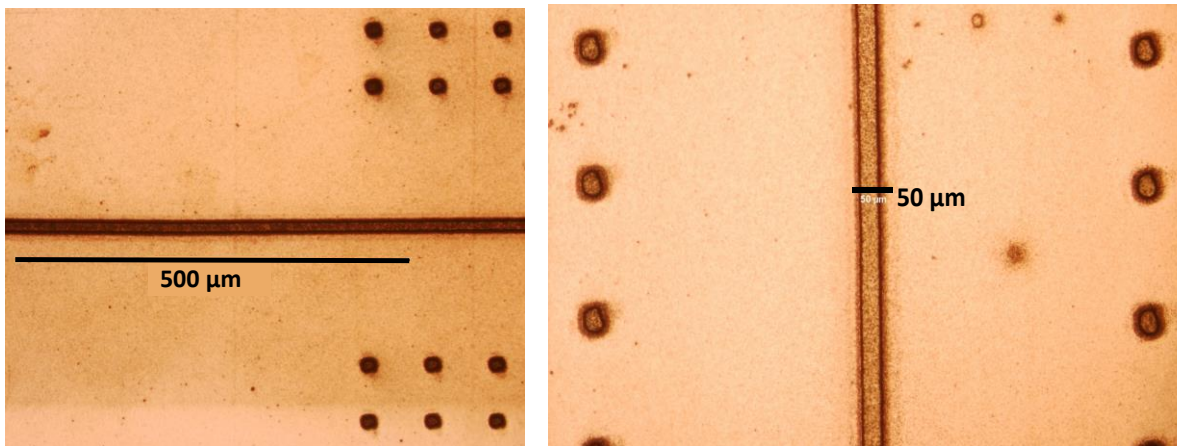
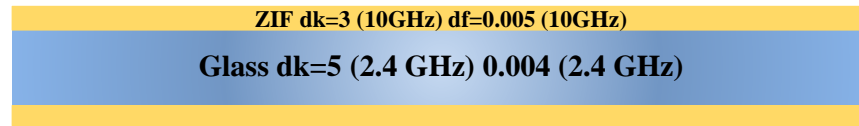
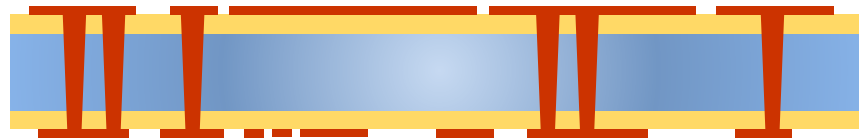


**Figure 101.** Top-view of the substrate with the laser-ablated trench and blind-vias.

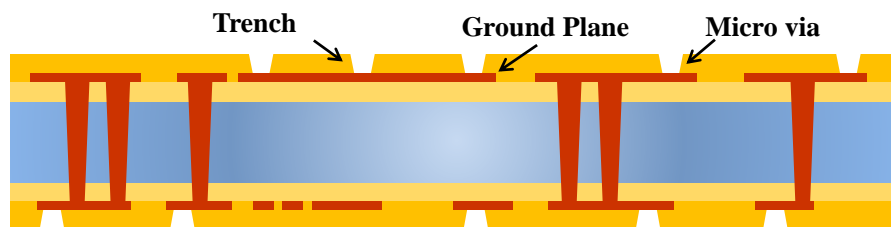
**Laminate the Polymer on 100 um Glass**



**TPV drilling, copper deposition, lithography, patterning**



**Build-up Polymer lamination and micro-via + trench drilling**



**Metallization of micro-via and trenches**

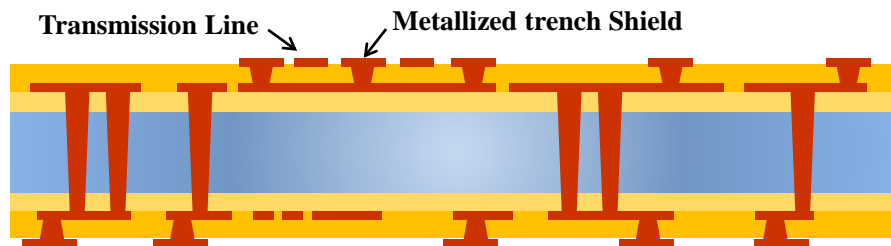


**Figure 102.** Fabrication process of multi-layer glass substrates.

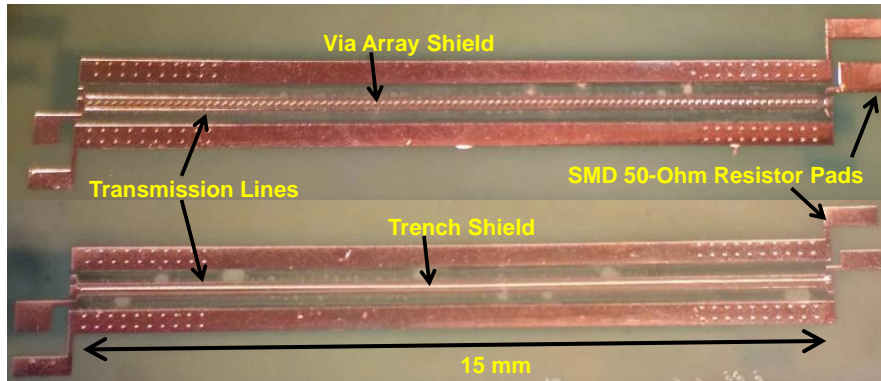


**Figure 103.** Transmission lines with via-array and trench shields, fabricated on ultra-thin glass substrates.

After the substrate fabrication, 50-Ohm SMD resistors were assembled onto the coupons to terminate the lines. Following this, RF characterization was carried out using GSG RF probes with a vector network analyzer. To characterize the EM interference between the lines, two-port S-parameters were measured. The results showed reasonable correlation with the simulations, with the trench structures offering up to 20dB of additional isolation between components, compared to via-array shields with discrete pads. Thus, the measurements demonstrate increased shielding effectiveness with trench structures compared to via-array shields, while also validating the simulations.

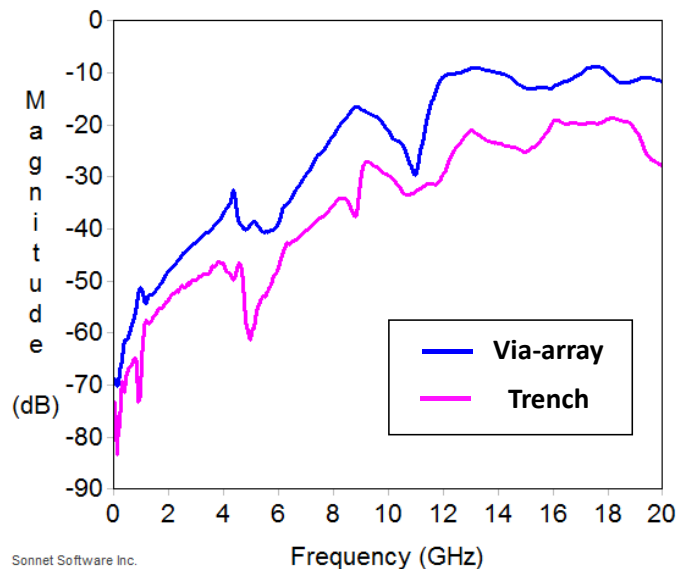


**Figure 104.** Comparison of measured TL-TL coupling in the presence of via-arrays and trenches.

## Summary

Component-level electromagnetic interference shields were developed for miniaturized WLAN RF modules, enabling 30dB – 60dB isolation in the frequency range of 1- 20GHz, between passives separated by less than 100 $\mu$ m. Trench-based shields having a width of 45 $\mu$ m were modeled, designed, fabricated and characterized to provide up to 20 dB of additional shielding between a pair of transmission lines, compared to via-array shields. To accomplish this objective, four sub-tasks were defined: a.)Modeling of EM radiation in RF modules, b.)Analytical modeling – Material and multi-layer stack-up design, c.)Modeling and design of component-level EMI shields, d.)Fabrication and characterization of EMI shields.

Electromagnetic coupling between various passives elements namely inductors, capacitors, TPVs and transmission lines was studied through 3D EM simulations. Component-dimensions from typical RF module designs were employed, with 400 $\mu$ m spacing between the components. The worst-case coupling for each pair of components was studied and it was observed that the coupling between two unmatched transmission lines was the maximum, followed by the coupling between two planar spiral inductors. Parallel-plate capacitors and transmission lines were found to interfere the least with each other and with other components. Based on these results, a simple set of guidelines were defined for the placement of such passives.

Analytical simulations were used to estimate the shield effectiveness of various single-layer and multi-layer shield materials. A novel multi-layer stack comprising 200nm of copper, 200nm CoZr and 20nm alumina was proposed. Analytical simulations showed that in the frequency range of 1-3GHz, the proposed multi-layer stack offered 6X reduction in thickness over single-layered copper shield. However, for the frequency range of 3-20GHz, copper was found to be more effective and stable shield material.

The shielding effectiveness of via-array-based shields and trench-based shields were compared through modeling, simulation and fabrication. It was deduced through simulations that trench-based shields were more effective in suppressing EM coupling between two transmission

lines, than via-array-based shields, when the via pads on the upper metal layer were discontinuous. However, when the via pads were merged together, the via-array was found to be as effective as trench-based shields in providing isolation. Further, when the trenches were extended vertically upwards by 20 - 40 $\mu$ m, the shield effectiveness was observed to increase by up to 6dB.

Glass substrates with four metal layers were fabricated to test the shield effectiveness of trenches and via-array-based shields. The trenches and via-array-based shields were fabricated and metallized using the standard multi-layer fabrication process without any additional process steps. Integration of these shield structures do not contribute significantly to the size of the module. It was observed that the trench-based shields offered up to 20dB of additional EM isolation between two microstrip transmission lines compared to via-arrays. The measurements also validate the 3D EM models and simulations, and establish their extensibility to other scenarios.

## **CHAPTER 5**

### **DESIGN AND DEMONSTRATION OF MINIATURIZED RF MODULES**

The final task is to model, design and demonstrate glass-based WLAN RF modules with low-loss embedded passives, LNA dies, and integrated component-level EMI shielding; using the 3D IPAC concept. The first part of the WLAN RF module demonstration consists of embedded thin-film passives and chip-last embedded actives using ultra-short Cu-Cu interconnections, on ultra-thin organic substrate. However, glass is expected to be the mainstream substrate material in future RF modules because of its several advantages described in Chapter 1 and 2. Therefore, the second part of the module demonstration focuses on glass-based RF WLAN module demonstration. The key innovations in the 3D IPAC glass module are miniaturized passives and EMI shields, double-side thin-films, through-vias in the substrate, and chip-last embedded actives integrated using low-temperature Cu-Cu interconnections. Double-side active component assembly, although feasible, is not a part of this 3D IPAC demonstration.

#### **Objectives**

The objectives of this task are to model, design, fabricate and demonstrate miniaturized WLAN RF modules with less than 1dB passive insertion loss, more than 20dB adjacent-band attenuation, and, less than -40dB internal noise-coupling using the 3D IPAC concept, as listed in Table .

**Table 11****Targets for Module Design**

<b>WLAN RF Receiver module</b>	Diplexer + LNA dies	<b>Design:</b> <ul style="list-style-type: none"> <li>• Miniaturized diplexer design using novel design schematic;</li> <li>• Integrated EM isolation shield using trench structures;</li> <li>• Glass substrate with through-vias and precision RDL;</li> <li>• Low loss substrate and dielectrics;</li> <li>• Ultrashort interconnect lengths with 3D integration</li> </ul>
<b>Passive Insertion loss</b>	<= 1 dB	
<b>Adjacent-band Attenuation</b>	>= 20 dB	
<b>Internal Noise Coupling</b>	< -40 dB	
<b>Frequency of operation</b>	2.4 GHz – 5 GHz	
<b>Reduction in X-Y size</b>	1.5X	<b>3D IPAC concept:</b> <ul style="list-style-type: none"> <li>• High component density:</li> <li>• Embedded components</li> </ul>
<b>Reduction in thickness</b>	2X	<ul style="list-style-type: none"> <li>• Ultra-thin 100um glass substrate with embedded passives.</li> </ul>
<b>Cost</b>	2X reduction	<ul style="list-style-type: none"> <li>• 500 mm x 500 mm panels</li> </ul>

**Module Description**

As described in Chapter 1, 3D IPAC concept is employed to design the WLAN RF receiver module in a) organic substrates to demonstrate miniaturization with enhanced performance using embedded filters and chip-last embedded actives, b) glass substrate with innovative embedded passives and shielding. The corresponding sub-tasks for each of these modules are: 1) Module design and EM simulation, 2) Fabrication, and 3) Characterization and model validation.

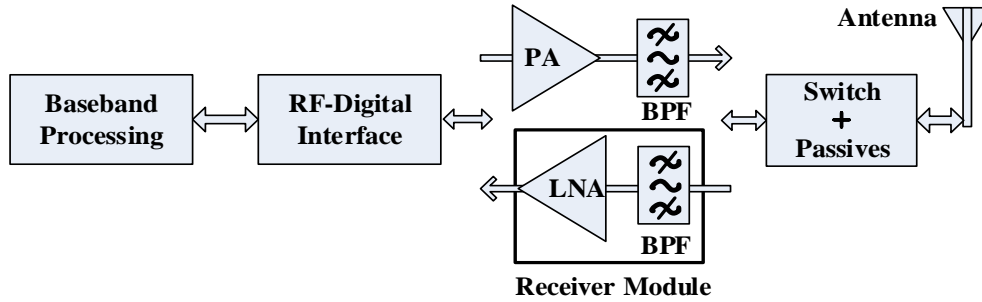


**Figure 105:** Components of a WLAN sub-system.

A typical WLAN RF receiver module consists of an LNA and a BPF, as represented in Figure 105. Two Gallium Arsenide (GaAs) actives are integrated with a WLAN band-pass filter to achieve adequate adjacent-band isolation for WLAN. When dual-band operation of the LNA is required, the BPF is replaced with a diplexer. Low-parasitic thermo-compression Cu-Cu interconnections are employed to interconnect the actives to the substrate. Further, the interconnection length and parasitics between the actives and passives is minimized by employing embedded passives. For this work, the dies are obtained from TriQuint Semiconductor, Inc. [60].

## Design and simulation of WLAN RF Module on Organic Substrate

### LNA schematic

The LNA schematic is shown in Figure 106. Only the 2.4 GHz side of the die was used for design and measurement. Both the RF chains at 2.4 GHz and 5 GHz operate independently. They are enabled by a switch die inside TriQuint's module. For example the 2.4 GHz chain can be enabled by supplying 3.3V on Pin 6 in TriQuint's current wire bond package. The input and output matching circuitry are located on the die. Two external decoupling capacitors (100pF on Pin 6 and 1 $\mu$ F on Pin 5) are required for operating the 2.4 GHz low noise amplifier.

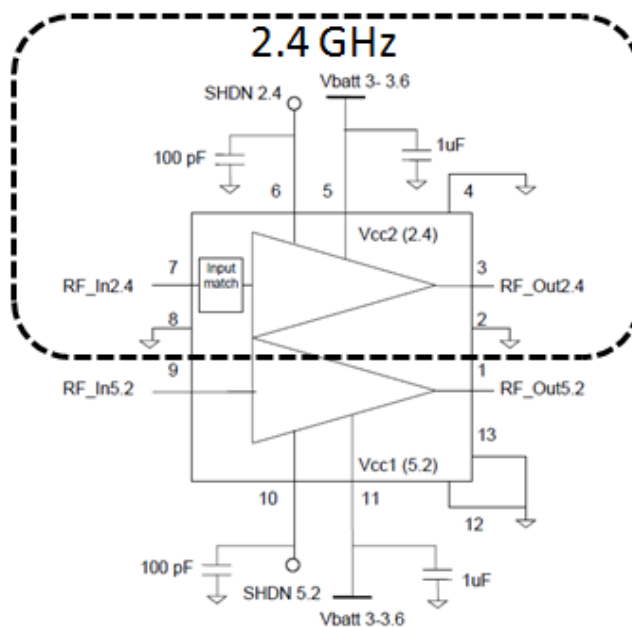


**Figure 106:** LNA Module schematic, as seen on TriQuint's datasheet.

### Substrate stack-up and design rules

To realize miniaturized high-Q passives, ZEONIF™ XL (X-L) – a low-loss organic material has been employed. Developed by Zeon Corp., X-L is a halogen-free glass-fiber-reinforced polymer laminate. The cross-section of the stack-up is illustrated in Figure 107.

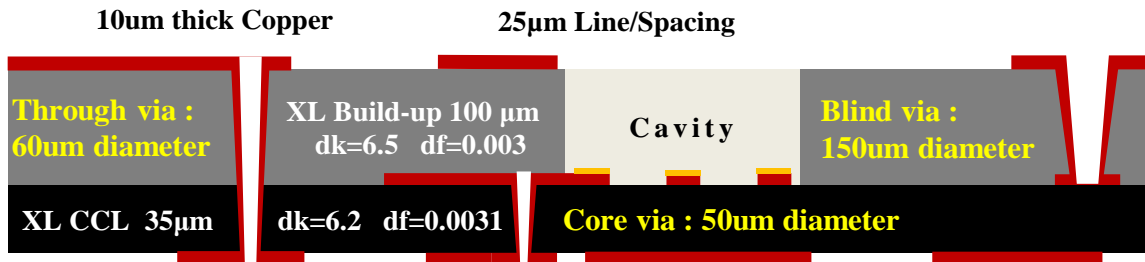
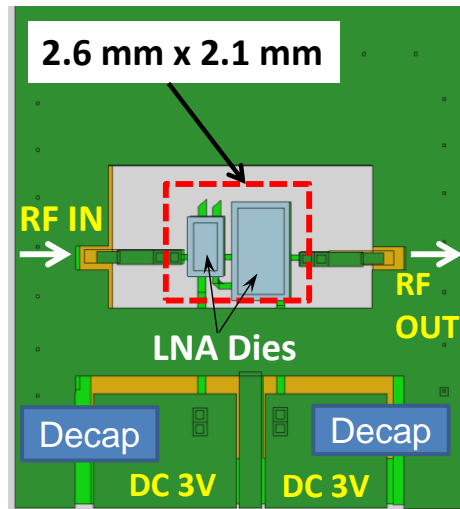


Figure 107: Stack up structure of the 3 metal-layer module.

The substrate stack-up consists of a core layer and a build-up film. To achieve this stack-up, a 100 µm-thick X-L prepreg (Dk=6.5, Df=0.0035) was laminated onto one side of an X-L copper-clad laminate (CCL) core (Dk=6.2, Df=0.0031) of thickness 30 µm.

### LNA module design

To demonstrate miniaturization without degradation in performance over the original LNA package (without filter), a LNA module was designed using only the LNA dies. The module consists of two embedded LNA dies, along with RF signal transmission-lines and DC power supply rails. The RF transmission lines were designed for 50Ω impedance. The dies were embedded in a cavity formed in the 100 µm-thick build-up layer, and were connected to landing pads on metal layer M2 with very short (15µm height) copper-copper interconnections using thermo-compression bonding [61]. Since the separation between the active side of the die and the ground plane (M3) is only 30 µm, the copper on M3 was etched away under the dies, to avoid eddy-current losses in the on-chip inductors. Metal patches were added to the power-supply rails on M1, to facilitate surface assembly of the decoupling capacitors. The LNA module occupied an area of 2.6 mm x 2.1 mm, as shown in Figure 108. However, the coupon for this module was designed bigger, to accommodate additional structures that aid in characterization. The thickness of this module is 160 µm.



**Figure 108.** Top view of M2 layer in the LNA module design.

### Filter design in organic substrates

The receiver module design essentially integrates the LNA module with an embedded band-pass filter. The circuit schematic of the filter was simulated using Agilent ADS [62]. Based on the schematic, the layout of the filter was designed and optimized using SONNET EM simulator [63] and is shown in Figure 109.

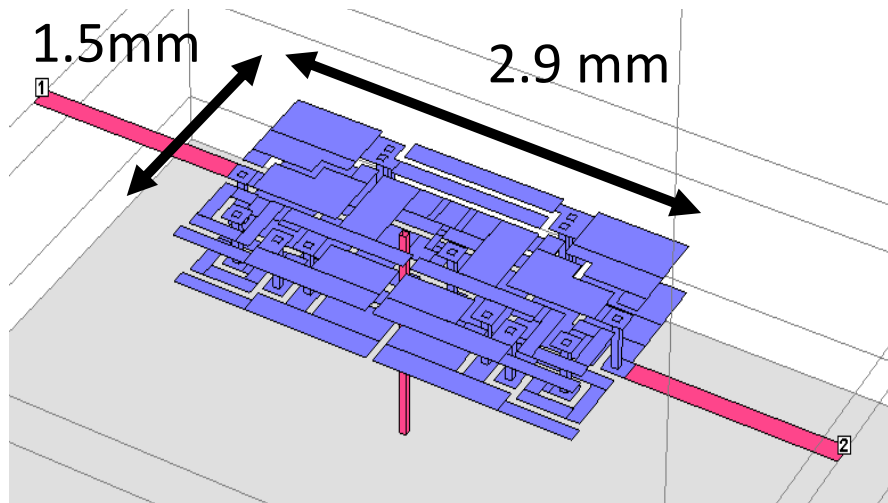


**Figure 109:** Layout of the WLAN band-pass filter

To achieve the highest capacitance density, the capacitors were designed between metal-layers M2-M3 across the thinner dielectric layer. The inductors were designed as two-layered structures across M2-M3 as well. This helped in increasing the mutual inductance. The metal on layer M1 was assigned as the ground plane of the filter. To minimize the effect of ground parasitics, all the capacitors on M2-M3 were designed as stitched capacitors [64]. The filter occupied an area of 1.5 mm x 2.9 mm and its simulated response is shown in Figure 110.

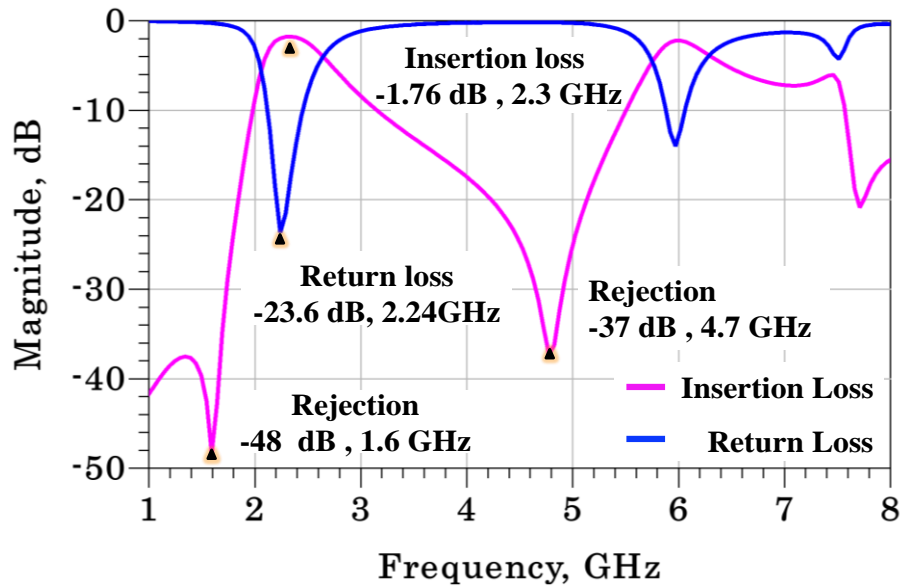
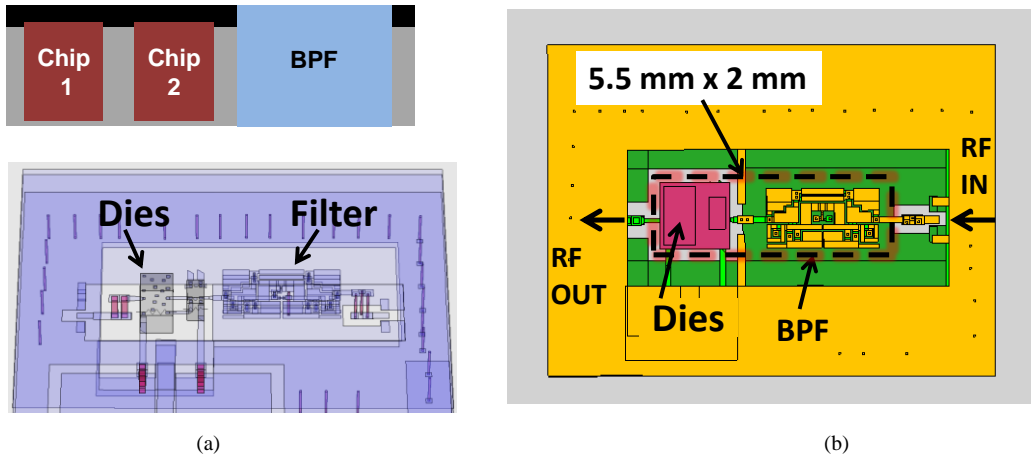


Figure 110: Simulated performance of the BPF.

#### WLAN RF Receiver module design on organic substrate

For the receiver module design, the BPF was integrated with the LNA module design such that the BPF is in the RF path from antenna to the LNA. For the characterization of this module, the antenna was substituted with a set of RF-probe pads. The schematic cross section, 3D view and top-view of the receiver module layout is shown in Figure 111. Its dimensions are 5.5 mm x 2 mm x 0.16 mm.



**Figure 111:** WLAN receiver module (a) schematic cross section and 3D view, and (b) top view.

### Full wave 3D EM simulation

The entire receiver module layout was simulated using HFSS [65], a 3D full-wave EM solver. The simulation flow shown in Figure 112 was employed.

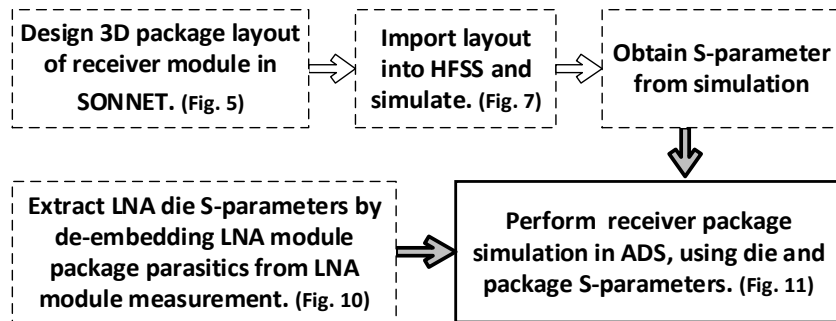


**Figure 112.** Simulation flow used for analyzing the receiver module layout.

The receiver module layout design was imported into HFSS, and set up for simulation. Setting-up the model included the following: a) specifying the substrate dimensions and assigning stack-up materials, b) creating tapered, conformally-metallized vias similar to the ones in the fabricated sample, c) defining metal types and thicknesses, and d) assigning ports. The metal thickness was set as 10  $\mu\text{m}$  on all the layers. Since EM models of the dies were not available, the input and output terminals of the dies were replaced with lumped ports. Further, to

include the effect of the die on the package resonances, a perfect electric conductor (PEC) sheet was introduced at the location of the die active surface. To capture any noise coupling from the power supply network to the receiver module input, a lumped port was located in the DC pads as well. The simulation was set-up for a driven terminal solution. A frequency sweep from 100 MHz to 20 GHz was defined in steps of 100MHz. The top view of the 3D model in HFSS is shown in Figure 113, identifying the die cavity, the BPF and the ports. This model was simulated and its S-parameters were obtained.

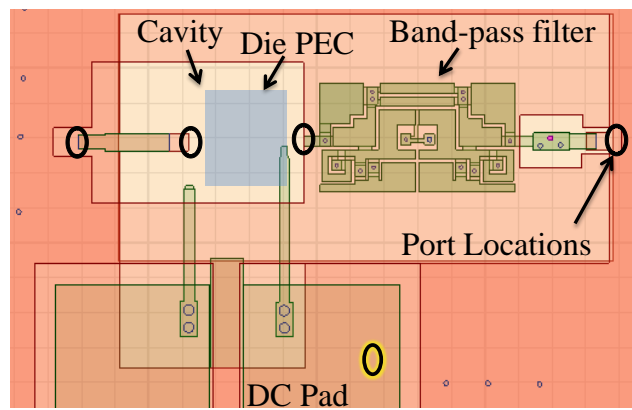


**Figure 113:** Top view of the WLAN receiver 3D model.

The signal loss in the input and output paths, and the coupling from the DC pads to the RF signal path is studied. The input signal path contains the BPF and its loss is 1.7dB as observed from Figure 110. The insertion loss of the output signal path is shown in Figure 114. It can be seen that the insertion loss at 2.4GHz was 0.3dB and return loss 15dB. Additionally, the noise coupling from the power supply network to the signal input and output paths was also obtained as shown in Figure 115. Very low noise coupling at the input is critical since the input signal level is low and any additional interference would lower the signal-to-noise ratio (SNR) at the input. It can be observed that even the worst-case noise coupling at the input is as low as -40dB, up to 10GHz. Thus the low insertion loss of the signal path and low noise coupling inside the package indicate that the noise added by the package is very low.

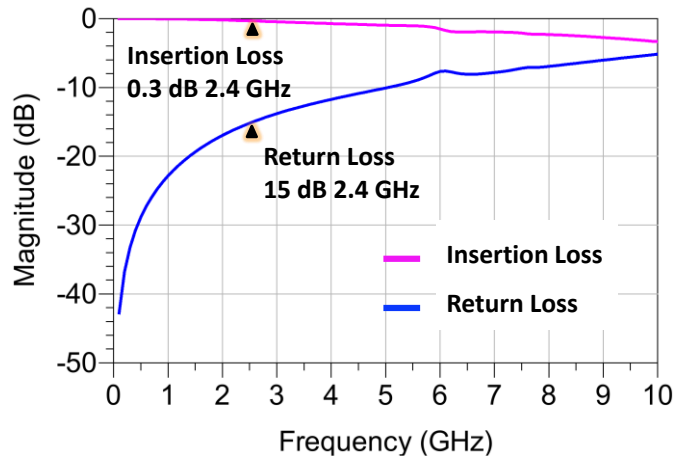


**Figure 114:** Characteristics of Output RF Signal Path.

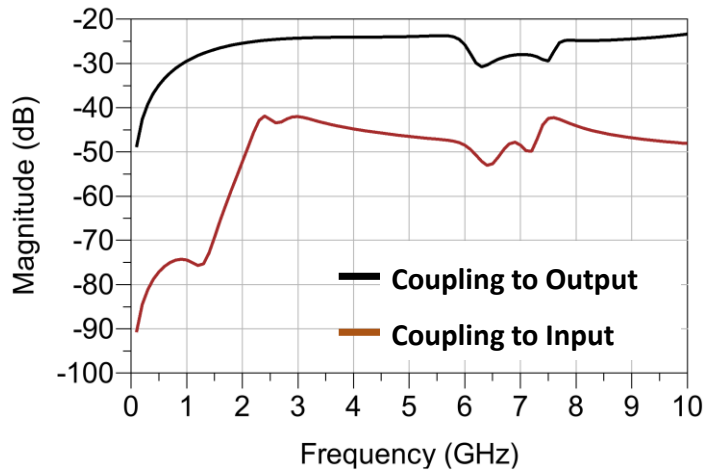


**Figure 115:** Coupling from DC pad to RF signal path.

Next, to obtain the S-parameter model of the LNA dies, the set-up shown in Figure 116 was used. First, the S-parameters of the package interconnections of the LNA module (no filter) were obtained through 3D EM simulations using HFSS. Following this, the LNA module (without filter) was fabricated and characterized. Then, the simulated S-parameters of the package interconnections were de-embedded from the characterized results of the LNA module. This yielded the S-parameter model of the LNA dies.

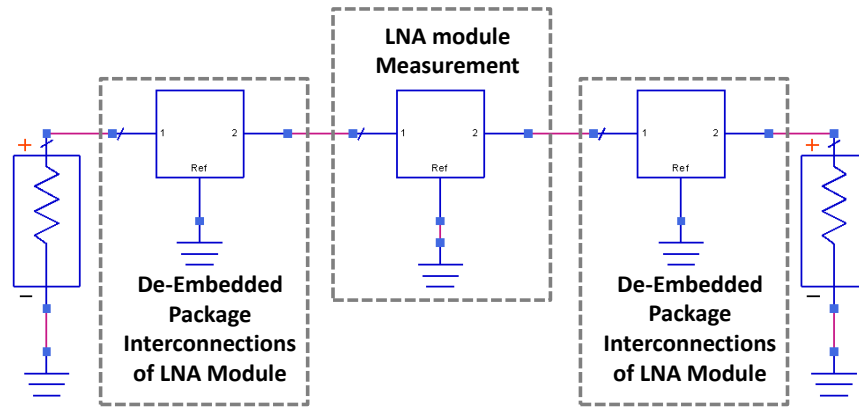


**Figure 116.** Agilent ADS set-up to extract LNA die S-parameters.

To simulate the complete receiver package along with the dies, the simulated S-parameter model of the receiver package and the de-embedded S-parameter model of the LNA dies were imported into Agilent ADS, as shown in Figure 117.

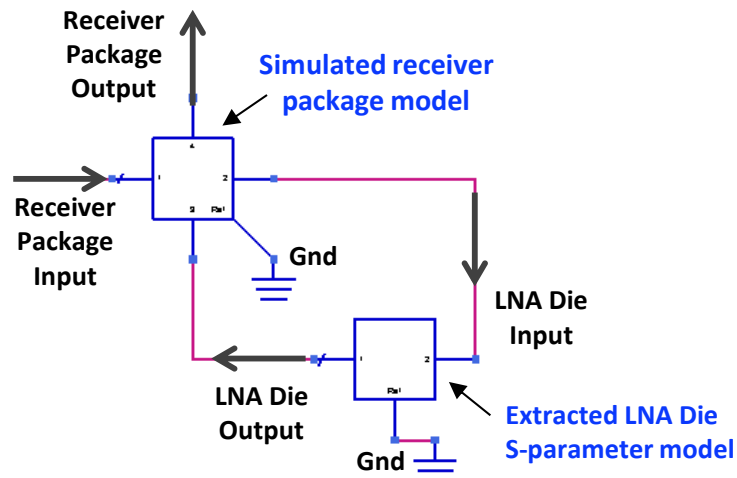


**Figure 117.** Complete package model created in Agilent ADS, indicating signal flow.

The die model was connected to its corresponding input-output port locations on the receiver package model. This set-up was then simulated in Agilent ADS to obtain the S-parameters of the complete package, as shown in Figure 118.

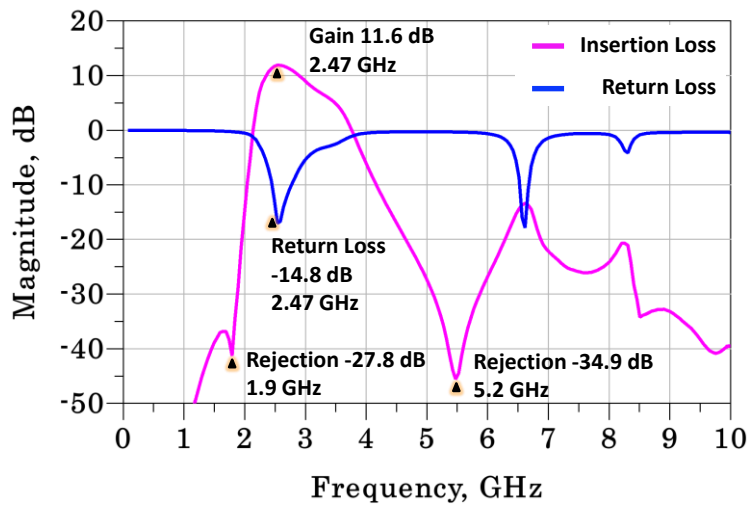


**Figure 118.** Complete receiver model simulated using HFSS and Agilent ADS.

## Fabrication, Assembly, and Characterization of RF Module on organic substrates

The module layout was panelized into a test-vehicle for fabrication. The top-view image of the test vehicle layout is shown in Figure 119.

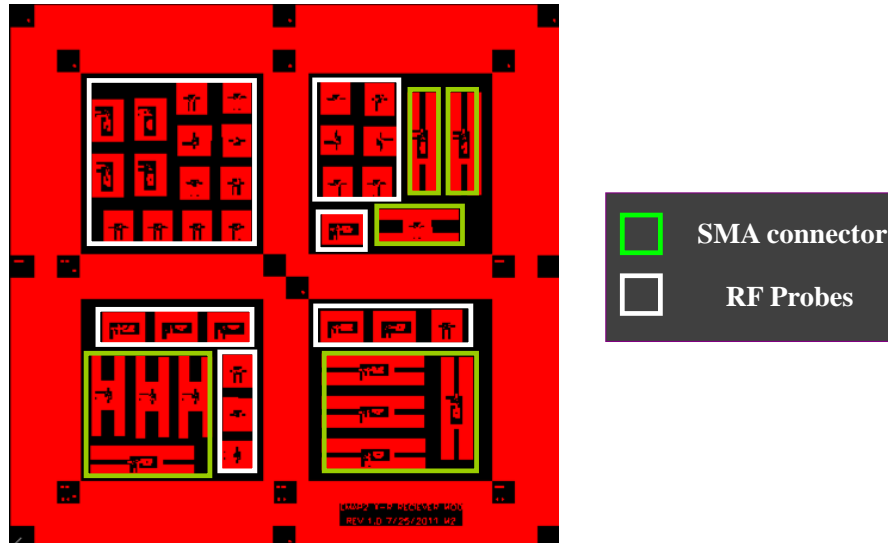


**Figure 119:** Image of the test vehicle mask layout.

The fabrication process steps are depicted in Figure 120. To achieve a good yield especially for the copper features with 30 $\mu\text{m}$  spacing, semi additive process (SAP) was employed for the metal patterning. The first step of substrate fabrication was the drilling of through-vias in the XL CCL using LASER, to obtain vias of diameter 50  $\mu\text{m}$ . Next, electroless plating was performed to metallize the vias with a seed layer of 1  $\mu\text{m}$  (Steps 1-2). This was followed by photoresist lamination on the top side and photolithography to pattern the photoresist so as to expose only the regions where the copper needs to be retained (Step 3). Subsequently, electrolytic plating was performed to increase the thickness of the exposed copper (Step 4). Once the thickness of the plated copper was close to 10  $\mu\text{m}$ , the photo-resist was stripped away and the seed layer removed through micro-etching (Step 5). Then, the prepreg material was laminated on the top side of the core (Step 6), followed by blind via drilling and metal patterning through subtractive etching (Steps 7-8). Finally cavities were formed on the

build-up layer for die embedding and nicked-gold surface finish was applied to the copper traces (Step 9). An image of the substrate just before assembly, along with an image of the top view of the cavity containing copper traces and die landing pads, is shown in Figure 121.

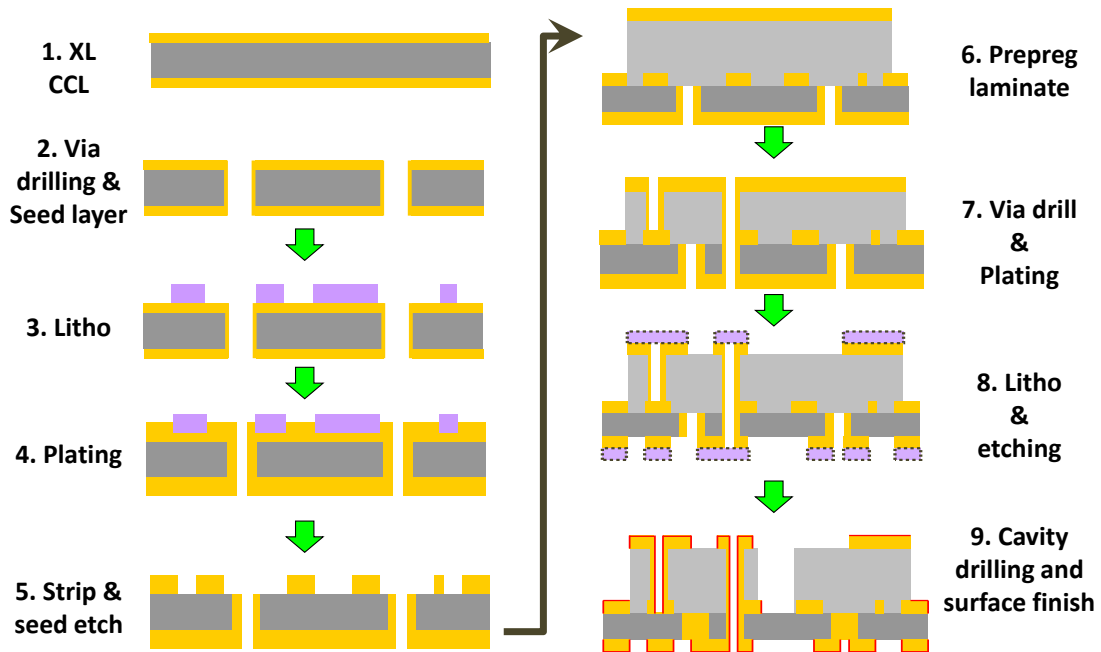


**Figure 120:** Fabrication process steps.

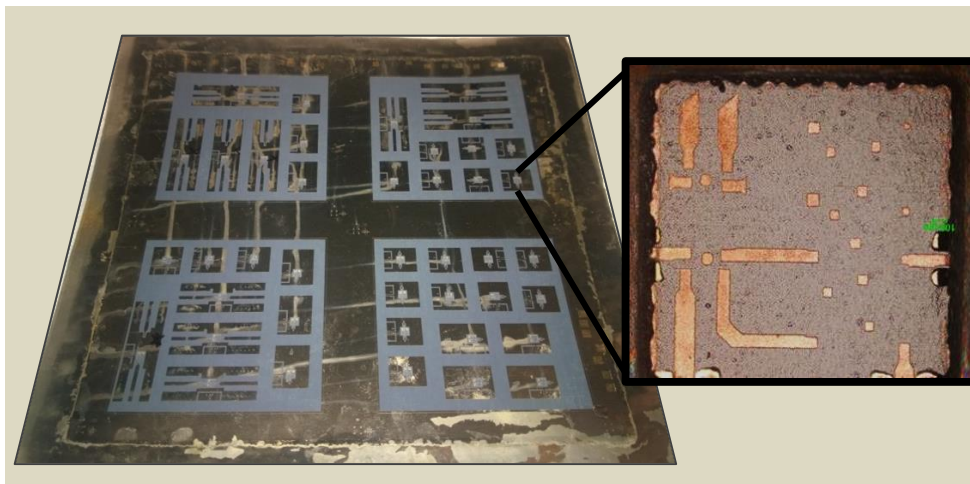


**Figure 121:** Images of, a) substrate prior to assembly, and b) top view of die cavity.

## Assembly

The ability to perform intermediate testing with chip-last approach helped determine the yield of the BPFs through characterization, prior to die assembly. The two LNA dies and the decoupling capacitors were assembled on tested “known-good” coupons. The top view of the assembled receiver module and its X-ray image [4] are shown in Figure 122. The ground planes on the backside of the dies were wire-bonded to each other and to the ground islands on the substrate. Multiple wire-bonds were used to achieve a low-inductance short between the substrate ground and the dies’ ground. After assembly, the modules were characterized using a Vector Network Analyzer (VNA), to study the model-to-hardware correlation. A cross-section of the fabricated receiver module is shown in Figure 123.

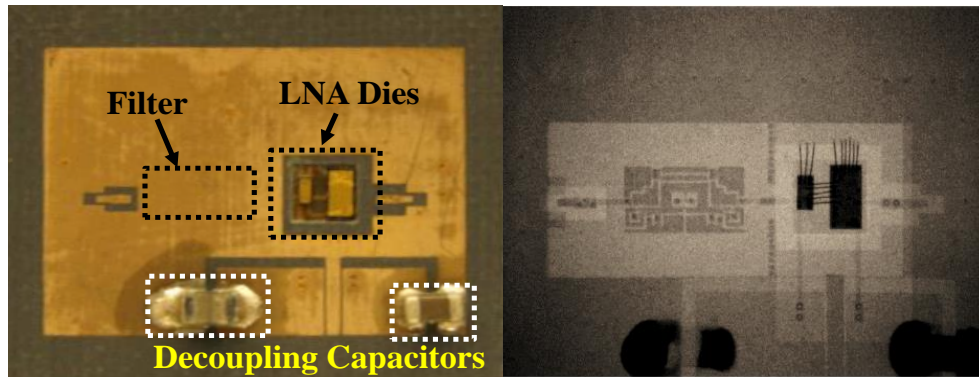


**Figure 122:** RF receiver module after assembly (left: top view, right: X-ray image).

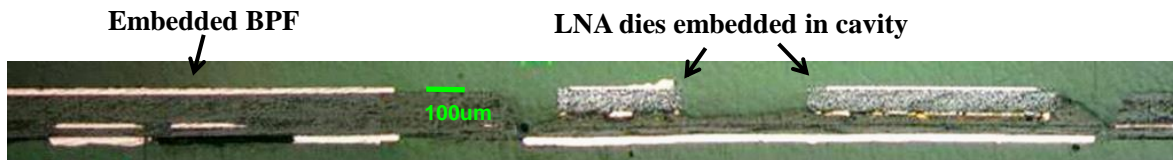


**Figure 123:** Cross section of RF receiver module.

## Characterization

After assembly, the modules were characterized using the following set-up:

- GSG RF probes: 500  $\mu\text{m}$  pitch,
- DC Supply: 3.3V, 14mA
- Two-port VNA,
- Short Open Load Thru (SOLT) Calibration.

The measured response of the LNA module is shown in Figure 125. The peak gain at 2.4 GHz was 14.13 dB with more than 15dB return loss. It is noteworthy that the measured gain of the LNA module is comparable to its datasheet performance [60] despite the fact that the LNA dies were designed and optimized for a wire-bond package.

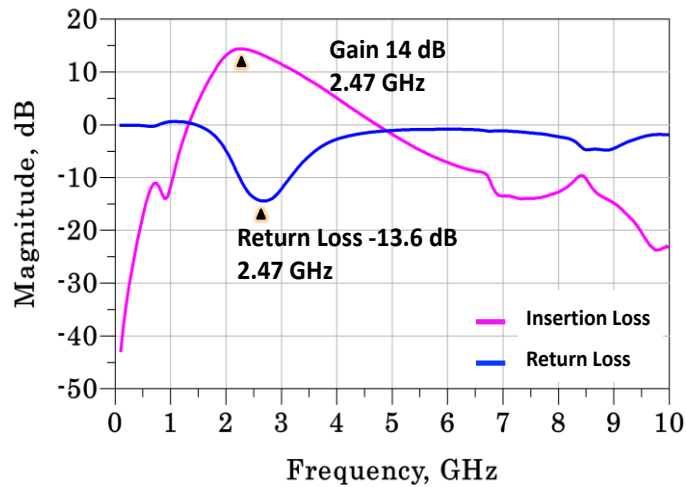


**Figure 124.** Measured response of LNA modules.

The measured response of the receiver module is shown in Figure 125. The peak gain of the receiver module was 11dB, and the gain at 2.4 GHz was 9.2dB, with more than 25dB adjacent band rejection (at 5.2GHz). The isolation of GSM band at 1.9GHz was 32dB. The shift in peak gain was attributed to the pass band of the BPF shifting to 2.6 GHz, reducing the gain of the receiver module at 2.4 GHz.

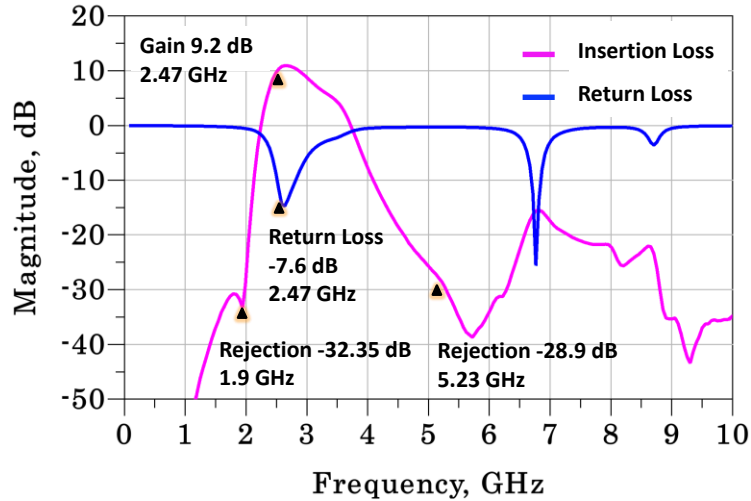


**Figure 125:** Measured response of RF receiver module.

### Analysis and Model validation

A comparison between the performances of the 3D full-wave EM simulation of the BPF and its measurement is shown in Figure 126. A slight drift in the performance, towards the higher frequencies was observed and is attributed to process variations that potentially cause a reduction in the capacitor or inductor values. Good correlation between the complete receiver package simulation and its measurement can be observed from Figure 127. This validates the simulation method employed to estimate the combined performance of the chip and package. The characterization result indicates more than 20dB suppression of the adjacent frequency band at 5-6GHz, with a package loss of 3dB, despite achieving 1.5X volume miniaturization, because of the low-loss substrate, shorter interconnection (Cu-Cu) between the die and the substrate, and chip-last embedding technology.

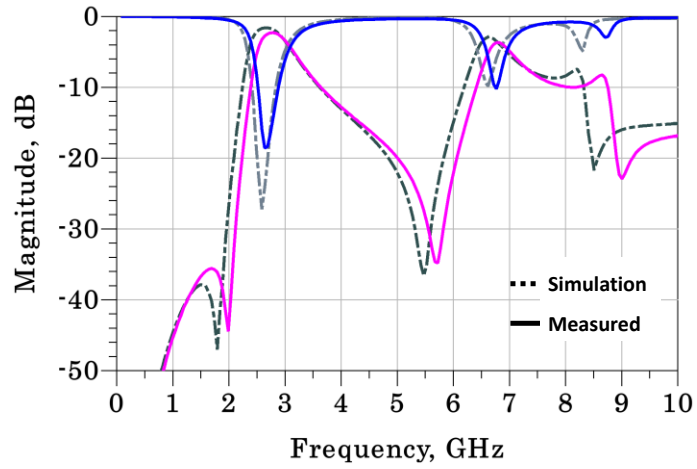


**Figure 126:** Comparison of the simulated and the measured responses of the filter.

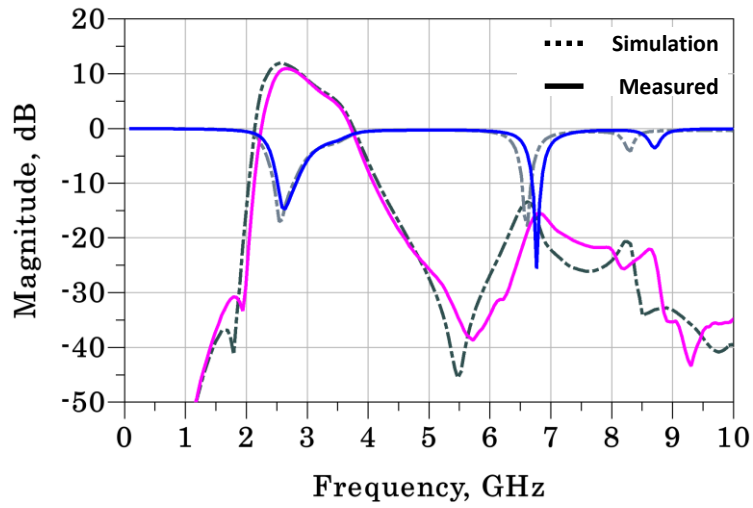


**Figure 127:** Comparison of the simulated and the measured responses of the receiver.

## **Design and simulation of RF Module on Glass Substrate**

To develop the WLAN RF receiver module (LNA + Filter) on glass substrates, both 2.4GHz and 5GHz bands were considered for the design. Further, to direct the signals between the two bands, the BPF was replaced with a diplexer. Trench-based electromagnetic shields were also integrated into the design to isolate the two bands and also to shield the filter from any noise from the DC pads. The design and simulation of the module will be discussed in this section, followed by the fabrication, assembly and test processes to realize the same.

### Substrate stack-up and design rules

The substrate stack-up consisted of four metal layers on a glass core having a thickness of 100  $\mu\text{m}$  with a polymer layer on both sides. The glass substrates were obtained from Corning, and had a dielectric permittivity ( $\epsilon_r$ ) of 5, and loss tangent ( $\tan\delta$ ) of 0.005 at 2 GHz. The core polymer, ABF-GX92 from Ajinomotto, had a thickness of 15  $\mu\text{m}$ , with  $\epsilon_r$  of 3.2 and  $\tan\delta$  of 0.017 at 10 GHz. The build-up polymer (ZS-100  $\epsilon_r$  of 3.0 and  $\tan\delta$  of 0.005 at 10 GHz) had a thickness of 17.5  $\mu\text{m}$ . The metal thickness on all layers was around 8  $\mu\text{m}$ . The pitch between two TPVs was 300  $\mu\text{m}$  and between blind vias was 100  $\mu\text{m}$ . The minimum width of the metal patterns and spacing was defined as 15  $\mu\text{m}$ . To enable interconnection of components on either side of the glass substrate and between metal layers, through package vias and blind vias were formed. The diameter of the TPVs was 100  $\mu\text{m}$  and that of the blind vias was 45  $\mu\text{m}$ . The stack-up cross-section is depicted in Figure 128.

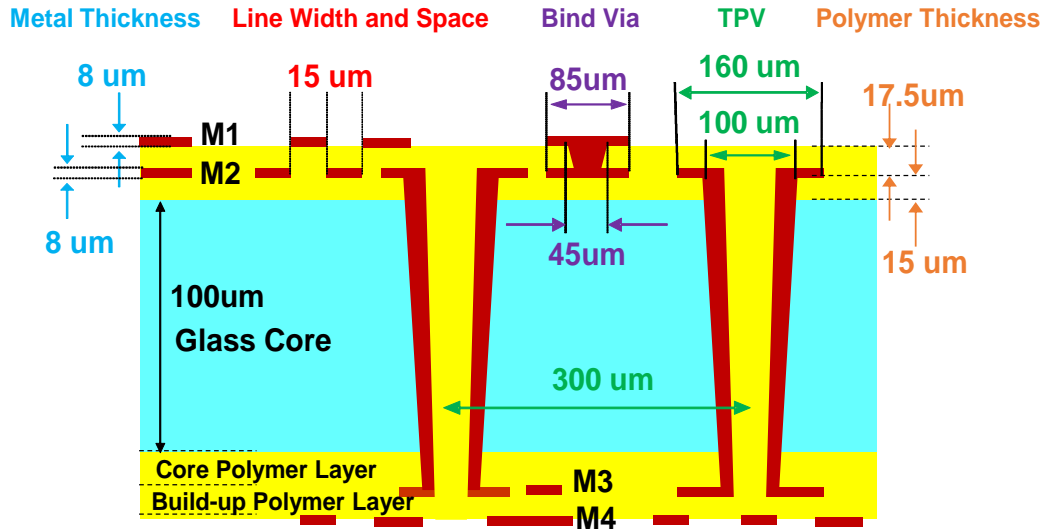


Figure 128: Stack-up cross-section of the multilayer glass substrate.

### Diplexer design on glass substrate

The diplexer used in the WLAN RF module was similar to the design described in Chapter 3. However, in this module design, the diplexer was realized as an embedded component and not as a separate 3D IPD component. To enable low-loss interconnections between the LNA and the diplexer, it was necessary to layout of the diplexer horizontally using only two metal layers. Hence the layout of the diplexer was performed using only the build-up metal layers (M1 – M2), with the low-band filter placed adjacent to the high-band filter. The top-view of the diplexer layout is shown in Figure 129. The dimensions of the filter were 1.2 mm x 1.1 mm. The simulated insertion loss and return loss of the diplexer are shown in Figure 130. The simulation was performed using Sonnet EM suite, a full-wave planar EM software.

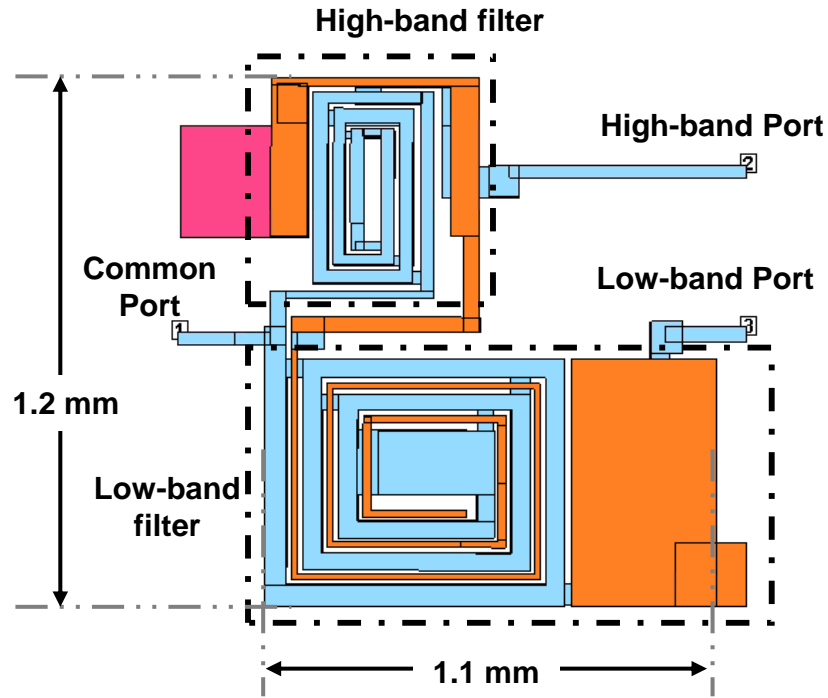


Figure 129: Top-view of the diplexer layout.

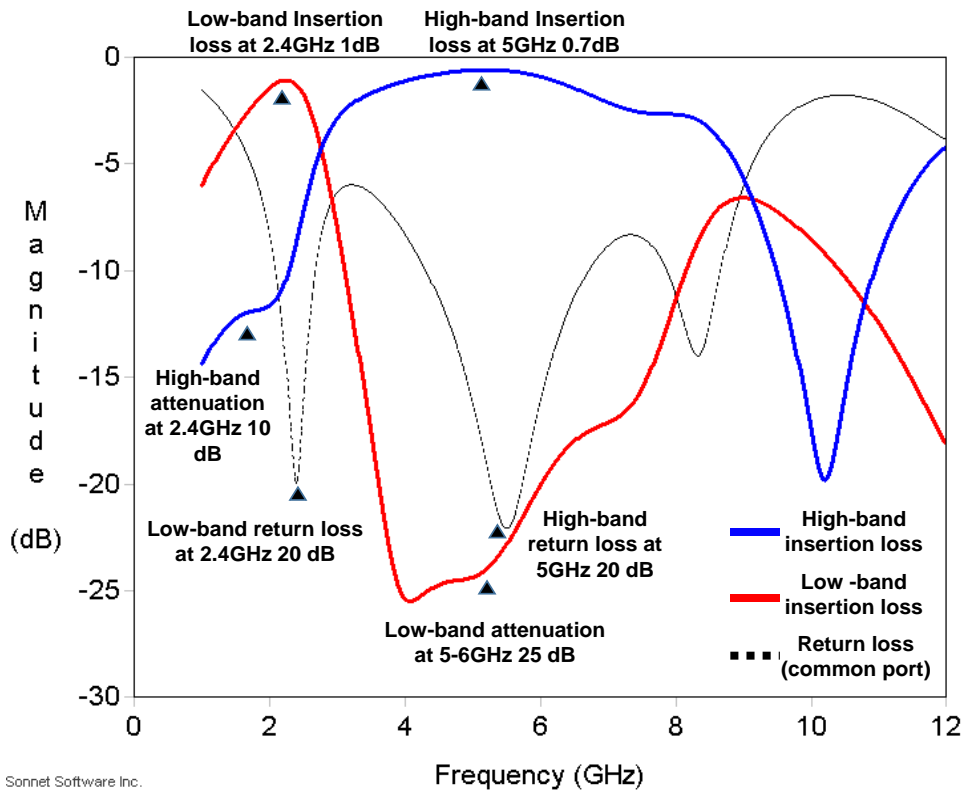
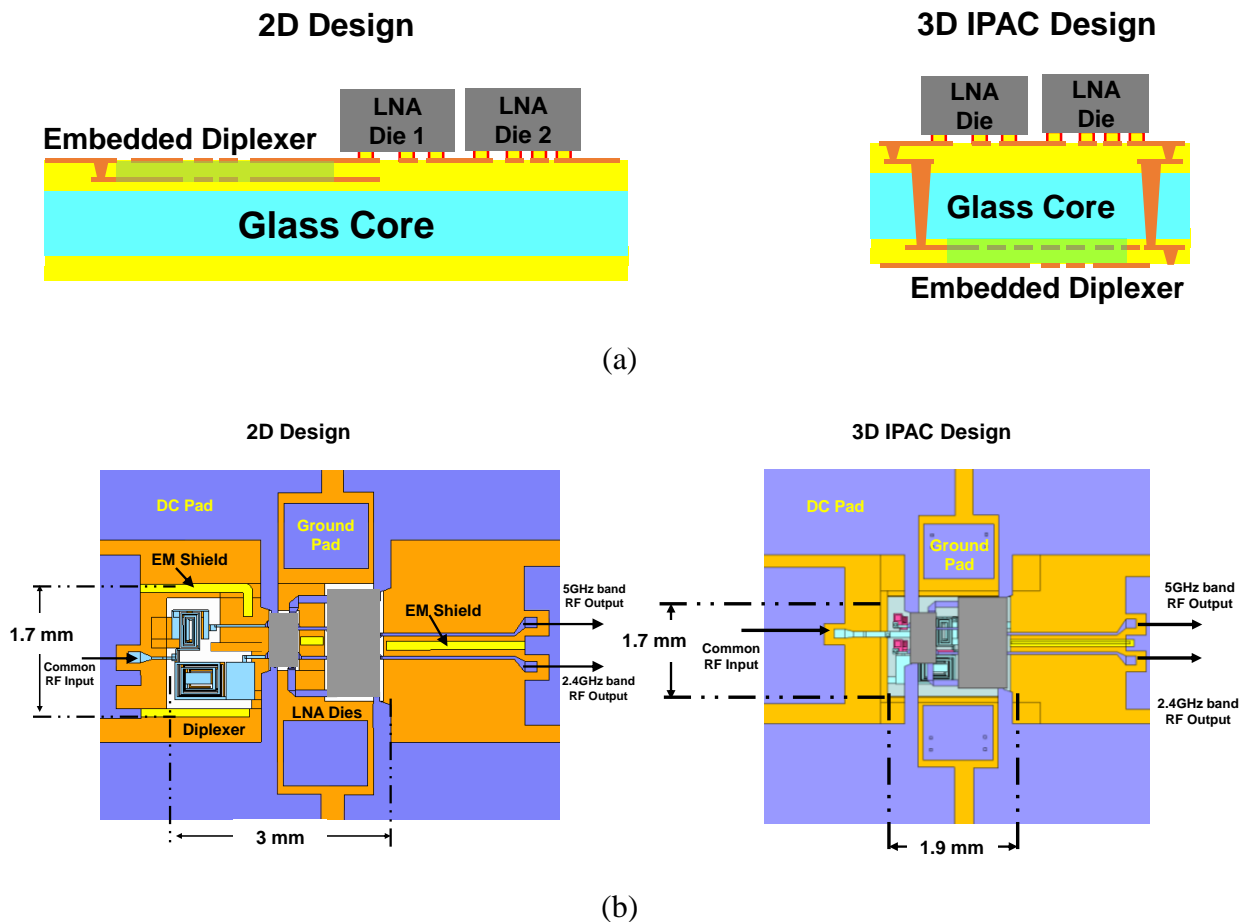


Figure 130: Simulated response of the diplexer.

## WLAN RF Receiver module design on glass substrate

The receiver module design consists of a diplexer and LNA dies. The diplexer was integrated with the LNA dies such that it is in the transition path from the antenna to the LNA. Since an antenna was not integrated, a set of GSG probe pads were substituted for the same. For the characterization of this module, the antenna was substituted with a set of RF-probe pads. The trench-based EM shields were integrated around the diplexer and between the 2.4GHz and 5GHz signal lines, to minimize noise and signal coupling between the actives and other system components such as DC pads and transmission lines. The schematic cross-section and the top-view of the 2D and 3D IPAC receiver module layout are shown in Figure 131. The dimensions of the 2D module are 3 mm x 1.7 mm, and those of the 3D IPAC module are 1.9 mm x 1.7 mm.



**Figure 131:** (a) Schematic Cross-section, and (b) Top-view, of the WLAN RF receiver Module.

## Full-wave EM simulations

The RF paths in the WLAN module were simulated using Sonnet [63] full-wave EM solver to estimate the loss and coupling. Since the input path is mostly dominated by the diplexer, only the output path was considered for the simulation. The output path, shown in Figure 132, comprises microstrip transmission lines for the 2.4GHz and 5GHz outputs with the EM shield trench in-between. The lines were 2 mm long, 40  $\mu\text{m}$  wide, and were impedance matched to 50 $\Omega$ . The trench was 45  $\mu\text{m}$  wide, with a capture pad width of 100  $\mu\text{m}$ . The distance between the two transmission lines was 280  $\mu\text{m}$  and the distance from the trench pad to the transmission line was 80  $\mu\text{m}$ .

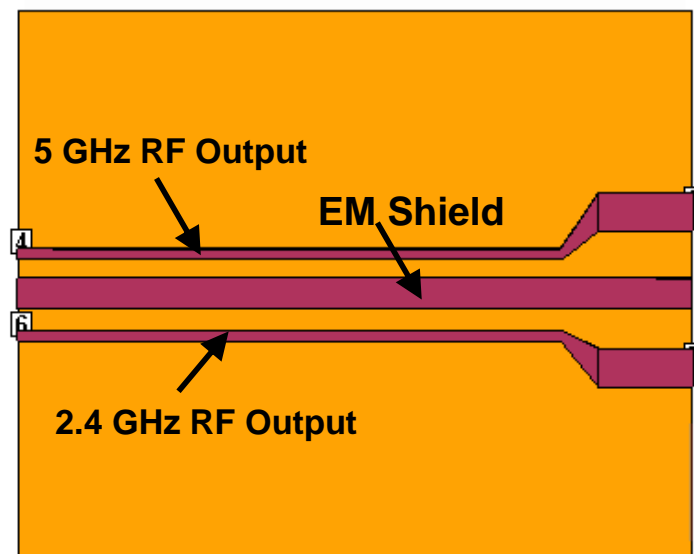


**Figure 132:** Top-view of the output section of the WLAN RF receiver Module.

The simulated response is shown in Figure 133. It can be observed that, since the transmission lines were impedance-matched and only 2mm long, the loss is very low with 0.1dB at 2.4GHz and 0.12dB at 5GHz. Further, the coupling between the transmission-lines is also below -60dB even up to 10GHz, as shown in Figure 134.

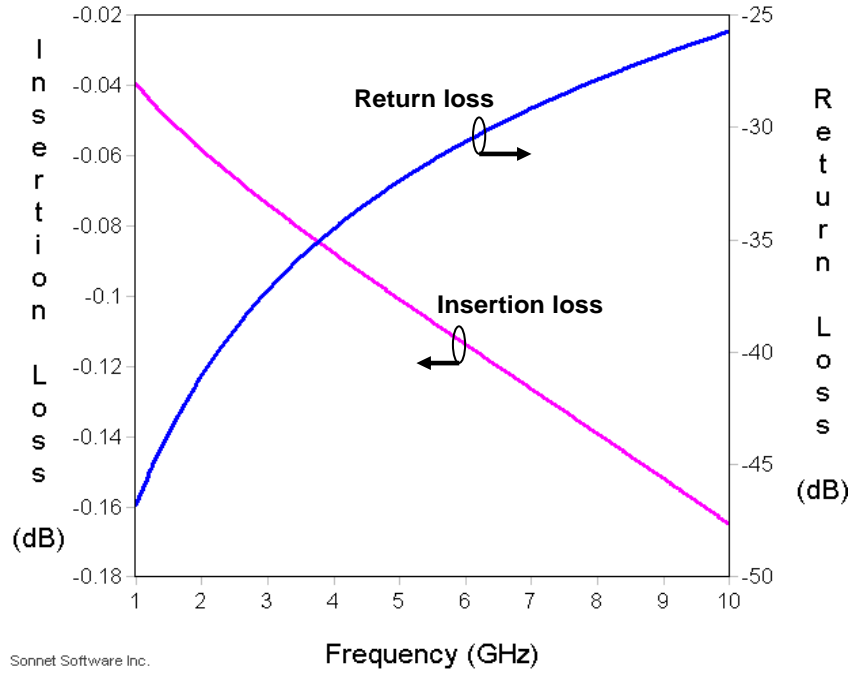


**Figure 133:** Simulated response of the output section of the WLAN RF receiver Module.

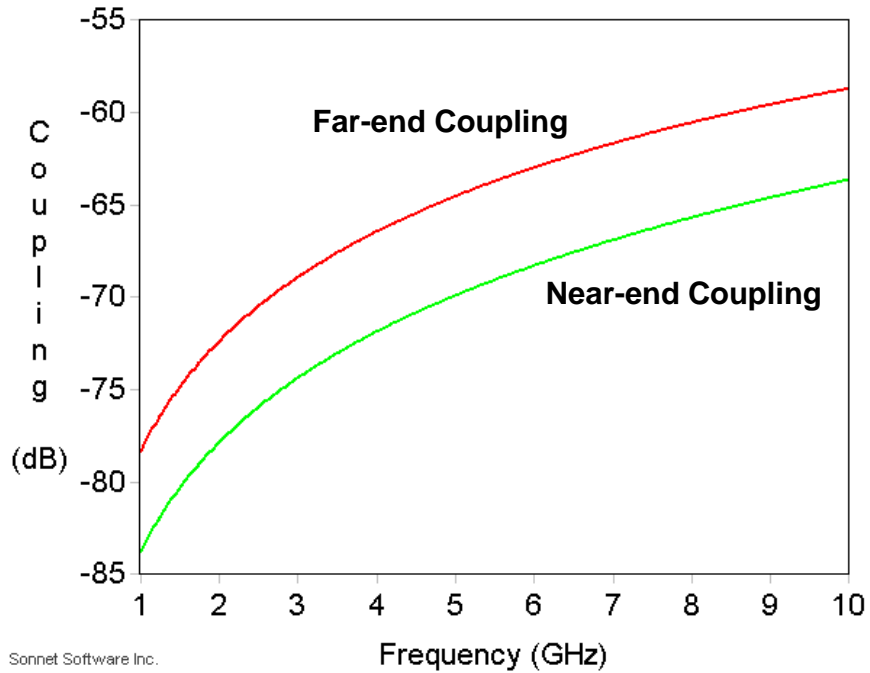


**Figure 134:** Simulated coupling of the output section of the WLAN RF receiver Module.

## **Fabrication and characterization of RF Modules on Glass Substrates**

### Fabrication process for glass substrates

The fabrication process for a two-metal layer substrate was described in Chapter 3. The same set of processes are employed for the four-metal layer substrate as well. For the four-metal-layer fabrication, the process is continued by laminating polymer (RXP4) build-up layers on each side of the two-metal-layer substrate. Micro-vias are formed on the build-up polymer using UV lasers, to electrically connect the metal layers on the inner layers to the ones on the surface. A semi-additive plating approach is used to pattern the surface metal layers, and complete the fabrication of the four metal layer stack-up.

### Assembly

Following the fabrication of the glass substrate, the substrates are visually inspected to eliminate defective coupons. Further, through 2-port S-parameter characterization of the diplexers, a few known-good coupons are selected for assembly of the actives. The same assembly process that is employed for the fabrication of the organic substrates is used to assemble the LNA dies and the decoupling capacitors on the glass substrate.

### Characterization and Model Validation:

The characterization process is similar to that used for the organic modules. The measured 2-port S-parameter response of the 2.4GHz BPF (fabricated separately), from Chapter 3, is shown in Figure 135.

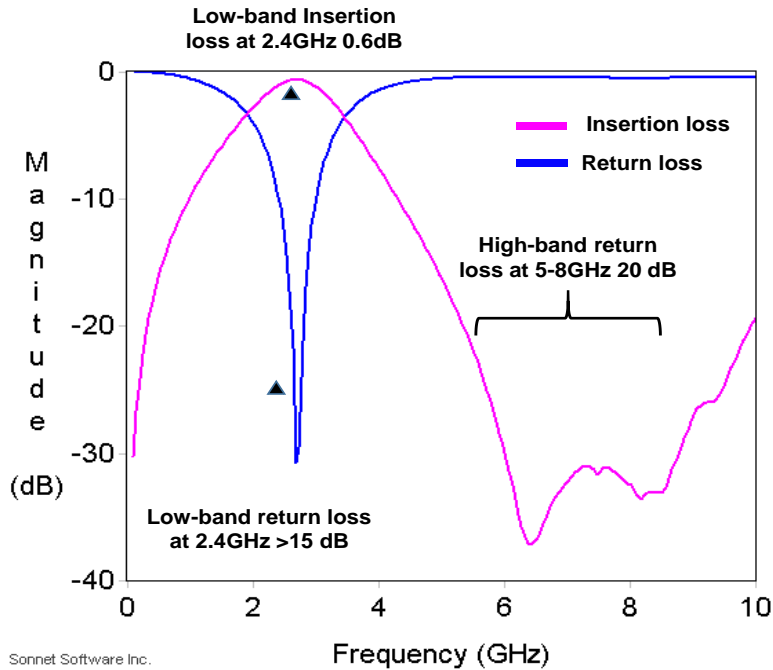


**Figure 135:** Measured response of the low-band BPF of the diplexer.

Further, using the de-embedded LNA response from the organic substrate, and the simulated output RF path, the low-band performance of the RF WLAN module on glass was estimated. The S-parameter responses of the individual building blocks were combined as shown in Figure 136, using the method depicted in Figure 117. The simulated response for the 2.4GHz chain is shown in Figure 137.

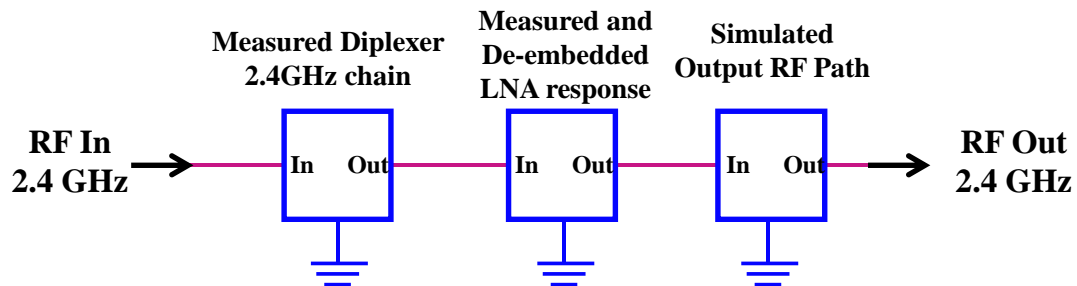


**Figure 136:** ADS schematic to estimate the low-band response of RF module on glass.

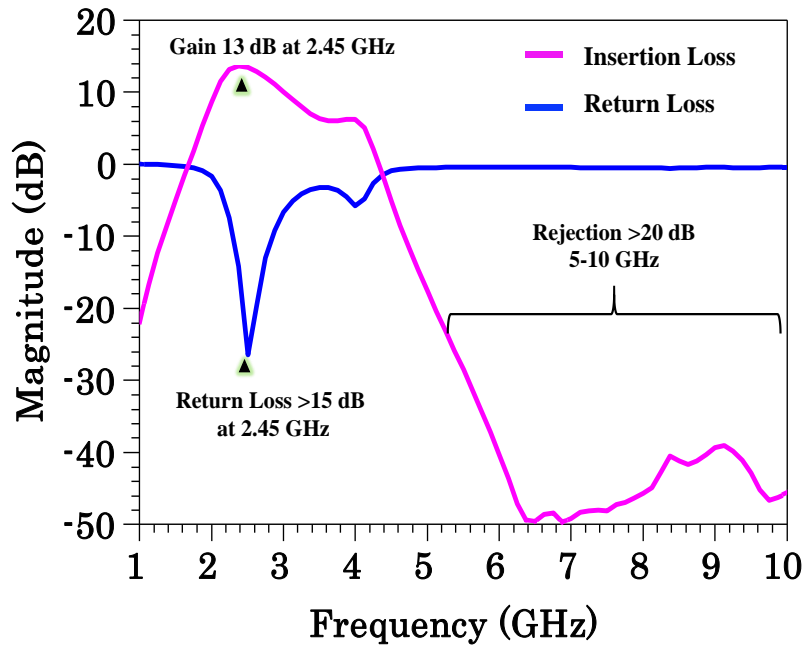


**Figure 137:** Estimated low-band response of WLAN RF module on glass substrate.

As seen in Figure 137, the gain at 2.4GHz is 13dB, which indicates that the combined loss from the diplexer and the package was only 1dB. Further, the out-of-band attenuation in the high frequencies indicate 20dB – 40dB of rejection in 5-6GHz band, and more than 35dB till 10GHz. Such attenuation characteristics indicate the efficacy of the diplexer.

## Summary

Advanced RF module technologies with superior electrical performance metrics: less than 1dB passive insertion loss, more than 20dB adjacent-band attenuation, less than -40dB internal noise-coupling, and atleast1.5X miniaturization at lower cost, were demonstrated using two examples: 1) Embedded thin-film passives and chip-last embedded actives with ultra-short Cu-Cu interconnections on organic substrates, 2) Glass substrates with embedded thin-film passives, integrated shields and ultra-short Cu-Cu interconnections on glass.

Chip-last embedded WLAN receiver module demonstration in low-loss organic substrates was described in the first part of the chapter. The LNA module with dimensions 2.6 mm x 2 mm x 0.16 mm, is more than 5x smaller in volume compared to current packages. It has a measured peak gain of 14dB. The receiver module has a gain of 9dB at 2.4 GHz. Comparing the performance of the LNA and the receiver modules, very good rejection of the adjacent frequency bands is observed in the receiver module, validating the effect of the BPF. The measured response of the receiver module correlates well with the results of the 3D EM simulations. The dimensions of the receiver module are 5.5 mm x 2 mm x 0.16 mm. Compared to current wire-bonded LNA packages without a filter, this receiver module, including the filter, is more than 5X smaller in volume.

As a next step, to achieve higher performance, increased miniaturization and lower cost; a glass-based dual-band LNA module with embedded diplexer and trench-based EM shields, was designed for demonstration using the 3D IPAC concept. The simulated performance of the diplexer showed 1dB insertion loss for both 2.4GHz and 5GHz, with more than 15dB rejection of adjacent band. The low-band BPF of the diplexer was measured and the insertion loss was 0.6dB at 2.6 GHz with more than 20dB attenuation for the high band. The BPF response was combined with the de-embedded LNA response and the simulated response of the RF path in the package. The estimated low-band response of the WLAN RF glass module shows a gain of 13dB with 20-40dB rejection in 5-10GHz. This indicates that the target performance specs of 1dB package loss, in addition to the adjacent-band rejection of more than 20dB and EM coupling of

less than -40dB; have been achieved. The WLAN glass substrate measured 1.7mm x 3mm x 0.2mm. Compared to the conventional WLAN LNA packages, the glass module with the miniaturized diplexer and EM shield achieves more than 3X reduction in area, resulting in more than 5X volume miniaturization from thickness reduction. Further, up to 8X volume reduction is possible by utilizing double-side integration enabled by glass 3DIPAC. Thus, 3D IPAC-based high-density integration of actives with embedded thin-film passives and EM shielding enables ultra-miniaturization without a significant performance degradation in RF modules for next-generation systems.

## CHAPTER 6

### SUMMARY AND FUTURE WORK

Smart mobile systems demand ultra-miniaturized integration of diverse functions such as access to high-definition media content on-the-move, health monitoring, GPS navigation, ability to control other devices such as smart home appliances and automobiles, and digital processing and wireless communication capabilities to enable these. Hence, there is a need to integrate multiple Radio Frequency (RF) communication standards such as GPS, WLAN, GSM, Bluetooth, and mm wave, in a highly miniaturized form-factor. Realization of such systems requires both high-performance and high-density functional components, and their integration into ultra-miniaturized modules, sub-systems and systems. This thesis focuses on two key passive-component building block technologies: diplexers and EMI shields for higher performance and density, and their integration with actives using an innovative 3D Integrated Passive and Active Components (3D IPAC) concept. A detailed survey of existing technologies was also performed to understand their advantages and limitations, and to propose and demonstrate suitable compelling alternatives using novel design and integration approaches. These approaches pave the way towards the development of ultra-miniaturized WLAN RF Front-end modules, and eventually towards fully integrated RF sub-systems on a single miniaturized multi-functional package. This chapter summarizes the key research findings and provides directions to extend this research further.

#### **Miniaturization of RF WLAN Diplexer**

A novel structure for a thin-film band-pass filter was proposed and a corresponding lumped-element circuit schematic was developed. Parametric structural design variations of the proposed filter and their effect on the RF performance were analyzed. In addition, topological

modifications to the circuit and their effect on the performance of the filter were also studied. The proposed filter structure was fabricated on ultra-thin glass substrate of thickness 30  $\mu\text{m}$ , and measured to obtain the S-parameter response. Based on the proposed filter structure, a WLAN diplexer was then designed, fabricated and characterized. To enhance the adjacent-band rejection and miniaturization, subsequent design improvements were carried out using grounded spirals and ground capacitor. A miniaturized diplexer with dimensions 1mm x 0.5mm x 0.2mm was designed with 0.9dB insertion loss and 12dB rejection. The low-band filter was also revised to improve the performance. The dimensions of the revised two-metal layer design were 1mm x 0.5mm. The measured insertion loss was 0.6dB and high-band rejection was more than 25dB. This revised design matched the target specifications. Hence, through the modeling, design, fabrication and characterization of a miniaturized diplexer on ultra-thin glass substrates, the proposed novel filter design has been shown to offer excellent potential to miniaturize RF passives, leading to ultra-miniaturized 3D IPD diplexer components.

### **Miniaturized Component-level EMI shielding**

Component-level trench-based electromagnetic interference shields were developed for miniaturized WLAN RF modules, enabling 30dB – 60dB isolation in the frequency range of 1- 20GHz, between passives separated by less than 100 $\mu\text{m}$ . The shielding issue in RF modules was addressed through four sub-tasks defined as: a.)Modeling of EM radiation in RF modules, b.)Analytical modeling – Material and multi-layer stack-up design, c.)Modeling and design of component-level EMI shields, d.)Fabrication and characterization of EMI shields.

Electromagnetic coupling between various passives elements was studied through 3D EM simulations to determine the worst-case coupling for a given pair of components. Based on these results, a simple set of guidelines were defined for the placement of such passives. Following this, analytical simulations were used to estimate the shield effectiveness of various single-layer and multi-layer shield materials, and a novel multi-layer stack was proposed. Subsequently, the

shielding effectiveness of via-array-based shields and trench-based shields were compared through modeling, simulation and fabrication. It was deduced through simulations that trench-based shields were more effective in suppressing EM coupling between two transmission lines, than via-array-based shields when the via pads on the upper metal layer were discontinuous. However, when the via pads were merged together, the via-array was found to be as effective as trench-based shields in providing isolation. Further, when the trenches were extended vertically upwards by 20 - 40 $\mu$ m, the shield effectiveness was observed to increase by up to 6dB. Multi-layer glass substrates were fabricated to test the shield effectiveness of trenches and via-array-based shields. It was observed that the trench-based shields offered up to 20dB of additional EM isolation between two microstrip transmission lines.

### **Design and Demonstration of miniaturized RF modules**

Advanced RF module technologies with higher electrical performance metrics such as less than 1dB passive insertion loss, more than 20dB adjacent-band attenuation, less than -40dB internal noise-coupling, and >1.5X miniaturization at lower cost, based on 3D IPAC concept were demonstrated using two examples: 1) Embedded thin-film passives and chip-last embedded actives with ultra-short Cu-Cu interconnections on organic substrates, 2) Glass substrates with embedded thin-film passives, integrated shields and ultra-short Cu-Cu interconnections on glass.

A chip-last embedded WLAN receiver module was fabricated on a low-loss organic substrate. The dimensions of the receiver module are 5.5 mm x 2 mm x 0.16 mm. Compared to current wire-bonded LNA packages without a filter, this receiver module, including the filter, is at least 1.5x smaller in volume. As the next step towards higher performance, increased miniaturization and lower cost, a glass-based dual-band LNA module with embedded diplexer and trench-based EM shields, was designed using the 3D IPAC concept. The estimated low-band response of the WLAN RF glass module shows a gain of 13dB with 20-40dB rejection in 5-10GHz. The 3D IPAC WLAN glass module measures 1.7mm x 1.9mm x 0.3mm. Compared to

the conventional WLAN LNA packages, the glass module with the miniaturized diplexer and EM shield achieves more than 2.5X reduction in area, resulting in a potential 8x volume miniaturization. Thus, high-density integration of actives with miniaturized passives and EM shielding enables ultra-miniaturization of RF modules for next-generation systems.

### **Key Contributions**

The key contributions and novelty of this dissertation are summarized as follows:

- Proposed a novel filter layout, developed an equivalent circuit schematic and analyzed the effect of process variations on the performance of the filter.
- First demonstration of band-pass filters on glass substrate of thickness 30  $\mu\text{m}$ .
- Developed component-level trench-based shields without requiring additional fabrication process steps.
- First design and demonstration of currently the thinnest (130  $\mu\text{m}$ ) WLAN RF receiver on organic substrate with embedded passives.

### **Future Research Directions**

Progress in science and engineering is a perennial process fueled by curiosity and an obsession for improvement. Discussed below are possible research directions to extend the research described in this thesis.

#### 3DIPD Diplexer

##### *Sputtered thin-films as dielectric materials*

Sputtered thin-films such as  $\text{SiO}_2$ ,  $\text{SiN}$ ,  $\text{Al}_2\text{O}_3$ , etc. can increase the capacitance by a factor of more than 10X and enable a similar factor of miniaturization. The primary challenges would involve forming a thin pin-hole-free layer of sputtered film with uniform thickness on a thick patterned metal layer. The second challenge would be to achieve precise lithography so as to achieve tight tolerance on large panels, which eventually controls the capacitances, and hence the frequency response of the filter.

### *LGA assembly of 3D IPD diplexer components*

Assembly of 3D IPD diplexers that are developed in this research is an important future research focus. By employing LGA assembly technology to integrate components onto the substrate, the interconnection parasitics can be lowered to enable better performance.

### EMI shielding

#### *Multi-layer shield integration into RF modules*

The multi-layer shields that have been developed through analytical simulations can be employed to shield a RF module package from external EM interference or integrated with trench-based structures to increase the internal EM isolation between sensitive components. This would involve the development of a novel process since the multi-layer shields are created through sputtering process while the rest of the metal structures are based on semi-additive copper plating.

#### *Trenches as external shields for packages*

The trenches developed as EM shields between components in this research could be extended to encompass the entire package and designed to act as an external EMI shield for the complete package. In regions where forming a trench is difficult, metallized ground vias could be employed as they can be as effective as trenches.

### RF modules

#### *Chip-last embedded RF modules on glass substrate*

Using thicker build-up layers, the WLAN actives could be embedded using chip-last embedding techniques and integrated with 3D IPD diplexers which could also be chip-last embedded, resulting in ultra-miniaturized profile-free WLAN RF front-end modules. There is

also scope for higher levels of integration using other front-end RF components such as power amplifiers and switches, and mixed-signal dies.

### **List of Publications**

#### Journal Publications

1. **Sitaraman, S.**, Suzuki, Y., et al. (2014). "Ultraminiaturized WLAN RF Receiver Module in Thin Organic Substrate." *Components, Packaging and Manufacturing Technology (CPMT), IEEE Transactions on* 4(8): 1276-1283.
2. Raj, P. M., Mishra, D., **Sitaraman, S.**, and Tummala, R., "Nanomagnetic Thinfilms for Advanced Inductors and EMI Shields in Smart Systems", *Journal of Materials NanoScience*, [S.l.], v. 1, n. 1, p. 31-38, sep. 2014. ISSN 2394-0867.
3. Gokul Kumar, **Sitaraman, Srikrishna**, Jounghyun Cho, Venkatesh Sundaram, Joungho Kim, Rao R Tummala, "Design and Demonstration of Effective Power Delivery Networks with Suppressed Resonances in Double-sided 3-D Glass Interposer Packages", *Components, Packaging and Manufacturing Technology, IEEE Transactions on*, 2015 (Accepted).

#### Conference Publications

4. **Sitaraman, S.**, et al. (2015). "Modeling, Design and Demonstration of Trench-based Electromagnetic Shielding in Miniaturized RF Glass Packages". *Electronic Components and Technology Conference (ECTC), 2015, IEEE 65th*.
5. **Sitaraman, S.**, et al. (2014). "Modeling, design and demonstration of multi-die embedded WLAN RF front-end module with ultra-miniaturized and high-performance passives". *Electronic Components and Technology Conference (ECTC), 2014 IEEE 64th*.

6. Gokul Kumar, **Srikrishna Sitaraman**, et al., "Power Delivery Network Analysis of 3D Double-side Glass Interposers for High Bandwidth Applications", ECTC 2013, IEEE 63rd.
7. Yoichiro Sato, **Srikrishna Sitaraman**, et al., "Ultra-miniaturized and Surface-mountable Glass-based 3D IPAC Packages for RF Modules", ECTC 2013, IEEE 63rd.
8. Gokul Kumar, **Srikrishna Sitaraman**, et al., "Chip-Last Die Embedded PA and Digital Modules towards an Ultra-miniaturized WLAN sub-system", ECTC 2012, , IEEE 62nd.
9. Yuya Suzuki, **Srikrishna Sitaraman**, et al., "Low cost System-in-Package module using next generation low loss organic material", ECTC 2012, , IEEE 62nd.
10. Sridharan, V.; Goyal, A.; **Sitaraman, S.** et al., "Ultra-miniaturized WLAN RF receiver with chip-last GaAs embedded active," Electronic Components and Technology Conference (ECTC), 2011 IEEE 61st , vol., no., pp.1371-1376, May 31 2011-June 3 2011

## REFERENCES

- [1] S. Dalmia, V. Govind, J. Dekosky, V. Sundaram, G. White, and M. Swaminathan, "Design and implementations of RF systems and sub-systems in LCP-type multilayer technology," in *Electronic Components and Technology Conference, 2006. Proceedings. 56th*, 2006, p. 5 pp.
- [2] R. Vaidya, D. Gupta, M. Bhakuni, and R. Prince, "A Miniature Low Current Fully Integrated Front End Module for WLAN 802.11b/g Applications," in *Compound Semiconductor Integrated Circuit Symposium, 2007. CSIC 2007. IEEE*, 2007, pp. 1-4.
- [3] P. M. Raj, J. Uei-Ming, D. Jinxiang, K. P. Murali, H. Sharma, D. Mishra, *et al.*, "3D IPAC &#x2014; A new passives and actives concept for ultra-miniaturized electronic and bioelectronic functional modules," in *Electronic Components and Technology Conference (ECTC), 2013 IEEE 63rd*, 2013, pp. 517-522.
- [4] Y. Suzuki, S. Sitaraman, A. Goyal, L. Fuhan, N. Kumbhat, M. Hashimoto, *et al.*, "Low cost system-in-package module using next generation low loss organic material," in *Electronic Components and Technology Conference (ECTC), 2012 IEEE 62nd*, 2012, pp. 1412-1417.
- [5] A. C. Kundu, M. Megahed, and D. Schmidt, "Comparison and analysis of integrated passive device technologies for wireless radio frequency module," in *Electronic Components and Technology Conference, 2008. ECTC 2008. 58th*, 2008, pp. 683-687.
- [6] C. Durand, F. Gianesello, R. Pilard, D. Gloria, Y. Imbs, R. Coffy, *et al.*, "High performance RF inductors integrated in advanced Fan-Out wafer level packaging technology," in *Silicon Monolithic Integrated Circuits in RF Systems (SiRF), 2012 IEEE 12th Topical Meeting on*, 2012, pp. 215-218.
- [7] "Industrial PCB Development Using Embedded Passive and Active Discrete Chips Focused on Process and DfR," <http://flex.icconnect007.media/index.php/article/41996/industrial-pcb-development-using-embedded-passive-and-active-discrete-chips-focused-on-process-and-dfr/41999/?skin=flex>, 2010.
- [8] T. Kamgaing, E. Davies-Venn, and K. Radhakrishnan, "A compact 802.11 a/b/g/n WLAN Front-End Module using passives embedded in a flip-chip BGA organic package substrate," in *Microwave Symposium Digest, 2009. MTT '09. IEEE MTT-S International*, 2009, pp. 213-216.
- [9] Z. Xiu Yin, D. Xin, K. Hsuan-ling, W. Bai-Hong, C. Ze Yu, and X. Quan, "Compact LTCC Bandpass Filter With Wide Stopband Using Discriminating Coupling," *Components, Packaging and Manufacturing Technology, IEEE Transactions on*, vol. 4, pp. 656-663, 2014.
- [10] Y. WanSuk, V. Sundaram, and M. Swaminathan, "High-**Q** Embedded Passives on Large Panel Multilayer Liquid Crystalline Polymer-Based Substrate," *Advanced Packaging, IEEE Transactions on*, vol. 30, pp. 580-591, 2007.
- [11] S. Hwang, S. Min, M. Swaminathan, V. Sundaram, and R. Tummala, "Thin-Film High-Rejection Filter Integration in Low-Loss Organic Substrate," *Components, Packaging and Manufacturing Technology, IEEE Transactions on*, vol. 1, pp. 1160-1170, 2011.
- [12] V. Sridharan, S. Min, V. Sundaram, V. Sukumaran, S. Hwang, H. Chan, *et al.*, "Design and fabrication of bandpass filters in glass interposer with through-package-vias (TPV),"

- in *Electronic Components and Technology Conference (ECTC), 2010 Proceedings 60th*, 2010, pp. 530-535.
- [13] H. Chang, J. J. Chen, V. Chen, and S. Leou, "Novel shielding structure for LTE and 3G RF design," in *Microwave Conference Proceedings (APMC), 2012 Asia-Pacific*, 2012, pp. 920-922.
- [14] S. Mostafazadeh, S. Chillara, and J. Belani, "Semiconductor component package assembly including an integral RF/EMI shield," ed: Google Patents, 1997.
- [15] K. Matsuge, S. Hiura, M. Ishida, T. Kitahara, and T. Yamamoto, "Full RF module with embedded filters for 2.4 GHz and 5 GHz dual band WLAN applications," in *Microwave Symposium Digest, 2004 IEEE MTT-S International*, 2004, pp. 629-632 Vol.2.
- [16] U. R. H. Madsen, Carsten, "Conformal technology delivers breakthrough in RF shielding," *Microwaves & RF*, p. p26, 2008.
- [17] N. Karim, M. Jingkun, and F. Jun, "Improving electromagnetic compatibility performance of packages and SiP modules using a conformal shielding solution," in *Electromagnetic Compatibility (APEMC), 2010 Asia-Pacific Symposium on*, 2010, pp. 56-59.
- [18] H. Chih-Ying, H. Chun-Hsiang, W. Chuen-De, L. Kuo-Hsien, S. Chia-Hsien, W. Chen-Chao, *et al.*, "Mold-based compartment shielding to mitigate the intra-system coupled noise on SiP modules," in *Electromagnetic Compatibility (EMC), 2011 IEEE International Symposium on*, 2011, pp. 341-344.
- [19] P. Jiwoo, H. Myunghyun, K. Jaemin, K. Donghee, C. Ho, K. Seyoung, *et al.*, "Design of a 3-D SiP for T-DMB with Improvement of Sensitivity and Noise Isolation," in *Electronics Packaging Technology Conference, 2008. EPTC 2008. 10th*, 2008, pp. 1387-1392.
- [20] A. Suntives, A. Khajooeizadeh, and R. Abhari, "Using via fences for crosstalk reduction in PCB circuits," in *Electromagnetic Compatibility, 2006. EMC 2006. 2006 IEEE International Symposium on*, 2006, pp. 34-37.
- [21] G. E. Ponchak, C. Donghoon, and Y. Jong-Gwan, "Characterization of plated via hole fences for isolation between stripline circuits in LTCC packages," in *Microwave Symposium Digest, 1998 IEEE MTT-S International*, 1998, pp. 1831-1834 vol.3.
- [22] G. E. Ponchak, C. Donghoon, Y. Jong-Gwan, and L. P. B. Katehi, "The use of metal filled via holes for improving isolation in LTCC RF and wireless multichip packages," *Advanced Packaging, IEEE Transactions on*, vol. 23, pp. 88-99, 2000.
- [23] V. Sukumaran, G. Kumar, K. Ramachandran, Y. Suzuki, K. Demir, Y. Sato, *et al.*, "Design, Fabrication, and Characterization of Ultrathin 3-D Glass Interposers With Through-Package-Vias at Same Pitch as TSVs in Silicon," *Components, Packaging and Manufacturing Technology, IEEE Transactions on*, vol. 4, pp. 786-795, 2014.
- [24] G. M. L. Y. E. Jones and L. Young, "Microwave Filters, Impedance Matching Networks and Coupling Structures," *Artech House*, 1964.
- [25] Z. Yunchi and K. A. Zaki, "LTCC Multi-layer Coupled Strip-Resonator Filters," in *Microwave Symposium, 2007. IEEE/MTT-S International*, 2007, pp. 1039-1042.
- [26] E. Arabi, M. Lahti, T. Vaha-Heikkila, and A. Shamim, "A 3-D Miniaturized High Selectivity Bandpass Filter in LTCC Technology," *Microwave and Wireless Components Letters, IEEE*, vol. 24, pp. 8-10, 2014.

- [27] Y. Tao, M. Tamura, and T. Itoh, "Super Compact Low-Temperature Co-Fired Ceramic Bandpass Filters Using the Hybrid Resonator," *Microwave Theory and Techniques, IEEE Transactions on*, vol. 58, pp. 2896-2907, 2010.
- [28] H. Chien-Hsiang, L. Yi-Chieh, H. Tzyy-Sheng, and H. Lih-Tyng, "Design of compact bandpass filter using transformer-based coupled resonators on integrated passive device glass substrate," in *Microwave Conference Proceedings (APMC), 2011 Asia-Pacific*, 2011, pp. 1921-1924.
- [29] T. Sudo, H. Sasaki, N. Masuda, and J. L. Drewniak, "Electromagnetic interference (EMI) of system-on-package (SOP)," *Advanced Packaging, IEEE Transactions on*, vol. 27, pp. 304-314, 2004.
- [30] C. Leseigneur, F. Fernandez, L. Ndez, P. Perez, et al., "Near-field coupling model between electronic systems and a transmission line," in *Electromagnetic Compatibility (EMC), 2010 IEEE International Symposium on*, 2010, pp. 22-27.
- [31] F. Vecchi, M. Repossi, A. Mazzanti, P. Arcioni, and F. Svelto, "A simple and complete circuit model for the coupling between symmetrical spiral inductors in silicon RF-ICs," in *Radio Frequency Integrated Circuits Symposium, 2008. RFIC 2008. IEEE*, 2008, pp. 479-482.
- [32] M. Lazarczyk, N. Barry, T. O'Donnell, and R. Meere, "Comparison of fields emitted from high frequency silicon-integrated, microfabricated inductors," in *Power Electronics and Applications, 2009. EPE '09. 13th European Conference on*, 2009, pp. 1-10.
- [33] T. Sato, H. Horiuchi, and K. Yaniasawa, "Local EMI in the monolithic DC-DC converter with on-chip planar inductor," in *Magnetics Conference, 2002. INTERMAG Europe 2002. Digest of Technical Papers. 2002 IEEE International*, 2002, p. EV3.
- [34] E. Diaz-Alvarez and J. P. Krusius, "Package and chip-level EMI/EMC structure design, modeling and simulation," in *Electronic Components and Technology Conference, 1999. 1999 Proceedings. 49th*, 1999, pp. 873-878.
- [35] H. Shall, Z. Riah, and M. Kadi, "Prediction of 3D-near field coupling between a toroidal inductor and a transmission line," in *Electromagnetic Compatibility (EMC), 2013 IEEE International Symposium on*, 2013, pp. 651-656.
- [36] H. Shall, Z. Riah, and M. Kadi, "A Novel Approach for Modeling Near-Field Coupling With PCB Traces," *Electromagnetic Compatibility, IEEE Transactions on*, vol. PP, pp. 1-8, 2014.
- [37] R. Minami, H. JeeYoung, D. Imanishi, K. Okada, and A. Matsuzawa, "Measurement of integrated PA-to-LNA isolation on Si CMOS chip," in *Microwave Conference Proceedings (APMC), 2010 Asia-Pacific*, 2010, pp. 1629-1632.
- [38] Y. Taesik, Y. Bayram, and J. L. Volakis, "Hybrid Analysis of Electromagnetic Interference Effects on Microwave Active Circuits Within Cavity Enclosures," *Electromagnetic Compatibility, IEEE Transactions on*, vol. 52, pp. 745-748, 2010.
- [39] H. W. Ott, *Noise reduction techniques in electronic systems*, 2nd ed. ed. Wiley: New York, 1988.
- [40] R. B. Schulz, V. C. Plantz, and D. R. Brush, "Shielding theory and practice," *Electromagnetic Compatibility, IEEE Transactions on*, vol. 30, pp. 187-201, 1988.
- [41] J. C. Volkers and W. R. Conley, "Alternating layers of high and conductivity metals or alloys," ed: Google Patents, 1985.

- [42] K. Yamada, M. Ishida, S. Yutaka, and M. Yamaguchi, "High-performance laminated thin-film shield with conductors and magnetic material multilayer," in *Electromagnetic Compatibility (EMC), 2011 IEEE International Symposium on*, 2011, pp. 432-437.
- [43] J. D. Le, R. C. Fitzer, C. L. Bruzzone, S. P. Maki, B. L. Givot, and D. A. Sowatzke, "Multilayer emi shielding thin film with high rf permeability," ed: Google Patents, 2011.
- [44] B. Bagdasarian, J. Blonski, N. Karim, and M. Jingkun, "RF-SiP design and integration," in *Microwave Conference Proceedings, 2005. APMC 2005. Asia-Pacific Conference Proceedings*, 2005, p. 4 pp.
- [45] H. Sasaki, V. Govind, K. Srinivasan, S. Dalmia, V. Sundaram, M. Swaminathan, *et al.*, "Electromagnetic interference (EMI) issues for mixed-signal system-on-package (SOP)," in *Electronic Components and Technology Conference, 2004. Proceedings. 54th*, 2004, pp. 1437-1442 Vol.2.
- [46] H. Morkner, M. Karakucuk, G. Carr, and S. Espino, "A full duplex Front End Module for WiFi 802.11.n applications," in *Wireless Technology, 2008. EuWiT 2008. European Conference on*, 2008, pp. 162-165.
- [47] H. Beom Cheol, D.-H. Kim, Y. Jong Min, J.-I. Ryu, J.-C. Kim, J.-C. Park, *et al.*, "A GPS/BT/WiFi triple-mode RF FEM using Si- and LTCC-based embedded technologies," in *Microwave Symposium Digest (MTT), 2012 IEEE MTT-S International*, 2012, pp. 1-3.
- [48] W. Min-Chung and C. Shyh-Jong, "A small SiP module using LTCC 3D circuitry for dual band WLAN 802.11 a/b/g front-end solution," in *Silicon Monolithic Integrated Circuits in RF Systems, 2006. Digest of Papers. 2006 Topical Meeting on*, 2006, p. 4 pp.
- [49] Y.-J. Ko, P. Jae Yeong, R. Jin-Hyung, L. Kyeong-Hak, and B. Jong-Uk, "A miniaturized LTCC multi-layered front-end module for dual band WLAN (802.11 a/b/g) applications," in *Microwave Symposium Digest, 2004 IEEE MTT-S International*, 2004, pp. 563-566 Vol.2.
- [50] S. Sakhnenko, D. Orlenko, B. Vorotnikov, O. Aleksieiev, P. Komakha, P. Heide, *et al.*, "Ultra-low-profile small-size LTCC front-end module (FEM) for WLAN applications based on a novel diplexer design approach," in *Microwave Symposium Digest, 2009. MTT '09. IEEE MTT-S International*, 2009, pp. 609-612.
- [51] M. Brunnbauer, T. Meyer, G. Ofner, K. Mueller, and R. Hagen, "Embedded Wafer Level Ball Grid Array (eWLB)," in *Electronic Manufacturing Technology Symposium (IEMT), 2008 33rd IEEE/CPMT International*, 2008, pp. 1-6.
- [52] V. K. Nair, C. Hanna, R. Spreitzer, and J. Swan, "Active die embedded small form factor RF packages for ultrabooks and smartphones," in *Electronic Components and Technology Conference (ECTC), 2014 IEEE 64th*, 2014, pp. 1278-1283.
- [53] "SESUB modules for smartphones "<http://www.epcos.com/epcos-en/374108/tech-library/articles/products---technologies/products---technologies/very-small-and-extremely-flat/171672>"."
- [54] L. Baik-Woo, V. Sundaram, B. Wiedenman, K. Y. Chong, V. Kripesh, M. Iyer, *et al.*, "Chip-last Embedded Active for System-On-Package (SOP)," in *Electronic Components and Technology Conference, 2007. ECTC '07. Proceedings. 57th*, 2007, pp. 292-298.
- [55] V. Sridharan, A. Goyal, S. Sitaraman, N. Kumbhat, N. Sankaran, H. Chan, *et al.*, "Ultra-miniaturized WLAN RF receiver with chip-last GaAs embedded active," in *Electronic Components and Technology Conference (ECTC), 2011 IEEE 61st*, 2011, pp. 1371-1376.
- [56] S. Sitaraman, Y. Suzuki, C. White, V. Nair, T. Kamgaing, F. Juskey, *et al.*, "Modeling, design and demonstration of multi-die embedded WLAN RF front-end module with

- ultra-miniaturized and high-performance passives," in *Electronic Components and Technology Conference (ECTC), 2014 IEEE 64th*, 2014, pp. 1264-1271.
- [57] V. Sukumaran, T. Bandyopadhyay, Q. Chen, N. Kumbhat, L. Fuhan, R. Pucha, *et al.*, "Design, fabrication and characterization of low-cost glass interposers with fine-pitch through-package-vias," in *Electronic Components and Technology Conference (ECTC), 2011 IEEE 61st*, 2011, pp. 583-588.
- [58] E. A. Logan, H. M. Clearfield, J. L. Young, and D. H. Bolton, "Advanced packaging of integrated passive devices for RF applications," in *Radio and Wireless Conference, 1998. RAWCON 98. 1998 IEEE*, 1998, pp. 289-292.
- [59] V. Sukumaran, Q. Chen, L. Fuhan, N. Kumbhat, T. Bandyopadhyay, H. Chan, *et al.*, "Through-package-via formation and metallization of glass interposers," in *Electronic Components and Technology Conference (ECTC), 2010 Proceedings 60th*, 2010, pp. 557-563.
- [60] TriQuint, "TQM3M7001 802.11a/b/g Dual-Band, Low Noise Amplifier Module.."
- [61] A. Choudhury, N. Kumbhat, P. M. Raj, Z. Rongwei, V. Sundaram, R. Dunne, *et al.*, "Low temperature, low profile, ultra-fine pitch copper-to-copper chip-last embedded-active interconnection technology," in *Electronic Components and Technology Conference (ECTC), 2010 Proceedings 60th*, 2010, pp. 350-356.
- [62] "Advanced Design System - ADS " *Keysight Technologies EEsof EDA*, 2015.
- [63] "Sonnet EM Suite," *Sonnet Software Inc.*, 2015.
- [64] S. Min, S. Hwang, C. Daehyun, M. Swaminathan, V. Sridharan, H. Chan, *et al.*, "Filter integration in ultra thin organic substrate via 3D stitched capacitor," in *Electrical Design of Advanced Packaging & Systems Symposium, 2009. (EDAPS 2009). IEEE*, 2009, pp. 1-4.
- [65] HFSS, "ANSYS, Inc.,," 2015.